High density polymer modification of proteins using polymer-based protein engineering

Submitted in partial fulfillment of the requirements for

the degree of

Doctor of Philosophy

in

Department of Biomedical Engineering

Chad S. Cummings

B.S., Polymer and Fiber Chemistry, Clemson University

Carnegie Mellon University

Pittsburgh, PA

August 2016

ACKNOWLEDGEMENTS

There are many people to acknowledge that have helped me during my five years as a PhD student. The work in this dissertation has been a success due to technical and personal contributions from a multitude of individuals.

First, I would like to thank my advisor and committee chair, Dr. Alan Russell, who has always given me encouragement to have confidence in the work I have done and what I am able to do. He allowed me to focus on projects that I thought were the most interesting, even if their chance of success was low. Looking back, transferring to Carnegie Mellon to stay in the Russell lab was an easy decision, but also one of my best decisions during graduate school due to the constant support I received from Alan. In addition, I would like to thank the members of my dissertation committee Dr. Krzysztof Matyjaszewski, Dr. Kathryn Whitehead, and Dr. Jonathan Minden. As core members of the Center for Polymer-based Protein Engineering, I collaborated with students from each of their labs, and each has helped me directly by giving constructive criticism to improve the scientific path of this dissertation.

I would also like to thank the many members, past and present, of the Russell lab that have each helped me in different ways: Jill, Rick, Hiro, Moncy, Collin, Sonia, Alan, Weihang, and Sheiliza. Without question, Dr. Hironobu Murata deserves a lot of my gratitude as he trained me when I first entered the Russell lab, and continued to answer questions I had for him throughout my career. In addition, the contributions of Kathy Fein and Becca Ball in the Whitehead group have been crucial to completing important cell based assays for the protein conjugates. Specifically, Kathy's contribution in the months leading up to my defense was vital to me finishing.

Lastly, but most importantly, I would like to thank my family and my fiancée, Tiffany, for their personal and emotional support during my time in graduate school. Their words of encouragement helped give the wherewithal to finish graduate school. Of utmost importance is Tiffany, as she is the one person who would constantly offer support and listen with the most open of ears to me when I would complain, gloat, or talk about my day at lab.

I also would like to acknowledge the CMU Deans for funding the Center for polymer-based protein engineering and this research.

ABSTRACT

Proteins and protein-based materials are used for a wide range of therapeutic, diagnostic, and biotechnological applications. Still, the inherent instability of proteins in non-native environments greatly limits the applications in which they are effective. In order to increase their utility, proteins are often modified, either biologically or chemically, to manipulate their bioactivity and stability profiles. In this work, covalent attachment of polymers to the enzyme chymotrypsin was used to predictably tailor protein bioactivity and stability. Specifically, atom transfer radical polymerization (ATRP) based polymer-based protein engineering (PBPE) was used to grow polymers directly from the surface of chymotrypsin. First, the temperature responsive polymers poly(*N*-isopropyl acrylamide) (pNIPAM), which has a lower critical solution temperature (LCST) and poly(dimethylamino propane sulfonate) (pDMAPS), which has an upper critical solution temperature (UCST), were separately grown from chymotrypsin. The temperature responsive properties of the polymers were conserved in the protein-polymer conjugates, and chymotrypsin bioactivity, productivity, and substrate specificity were predictably tailored at different temperatures depending on the structural organization of the polymers. Next, a dual block polymer-chymotrypsin conjugate was synthesized by growing poly(sulfobetaine methacrylamide) (pSBAm)-*block*-pNIPAm conjugates from the surface of chymotrypsin. The CT-pSBAm-*b*-pNIPAm conjugates showed temperature dependent kinetics, due to UCST or LCST driven polymer collapse at high and low temperature. Most interestingly, the dual block conjugates were dramatically more stable than native chymotrypsin to low pH. In order to further investigate the effect of polymer conjugation on chymotrypsin stability at low pH, four distinct and uniquely charged polymers were grown from the surface of chymotrypsin. With these new conjugates, we confirmed that chymotrypsin low pH stability was dependent on the chemical

structure of polymers covalently attached to chymotrypsin. Indeed, positively charged polymers stabilized chymotrypsin to low pH, but negatively charged and amphiphilic polymers destabilized the enzyme. Lastly, after developing strategies for low pH stabilization, new protein-polymer conjugates with the chemical permeation enhancer 1-phenylpiperazine were designed to enable protein transport across the intestinal epithelium. Bovine serum albumin-poly(oligoethylene methacrylate)-*block*-poly(phenylpiperazine acrylamide) BSA-pOEGMA-*b*-pPPZ conjugates induced dose dependent increases in Caco-2 monolayer permeability and transported across an *in vitro* intestinal monolayer model with low cell toxicity.

TABLE OF CONTENTS

LIST OF TABLES

LIST OF FIGURES

Chapter 1 : Introduction

1.1 Protein-Polymer Conjugates

Protein modification has long been used to manipulate the bioactivity, stability, and solubility of proteins. Biological modification techniques such as site directed mutagenesis[1, 2] or directed evolution[3] and chemical modification strategies such as polymer covalent attachment[4, 5] or surface immobilization[6] have resulted in protein materials with higher stability, modified pH activity profiles, and changes in solubility. Specifically, the first demonstration of polymer conjugation to a protein was the attachment of poly(ethylene glycol) to bovine serum albumin in 1977.[7, 8] Since the first demonstration of protein-polymer conjugates, the methods and applications of protein-polymer conjugates have continued to expand. Protein-polymer conjugates are used frequently because they have several benefits over native proteins including increased stability, recovery, and solubility.[9, 10] In addition, structural and functional properties of polymers are transferred to protein-polymer conjugates to enable tailorable bioactivity and substrate binding. When designing protein-polymer conjugates several factors must be considered, as the understanding of the ultimate application of the conjugates is dependent on synthesizing well-defined and well characterized conjugates. The protein of interest must be commercially or biosynthetically available, the polymer synthesis must be well controlled, the conjugation chemistry must be mild to ensure protein stability, and the polymer attachment should be optimized to maintain desired protein bioactivity.[11]

1.1.1 Synthesis of Protein-Polymer Conjugates

Protein-polymer conjugates are synthesized using either a “grafting from” or a “grafting to” chemical modification strategy. (**Figure 1.1**) In “grafting to”, polymers are synthesized to a desired molecular weight or degree of polymerization (DP) prior to covalent conjugation with

the protein. Once synthesized, end group functionality on the polymer is exploited to covalently attach polymer chains to surface accessible and reactive amino acid residues on the protein of interest. In the "grafting to" method, the achievable polymer density around the biomolecule is often limited due to steric hindrance between each bound long polymer molecule and subsequent polymer chains attaching to the protein. In addition, the specific polymer chain attachment site to the biomolecule is often unknown when using the "grafting to" approach. Lastly, purification of unreacted free polymer from protein-polymer conjugate is often difficult due to their comparable size and molecular properties. Advantageously, the reaction conditions for polymerization, such as temperature or solvent, do not need to be optimal for protein stability in "grafting to." Indeed, high temperatures and organic solvents are often used during "grafting to" polymerization. Because polymers are attached to the protein after polymerization is complete, there is no need to consider protein stability when optimizing polymerization reaction conditions.

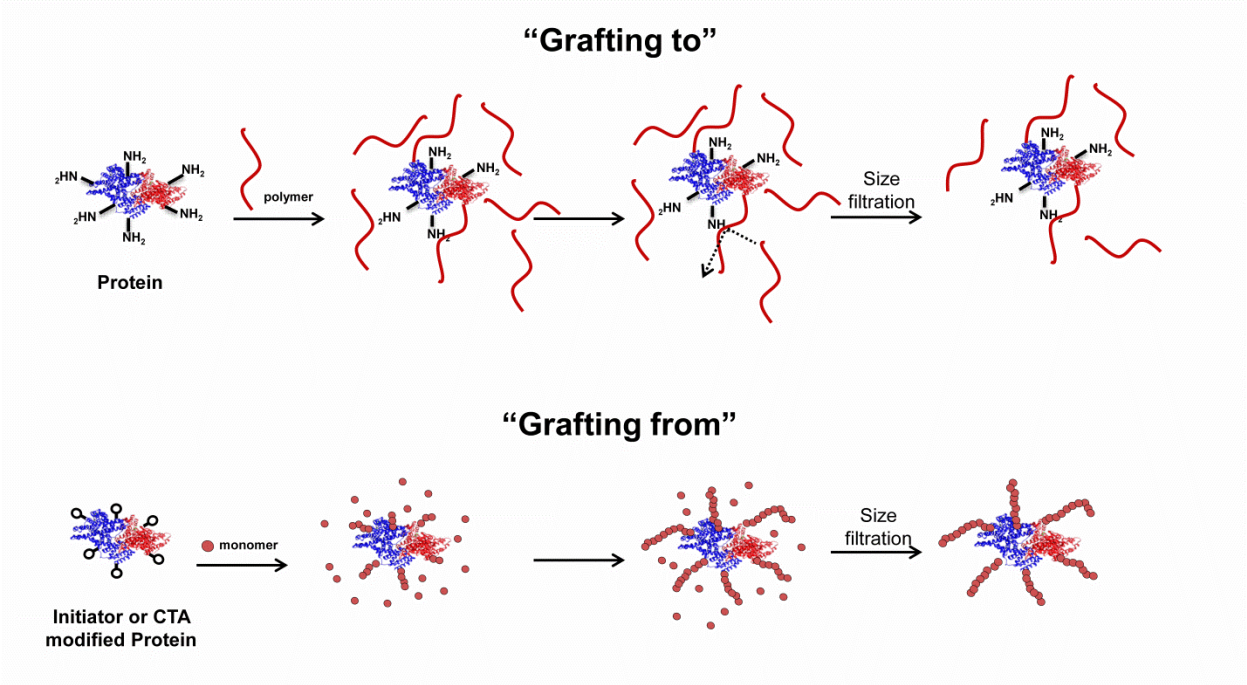

Figure 1.1 Synthesis of protein-polymer conjugates using "grafting from" and "grafting to" reactions

Conversely, in the "grafting from" approach, protein molecules serve as the initiating site for controlled radical polymerization (CRP) reactions. Most often, either atom transfer radical polymerization (ATRP) or reversible addition-fragmentation chain-transfer polymerization (RAFT)[12] are used when synthesizing polymer conjugates using the "grafting from" approach. In "grafting from," ATRP initiator molecules or RAFT chain transfer agents (CTA) are covalently attached to surface accessible amino acids, often lysine[13] or cysteine[14], the *N*-[15] or *C*-[16, 17] terminus, or noncanonical amino acids[18]. Then, polymer is grown directly outward from the surface of the initiator modified protein. Using "grafting from," reaction conditions are easily manipulated to predictably tune the polymer chain length or molecular weight while maintaining a low polydispersity index (PDI) and high uniformity. Since the polymer is grown directly from the surface of protein, there is often a higher degree of polymer modification in protein-polymer conjugates synthesized using "grafting from" compared to "grafting to." If desired, it is also possible to reduce the number of polymers per protein molecule by simply modifying molar ratios of reactants during the initiator or chain transfer agent immobilization reaction. In "grafting from", the separation of unreacted monomer from protein is a facile process due to the large size differences between monomer and protein-polymer. However, mild polymerization reaction conditions are required when using "grafting from" synthesis. Because the protein is present in the polymerization solution, the reaction must be done in aqueous buffer with ambient temperatures (<37 °C), depending on the protein, in order to not denature the protein. Unfortunately, ATRP and RAFT are more difficult to control in aqueous buffers compared to organic solvents, resulting in less uniformity. Still, many aqueous based protocols have been developed to better control CRP in water.[19-21] Another disadvantage of "grafting from" is that CRP initiator insolubility limits the maximum number of

polymers per protein. Less hydrophilic initiators reduce initiator immobilization homogeneity or necessitate biphasic reaction conditions.[13, 22]

Table 1.1 Synthesis of protein-polymer conjugates using "grafting from"

Initiator	Site of modification	Type of polymerization	Polymer	Percentage of Total Sites Modified	Unmodified Protein Remaining?
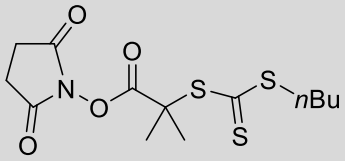	Lysine	RAFT	pNIPAm-*b*-pDMA	20 %	Yes[23]
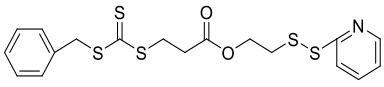	Cysteine	RAFT	pPEG-A	100%	No[24]
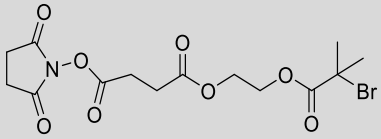	Lysine	ATRP	pOEGMA	50%	No[25]
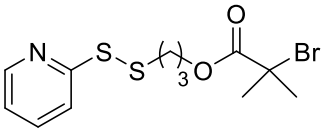	Cysteine	ATRP	pNIPAm	33%/100%	No[14]
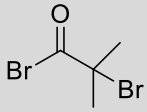	Lysine	ATRP	pMPEG-MA	15%	Yes[13]
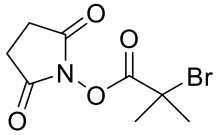	Lysine	ATRP	pMPC-MA	40%	Yes[26]

The "grafting from" technique has been used extensively to synthesize conjugates using both ATRP and RAFT. (**Table 1.1**) "Grafting from" protein-polymer synthesis has been used to synthesize protein conjugates with modified immunogenicity, manipulated bioactivity, enhanced solubility, and increased stability.[27-32] Most often in "grafting from", ATRP initiators or RAFT chain transfer agents are covalently attached to lysine or cysteine amino acid residues.

Attachment at lysine residues enables highly modified protein-polymer conjugates and high concentrations of initiator/CTA per protein which helps to control targeted degree of polymerization and the rate of reaction.[33] However, attaching at a large number of lysine residues can negatively affect protein bioactivity. Cysteine residues are less abundant on the protein surface, which allows for more site specific modification of polymers onto the protein. However, the enhanced properties added by the polymer maybe limited due to the low degree of modification. Similar to cysteine modification, modification of an ATRP initiator at the *N*-terminus can be used for site specific modification of polymers onto proteins. In one specific example, a cationic amine-functionalized polymer was grown from an ATRP initiator specifically attached to the *N*-terminus of myoglobin.[34] Post polymerization modifications resulted in a zwitterionic polymer-myoglobin conjugate that was injected into mice and compared to myoglobin-PEG conjugates. Zwitterionic-myoglobin conjugates showed increased plasma half-life compared to myoglobin-PEG conjugates and native myoglobin. Incorporation of non-canonical amino acids can also be used for site specific modification of polymers using "grafting from".[18, 35] Incorporation of the initiator molecule directly into the protein backbone removes the initiator immobilization step, but implementation of the non-natural amino acid can be laborious.

1.1.2 Moving Beyond PEGylation

The most commonly used technique to modify proteins for therapeutic applications is known as PEGylation. In PEGylation, proteins are covalently attached to polyethylene glycol (PEG) polymer chains via surface accessible and reactive amino acid residues using the "grafting to" process. PEGylation is therapeutically effective by reducing *in vivo* immunogenicity and increasing *in vivo* blood circulation time.[8] PEGylated proteins are currently FDA approved to

treat a multitude of diseases including gout, acute lymphoblastic leukemia, severe combined immunodeficiency disease, and chronic hepatitis C.[36]

The increased effectiveness of PEGylated protein drugs is largely due to two factors. First, PEG is a hydrophilic, uncharged polymer that has minimal interactions with the immune system. PEGylation is described as giving proteins a "stealth" behavior, as the PEG molecules shield the protein surface to mask and hide protein epitopes that could be recognized by patient immunogenic derived B and T cells.[36] In addition, PEG molecules increase the overall hydrodynamic diameter of the molecule, which reduces reticuloendothelial system clearance and increases residence time in blood. Each of these beneficial factors increase *in vivo* circulation time of PEGylated drugs, which leads to less frequent dosage schedules and increased patient compliance compared to unmodified proteins.

One specific example of a PEGylated drug is Pegloticase, an FDA approved drug for the treatment of chronic gout, a disease which causes a buildup of uric acid crystals leading to pain and inflammation in the joints.[37] In Pegloticase, PEG molecules are covalently attached to lysine amino acid residues on the surface of uricase,[38] an enzyme not natively synthesized by humans that breaks down uric acid in the blood. Since humans do not natively synthesize uricase, a porcine like uricase is used instead, which necessitates PEGylation to reduce immunogenicity of the non-human protein. Without PEGylation, uricase is cleared from circulation quickly due to high immunogenicity associated with non-human proteins.

Although it is clear that PEGylation increases beneficial properties for proteins, concerns still exist over the immunogenicity[39] and activity[40] profiles after PEG attachment. Thus, PEGylation must be optimized for each individual protein, and might not be suitable in certain instances. In addition, the long term stability of PEG is limited due oxidative degradation, which

was demonstrated by a loss of function of PEG coatings when implanted *in vivo* for extended times.[41] Indeed, a large amount of work has been explored in order to move beyond simple "grafting to" PEGylation of linear polymers by synthesizing conjugates with polymers other than PEG and with distinct architecture. [30, 42]

While PEGylated proteins work effectively in a variety of diseases, a large reduction in biological activity is seen for many enzymes after PEGylation, greatly reducing their therapeutic efficacy. Keefe *et al.* developed a chymotrypsin-poly(zwitterion) conjugate that showed increased substrate binding compared with PEGylation.[43] In this work, poly(carboxybetaine) (pCB) was conjugated to chymotrypsin via covalent bonding at surface lysines on chymotrypsin. pCB is a zwitterion, with one positive charge and one negative charge in the side chain of the polymer, resulting in an overall neutral polymer. Chymotrypsin-pCB conjugates showed higher substrate specificity and higher structural stability than PEGylated chymotrypsin in *in vitro* stability experiments when incubated in both urea and at high temperature. The authors hypothesized that the zwitterion polymer allowed better access of the substrate to the active site while maintaining high structural stability due to specific charge interactions between the substrate, water, and polymer that are not present for PEGylated proteins.

Liu *et al.* compared the immunogenic and bioactivity properties of linear versus non-linear PEG based polymers.[44] They synthesized L-asparaginase-polymer conjugates using both "grafting to" and "grafting from" strategies. "Grafting to" synthesis of asparaginase conjugates was completed using well-defined linear α-methoxy-poly(ethylene glycol) polymers and "grafting from" was completed using poly(olgioethylene glycol monomethyl ether methacrylate) (pOEGMA), a PEG mimic with similar structure, but distinct comb-shaped architecture. Conjugates with equivalent size and molecular weight were synthesized for comparison. The

comb shaped pOEGMA conjugates showed both higher bioactivity and lower *in vivo* immunogenicity compared to linear PEG conjugates, indicating that polymer architecture provides a unique opportunity to manipulate therapeutic efficacy.

PEG is the only polymer incorporated into FDA approved protein-polymer conjugates, but many other polymers are generally considered biocompatible including poly(*N*-(2-hydroxypropyl)methacrylamide) (pHMPA),[45] poly(vinylvpyrrolidone) (PVP),[46] and poly(2-oxazolines) (pOX)[47]. One specific example of pOX conjugates was completed by Mero *et al.*, who synthesized pOX conjugates with trypsin, a serine protease, and Ara-C, a known pyrimidine nucleoside analogue used to treat leukemia.[48] POX conjugates were synthesized to be the same size as the PEG conjugates and the activity and stability profiles were tested for each. Trypsin-pOX conjugates retained activity to small molecule substrates, but had lower activity to large molecule substrates. Ara-C-pOX conjugates maintained similar stability to a degrading enzyme and similar *in vitro* cytotoxicity to PEG derivatives. Thus, the authors concluded these conjugates represented a viable alternative to PEG conjugates, as the pOX polymers were easier to synthesize, allowed for more monomer modification, and could increase drug loading.

From the examples in this section, it is clear that several viable replacements to PEGylation do exist. While effective, the developing immunogenicity of PEG and common reduction in bioactivity after PEGylation represent sufficient motive to explore alternative opportunities.

1.1.3 Stimuli Responsive Polymers

One more class of protein-polymer conjugates are stimuli-responsive conjugates, where specific polymer functionality is transferred from polymer to the conjugate.[49] Stimuli-responsive polymers respond to an external stimulus, most commonly pH, temperature, or light,

by changing their conformation or chemical composition. This reversible response to an external stimulus is used as an on-off switch for protein bioactivity, solubility, or stability, depending on the application. Stimuli-responsive polymers have been incorporated into a variety of materials including films, particles, and proteins.[29]

One of the first demonstrations of a stimuli responsive protein-polymer conjugate was reported by Stayton *et al*. in which poly(*N*-isopropyl acrylamide) (pNIPAm) was covalently attached to a genetically modified cysteine near the binding pocket of streptavidin.[50] Strepavidin-pNIPAm conjugates showed temperature dependent binding with biotin, whereas unmodified streptavidin activity showed no dependence on temperature. They hypothesized the temperature dependent binding was due to the structural conformation of pNIPAm at different temperatures. PNIPAm is a temperature responsive polymer that has a lower critical solution temperature (LCST). Above the LCST, pNIPAm is a collapsed globule and phase separates in aqueous media, but below the LCST, pNIPAm is fully hydrated and has a random coil conformation. This change in structural conformation is reversible and is due to the varying hydration of the isopropyl group at different temperatures. Since the LCST of pNIPAm (31 °C) lies between room temperature (25 °C) and body temperature (37 °C), it has been used frequently for therapeutic applications.[51, 52] Other synthetic and natural polymers that exhibit LCST behavior include pDMAEMA,[53] pOEGMA,[54] and elastin like peptide[55]. Similar to an LCST, some polymers exhibit upper critical solution temperature (UCST) behavior where the polymers are in a random coil, chain extended state above a certain temperature, but in a collapsed globule orientation when below the same temperature.[56] Both LCST and UCST values are dependent on polymer molecular weight, chemical structure, and solution salt concentration. [57, 58]

In addition to temperature, light is used as an external stimulus to manipulate polymer structural conformation.[59] When exposed to light, photo responsive molecules adopt different photoisomeric states compared to the light absent photoisomeric state. When attached to a protein, these molecules alter substrate access and modify binding recognition sites. [60, 61] Like most temperature responsive polymers, these changes in biological activity are reversible and cyclical. Rather than direct attachment of responsive molecules to proteins, another approach to modulate protein bioactivity based on light involves the immobilization of a protein into a photochromic-functionalized polymer matrix. In one system, chymotrypsin activity was dependent on the presence of light due to photoisomeric state of spiropyran units in a crosslinked acrylamide polymer. This dependence of chymotrypsin activity on light was due to differences in permeability of the substrate across the polymer membrane with or without light.[62] For biomedical applications, the necessity of most of these systems to be switched on or off by UV light is still a hurdle. Administration of UV light to the body would only be practical for peripheral tissues where depth penetration is not a significant issue. Approaches that use infrared or near-infrared light triggered switches would be more appropriate for *in vivo* applications.[63]

Lastly, pH responsive polymers have been explored for therapeutic applications, especially uses related to cancer therapy, as the pH in tumor vasculature (~pH 6.5-7) is slightly lower than in circulating blood (pH 7.4), the gastrointestinal tract, where the pH changes from ~pH 1 in the stomach to ~pH 7 in the intestines,[64] and cell internalization where the low pH of endosomes (~pH 5) triggers specific responses after internalization. One of the most common uses of pH responsive polymers are enteric coated delivery systems in the GI tract.[65] These coatings usually consist of methacrylic acid or cellulosic based polymers that contain carboxylic

acid moieties. The pH responsive properties come from carboxylic acid moieties that are protonated at low pH in the stomach and deprotonated in the intestines, where the pH is closer to physiological pH. These coatings serve to protect the protein in the stomach, but allow the protein to be released once leaving the harsh environment of the stomach.[66] Similarly, pH responsive polymers have been used as polymeric drug carriers for delivery into cells.[67] When in the acidic endosome after cell internalization, these polymers are below their pKa and, thus, protonated and more hydrophobic. Due to the relative hydrophobicity, the polymers disrupt the endosome lipid bilayer and release the drug into the cytosol.

Tumor vasculature also provides an opportunity for pH responsive polymers to be used. Rather than carboxylic acid based polymers used in GI tract applications, pH responsive polymers used for tumor applications are often amine based, where they are charged and extended below their pKa, but uncharged and collapsed above their pKa. Commonly for tumor delivery, pH responsive polymers are incorporated into a block copolymer that forms pH dependent micelles. Indeed block copolymer-drug micelles showed 11 fold higher targeting ability compared to control micelles,[68] due to the ionization state of the pH responsive polymer poly(β-amino ester). Drug loaded polymer micelles fell apart at the lower pH of the tumor vasculature, releasing drug, but stayed intact at physiological pH in circulation.

1.2 Osmolyte Induced Protein Stabilization

Many small molecules readily destabilize and stabilize proteins by affecting protein structural organization. Molecules such as urea and guanidine hydrochloride structurally denature a wide variety of proteins, although the molecular mechanisms of destabilization are still not fully understood and are likely different for each molecule.[69] While known to destabilize proteins, some organisms, including sharks and rays, still have a large concentration

of urea in their cells, upwards of 600 mM in *Dasyatis americana* rays.[70] However, in order to counteract the destabilizing effects of urea in these organisms, there is also a large concentration of trimethylamine *N*-oxide (TMAO), a protein stabilizing methylamine osmolyte.[71] Indeed, TMAO has been shown frequently to counteract the destabilizing properties of urea on multiple proteins, [72-74] and this effect is general, where it is conserved for proteins that evolved in the presence of the osmolyte and also for proteins that did not.[75] Osmolytes are organic molecules that have been utilized in nature to stabilize proteins that might see adverse changes of environment. Osmolytes are generally characterized into three classes: (1) carbohydrates, which includes sorbitol, glycerol, and trehalose, (2) amino acids and their derivatives, which includes glycine, alanine, and proline, and (3) methylamines, which include betaine and TMAO.[76] As these molecules stabilize native proteins to a high degree, a large amount of work has been completed to examine the mechanism of their stabilization effect.[77] It has been determined that the stabilization effect of these osmolytes is related to their preferential exclusion from the surface of the protein. Osmolyte exclusion from the protein surface necessitates an increase in the relative hydration around the protein. Consequently, this hydration leads to tighter protein packing, which is responsible for reducing the tendency of the protein to unfold in response to thermal or chemical treatments.[78] Conversely, denaturing molecules have been shown to preferentially bind to the protein, which displaces the water hydration layer, causing destabilization. Unfortunately, the specific molecular mechanisms of these stabilizing and destabilizing properties are unknown. It has been hypothesized that the effects are due to a global change in water structure, direct interactions with the protein backbone[69] or specific amino acid residues,[79] or a combination of both[74]. In any case, the general stabilizing properties of methylamines is conserved for many different proteins. The study of protein stabilization by

osmolytes has proved useful in understanding the factors that contribute to *in vivo* protein misfolding and aggregation for diseases such as Alzheimer's and prion diseases.[80]

1.3 Protein Oral Delivery

Protein therapeutic delivery through the oral route represents the most patient friendly option. However, the gastrointestinal (GI) tract has evolved with the specific purpose of breaking down proteins for nutrient absorption. The two main challenges that must be overcome to make oral protein delivery effective are (1) low protein stability to the harsh conditions in the stomach and intestines and (2) low absorption of macromolecules across the intestinal epithelium. Proteins for therapeutic applications in the GI tract need to only overcome the low stability in the GI tract, while protein therapeutics that act somewhere else in the body must overcome both challenges.

1.3.1 Gastrointestinal Tract Anatomy and Physiology

The gastrointestinal (GI) tract is the series of organs, including the mouth, pharynx, esophagus, stomach, small intestine, colon, rectum, and anus, that form a passageway for food to pass through and be digested. The GI tract is one of two major divisions of the digestive system, the other being the accessory glands, which includes salivary glands, pancreas, and liver-each of which aid in digestion by secreting various fluids and enzymes into the GI tract. [81]

Structurally, the wall lining of the GI tract is conserved in most of the organs and has four distinct layers: the mucosa, submucosa, muscularis externa, and the serosa. Within the mucosa, there are three distinct sublayers; (1) the mucous membrane, the innermost layer of cells, (2) the lamina propia, and (3) muscularis mucosae, an outer layer of smooth muscle. The mucous membrane is a continuous layer of epithelial cells know as enterocytes. Enterocytes serve to separate the GI tract lumen from the rest of the body, and are classified as absorptive, endocrine,

or exocrine. Absorptive enterocytes are specialized to absorb nutrients and endocrine enterocytes secrete hormones into the bloodstream. Exocrine enterocytes are responsible for secretions into the GI tract lumen. One specific type of exocrine enterocytes are goblet cells, which secrete mucus, a sticky, viscous fluid containing mucin glycoproteins. Mucus is important for lumen protection from harsh conditions and physical abrasion that the lumen is exposed to during digestion. The lamina propia is a layer of connective tissue that contains many small blood vessels, nerves, and lymphatic vessels, each of which are important for nutrient absorption and digestion related signaling pathways.[81]

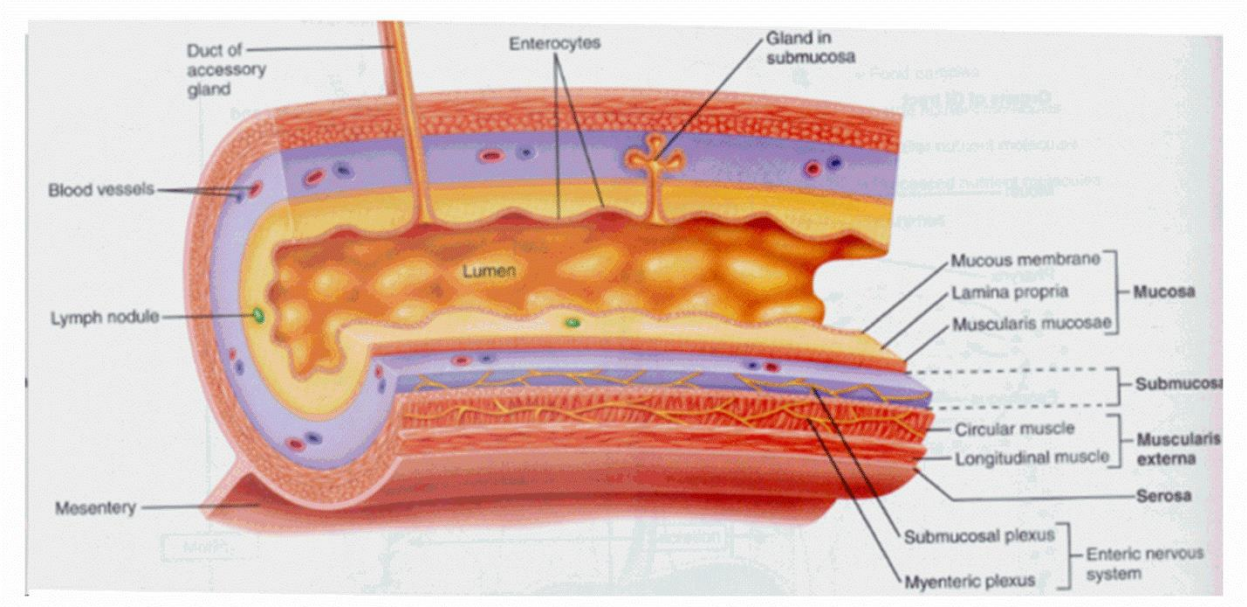

Figure 1.2 General structure of the gastrointestinal (GI) tract wall. The wall of the GI tract is conserved for many organs in the GI tract and consists of mucosa, submucosa, muscularis externa, and serosa layers. Image adapted from "Principles of Human Physiology." [81]

Of most importance to oral protein delivery are the stomach and the small intestine, because these are the organs of the GI tract where the harshest conditions are seen and most nutrient absorption takes place, respectively. The pH of the stomach is very low, between 0.9 and 2, which is a result of the secretion of gastric juice, made up of hydrochloric acid, sodium

chloride, and potassium chloride, by stomach gastric glands. Also secreted in the stomach, by chief cells, is pepsinogen, the precursor for the proteolytic enzyme pepsin. The presence of low pH and pepsin starts the breakdown of proteins during digestion. Low pH causes structural unfolding and pepsin cleaves the protein into smaller peptide fragments. [82]

After traveling through the stomach, chyme (the mixture of food and gastric juice) enters the small intestine via the pylorus. The small intestine is where most nutrient absorption takes place, and the increased absorption is due to specific anatomical differences in this region of the GI tract. The small intestine is divided into three sections, the duodenum, which is approximately the first 30 cm after the pylorus, the jejunum, which comprises the next 1 meter, and the ileum, which is the distal 1.5 meters that connects with the colon. In the duodenum, proteins are further digested by protease enzyme in pancreatic juice secreted by the pancreas. Pancreatic juice contains a mixture of the enzymes chymotrypsin, trypsin, and lipase and bicarbonate, which neutralizes the acid in chyme to slightly basic pH. The high absorptive efficiency of the small intestine is attributed to the presence of villi in the mucosal surface of the small intestine. Villi are small folds in the mucosal membrane that serve to increase the surface area 10 fold compared to a lining with no villi. Blood vessels are within the head of each villus, which is crucial for nutrient absorption. In addition to villi, the epithelial cells in the small intestine also contain microvilli which are even smaller folds on the apical surface of the enterocytes. These microvilli make up the brush border, which also contains brush border enzymes that aid in digestion and absorption. Collectively, the large surface area in the small intestine promotes high nutrient absorption. Once absorbed by the intestines, nutrients travel via the bloodstream to the liver for further processing and filtration.[81]

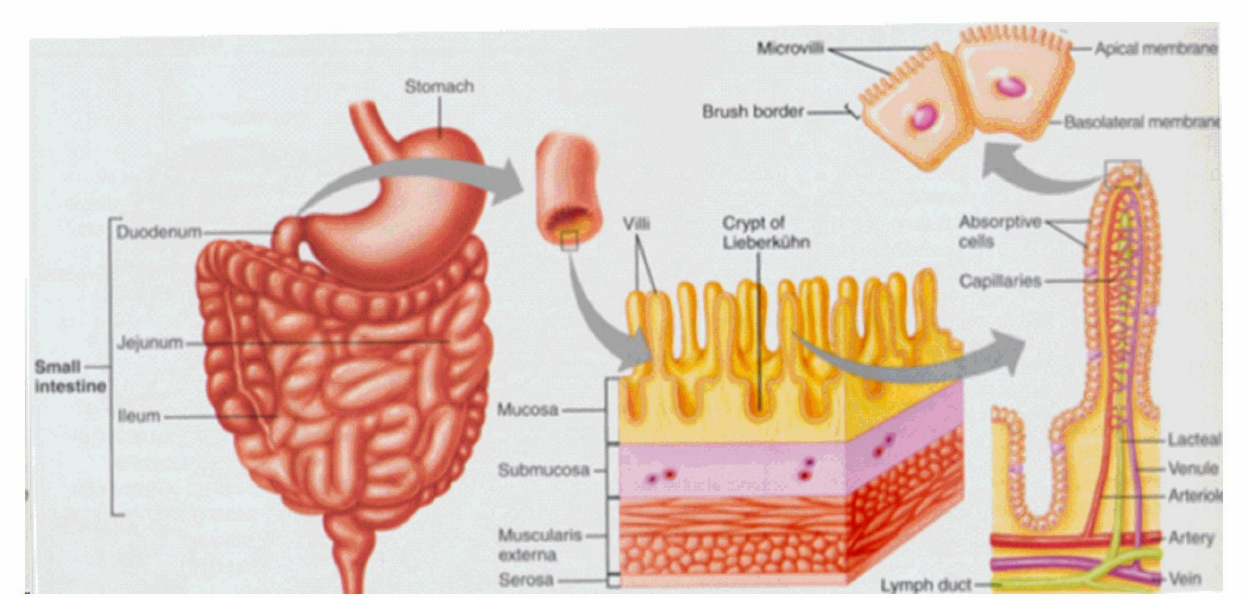

Figure 1.3 Anatomy of the small intestine. Anatomy of the small intestine is specialized to maximize surface area, which increases nutrient absorption. Image adapted from "Principles of Human Physiology." [81]

The absorptive process in the GI tract was not designed to maintain protein structural stability. Due to stomach acidic pH and digestive enzymes, proteins are readily unfolded and broken down into smaller peptide and amino acid fragments. Even if a protein is stable enough to avoid denaturation, the absorptive processes in the small intestine was designed to only allow small fragments into circulation. Indeed, in order for a protein to be delivered *via* the oral route, significant modifications must be made.

1.3.2 Mucoadhesive Polymers

Mucoadhesive polymeric systems increase absorption across the intestinal membrane by associating with mucosa and increasing the residence time of the drug around the membrane.[83] The two main classes of polymers that show mucoadhesive properties are carboxylic acid based polymers and positively charged polymers. Poly(acrylic acid) polymers, cellulosic polymers, and their derivatives, such as carbopol, poly(methacrylate), carboxymethyl cellulose, and

methylcellulose have all been used alone or with thiol group modifications[84] to increase effectiveness of orally delivered proteins. In order to increase the oral bioavailability of heparin for anti-coagulant therapy, Schmitz *et al.* developed a mucoadhesive system that used a thiolated polycarbophil to increase delivery across the intestinal membrane and increase therapeutic efficacy.[85] Heparin of different molecular weights was added with the thiolated polycarbophil and the permeation mediator, reduced glutathione (GSH), in a tablet form and then tested *in vivo* in rats. Hydroxyethylcellulose (HEC) was used as a control material for a standard drug delivery system. The thiomer/GSH system showed higher heparin plasma concentration than control HEC delivery vehicle, and this result was attributed to the mucoadhesive behavior. Poly(acrylic acid) based polymers are hypothesized to increase mucoadhesion through hydrogen bonding with mucin proteins, while thiolated polymers form crosslinks, via disulfide bridging, with mucin proteins and within the polymer itself.[86]

Positively charged polymers, including amine based polymers and chitosan, also exhibit mucoadhesive properties. Rather than associate solely through hydrogen bonding, these polymers also associate with mucin protein through electrostatic interactions. In order to examine the molecular mechanisms of chitosan mucoadhesion, mucin and chitosan were incubated together and crosslinking of mucin particles by chitosan, as a marker for mucoadhesion, was quantified using turbidity measurements.[87] Sodium chloride, ethanol, and urea were added to solutions to determine if electrostatic attraction, hydrogen bonding, or hydrophobic effects, respectively, were responsible for mucoadhesion. The authors concluded that electrostatic attraction was the main driving force of mucoadhesion, but that hydrogen bonding and hydrophobic effects were secondarily responsible. Conversely, electrostatic

attraction was determined to be solely responsible for polycationic dendronzied polymer mucoadhesion at pH 4.5 and pH 8, but hydrogen bonding did contribute at pH 1.8.[88]

Mucoadhesive polymers effectively increase the residence time of drugs in the GI tract by forming associations with the mucous membrane in the GI tract wall. As a result, permeation of large molecules across the intestinal membrane increases. In addition, mucoadhesive delivery vehicles can be used to extend the residence time of a GI tract therapeutic. This extended residence time at the site of action leads to a more efficacious therapy and a lower required dose.

1.3.3 Permeation Enhancers

Tight junctions, which control the flow of ions and nutrients and prevent paracellular transport of toxins into the body, are integral components of the effective barrier set up by enterocytes in the GI tract.[89] Tight junctions are composed of both transmembrane and cytosolic proteins. While not all of the proteins involved in tight junctions have been determined, several have been verified to be important for tight junction integrity including occludin, claudin, and junctional adhesion molecule (JAM).[90] Not surprisingly, increased expression of the tight junction proteins occludin and claudin correlated well with increases in TEER when Caco-2 cells were incubated with naringenin, a tight junction barrier integrity enhancer.[91] Intracellular domains of the transmembrane proteins interact with cytosolic proteins including zonula occludens proteins, which link to the actin cytoskeleton. [92] This link between transmembrane proteins and the actin cytoskeleton of the enterocytes is critical for tight junction barrier integrity.

Permeation enhancers increase macromolecule transport by disrupting tight junctions between enterocytes in the lining of the small intestine. They also decrease mucous viscosity and increase transcellular transport by disrupting cell membranes to increase membrane fluidity.

Permeation enhancers come from a wide variety of chemical classes, including surfactants, fatty acids, steroidal detergents, and chitosans.[93] Generally, nonionic surfactants are hypothesized to act as permeation enhancers by solubilizing membrane components. While many fatty acids in general have been examined for permeation enhancement, sodium caprate has been investigated most commonly. Indeed, sodium caprate increased permeability of the large molecule markers mannitol, PEG, and FITC-dextran.[94] Steroidal detergents, most often bile salts, which are natively secreted into the GI tract, also have permeation enhancing effects due to their ability to solubilize phospholipids.[93] Chitosans, which are also mucoadhesive, are potential permeation enhancers due to their positive charge, but have pH dependent effects because of their low solubility in neutral and basic pH.[95] Chemical modification of chitosans via quaternization enabled a pH independent positive charge, which promoted absorption enhancement of mannitol and FITC dextran with low cell toxicity.[96]

The success of permeation enhancers to increase oral protein bioavailability depends on careful determination of effective but safe concentration ranges. Since permeation enhancers actively interact with the intestinal membrane to modulate tight junctions, it is not surprising that these molecules can be toxic at high concentrations. *In vivo*, appropriate temporal delivery of permeation enhancers is important so that permeation enhancer and protein molecule arrive at the site of absorption at the same time. If buffering or solubility differences exist between the molecules along the GI tract, the permeation enhancer might cause acute toxicity with no increase in therapeutic bioavailability. In addition, the molecular mechanisms of many permeation enhancers are still unknown. In order to most effectively design permeation enhancement drug delivery strategies, these mechanisms must be elucidated.

Chapter 2 : Tailoring Enzyme Activity and Stability using Polymer-Based Protein Engineering

2.1 Introduction

Protein-polymer conjugates have long been used to manipulate the native properties of proteins. Many bioconjugates have been synthesized with poly(ethylene glycol) (PEG), which helps to increase protein stability and the half-life of proteins in circulation in blood [97]. More recently, efforts have been devoted to attaching stimuli responsive polymers that create "smart" bioconjugates [98-100] that add functionality to enzymes. We have become interested in whether the attachment of temperature-responsive polymers to proteins might impart unique properties on the enzyme. Two polymers that show temperature responsiveness are poly(*N*-isopropylacrylamide) (pNIPAm) and poly[*N,N'*-dimethyl(methacryloylethyl) ammonium propane sulfonate] (pDMAPS), though they respond to temperature in sharply distinct ways. pNIPAm exhibits lower critical solution temperature (LCST) behavior [101], where above ~32 °C the polymer experiences a reversible change in conformation, increasing its hydrophobicity and becoming immiscible in water. The same reversible change is seen for pDMAPS, except that the polymer is immiscible below the upper critical solution temperature (UCST). The UCST of pDMAPS has been shown to have strong dependence on polymer chain length and solution ionic strength [102], while the LCST of pNIPAm is less variable [54], but is still affected by several factors, such as degree of chain branching and molecular weight [103]. Changes in polymer structural conformation and solubility can be used as a method to filter proteins during separation processes. Advantageously, responsive behavior of polymers below ambient temperature allow for protein stability to be maintained during separation processes.

Previous studies have described syntheses of pDMAPS and pNIPAm bioconjugates using various proteins [104-106]. However, these studies did not address the effects of the polymer on

enzyme kinetics, stability, and substrate affinity or they utilized the "grafting to" approach. Recently, greater efforts have been applied towards developing aqueous based "grafting from" approaches to limit potential protein denaturation in organic solvents during conjugation. Averick *et al.* [25] described the synthesis of bovine serum albumin-oligo(ethylene oxide) methacrylate (BSA-OEOMA) conjugates in biologically relevant conditions. More recently, we have reported[107] on the synthesis of a novel water-soluble ATRP initiator molecule that was used to synthesize CT-poly(*N*,*N*-dimethylaminoethyl methacrylate) (CT-pDMEAMA) conjugates with pH-dependent enzyme kinetics and stability. This more water soluble initiator enabled high density growth of polymers from proteins that increased the molecular weight of conjugates by more than an order of magnitude.

In the study described herein, chymotrypsin (CT) was chosen as a model protein to modify with polymers that exhibit temperature-dependent changes in conformation. CT is a serine protease enzyme that acts in the small intestine by aiding in digestion. CT degrades itself via autolysis (self-digestion), and the mechanism and kinetics of CT have been studied exhaustively over a wide temperature and pH range [108, 109]. In addition, chymotrypsin has potential applications in detergents, biocatalysts, or as an exogenous enzyme therapy for pancreatic insufficiency.

The goal of the study described herein was to predictably manipulate the kinetics and stability of CT-pDMAPS and CT-pNIPAm bioconjugates using temperature as the trigger for a change in enzyme function. Both pNIPAm and pDMAPS were chosen in order to examine changes in relative enzyme activity and stability at stimuli responsive temperatures both above and below ambient temperature. The contrasting temperature responsive behavior of the UCST

and LCST bioconjugates provided an attractive approach to examine how polymer chain collapse at varying temperatures affects enzyme bioactivity, stability, and substrate affinity.

2.2 Materials and Methods

2.2.1 Materials

α-Chymotrypsin (CT) from bovine pancreas (type II), copper (I) bromide, 1,1,4,7,10,10-Hexamethyltriethylenetetramine (HMTETA) , *N*-succinyl-L-Alanine-L-Alanine-L-Proline-L-Phenylalanine-*p*-nitoroanilide (Suc-AAPF-pNA), [2-(Methacryloyloxy)ethyl]dimethyl-(3-sulfopropyl) ammonium hydroxide) (DMAPS), bicinchoninic acid (BCA) solution, copper (II) sulfate solution, and 4-hydroxy-3,5-cimethoxycinamic acid (sinapinic acid) were purchased from Sigma Aldrich (St Louis, MO) and used without further purification. *N*-isopropylacrylamide was purchased from Sigma Aldrich (St. Louis, MO) and purified by recrystallization using hexane. Me6TREN was synthesized as described previously by Ciampolini and Nardi[110]. Dialysis tubing (molecular weight cut off, 25-, 15- and 1.0-kDa, Spectra/Por®, Spectrum Laboratories Inc., CA) for conjugate isolation were purchased from Fisher Scientific (Pittsburgh, PA).

2.2.2 Measurements

^{1}H-NMR spectra were recorded on a spectrometer (300 MHz, Bruker Avance) in the NMR facility located in Center for Molecular Analysis, Carnegie Mellon University, Pittsburgh, USA) with Deuterium oxide (D_2O). Matrix assisted laser desorption ionization-time of flight mass spectroscopy (MALDI-TOF MS) measurements were recorded using a PerSeptive Voyager STR MS with nitrogen laser (337 nm) and 20 kV accelerating voltage also located at CMA, CMU, Pittsburgh, USA. Sinapinic acid and a gold sample plate were used for all samples. Apomyoglobin, cytochrome C, and aldolase were used as calibration samples. MALDI-TOF MS instrumentation was supported by an NSF grant (CHE-9808188).

2.2.3 Reaction between the ATRP Initiator and Chymotrypsin

Synthesis of the ATRP initiating molecules was carried out as described previously ([107]). Following synthesis, initiator molecule (469 mg, 1.4 mmol) and CT (1.0 g, 0.04 mmol protein, 0.56 mmol -NH_2 group in lysine residues) were dissolved in sodium phosphate buffer (100 mL of 0.1 M at pH 8.0). The solution was stirred at 4 °C for 3 hours, then dialyzed against deionized water, using dialysis tubing with a molecular weight cut off of 15 kDa, for 24 hours at 4 °C and then lyophilized.

2.2.4 Surface Initiated ATRP from CT-Initiator

To synthesize the CT-pDMAPS conjugates, the CT-Initiator complex (50 mg, 0.024 mmol initiator) and DMAPS (335 mg, 1.2 mmol) were dissolved in sodium phosphate buffer (20 mL, pH 6.0). In a separate flask, HMTETA (33 μL, 0.12 mmol) was dissolved in deionized water (10 mL) and bubbled with Argon for 10 min. Cu(I)Br (17 mg, 0.12 mmol) was added to the HMTETA solution and Argon was bubbled for an additional 50 minutes prior to addition of the copper catalyst solution. The solution was then stirred for 18 hr at 4 °C. Lastly, the solution was purified using dialysis tubing with a molecular weight cutoff of 25 kDa for 48 hours against deionized water at 4 °C, and then lyophilized.

For CT-pNIPAM synthesis, CT-Initiator conjugate (50 mg, 0.024 mmol initiator) and NIPAm (271 mg, 2.4 mmol) were dissolved in deionized water (20 mL). In a separate flask, Me6TREN (32 μL, 0.12 mmol) was dissolved in deionized water (10 mL) and bubbled with Argon for 10 min. Cu(I)Br (17 mg, 0.12 mmol) was added to the Me6TREN solution and Argon was bubbled for an additional 10 min. The procedure for CT-pNIPAM synthesis from this point forward was the same as described above for CT-pDMAPS synthesis.

2.2.5 Polymer Cleavage from CT surface

Both pDMAPS and pNIPAm were cleaved from the surface of CT using acid hydrolysis. CT-pDMAPS conjugates were incubated (15 mg/mL) in 6N HCl at 110 °C under vacuum for 24 hours. CT-pNIPAm (20 mg/mL) conjugates were incubated in 4.5N *p*-toluene sulfonic acid at 80 °C under vacuum for 72 hours. Following incubation, samples were isolated from CT using dialysis tubing (MWCo 1K Da) for 48 hours, and then lyophilized. Lastly, polymer molecular weight was determined using GPC.

2.2.6 CT Conjugate MW Determination

For both bicinchonic acid (BCA) and absorption protein assays, wt % of CT in the conjugate was determined by comparison to standard curve. From the wt % value, MW of the CT-polymer conjugate was calculated using the following formulas for CT-pDMAPS and CT-pNIPAm:

$$Mw_{CT\text{-}pDMAPS} = \frac{\frac{wt\ \%\ pDMAPS}{279\ g/mol\ DMAPS}}{\frac{wt\ \%\ CHT}{25500\ g/mol\ CHT}} * 279\ g/mol\ DMAPS + 25500\ g/mol\ CHT$$

$$Mw_{CT\text{-}pNIPAm} = \frac{\frac{wt\ \%\ pNIPAm}{113\ g/mol\ NIPAm}}{\frac{wt\ \%\ CHT}{25500\ g/mol\ CHT}} * 113\ g/mol\ NIPAm + 25500\ g/mol\ CHT$$

2.2.7 BCA Assay

25 μL of sample solution in de-ionized water (1.0 mg/mL) was mixed with 1.0 mL of mixture of bicinchonic acid (BCA) solution and copper (II) sulfate solution (50:1 vol:vol). The sample solution was incubated at 60 ºC for 15 min. Absorbance of the sample at 562 nm was recorded by UV-VIS spectrometer. CT concentration (wt%) of the conjugate was determined by comparison of the absorbance to the standard curve. Standard curves were obtained from

mixtures of native CT and free pDMAPS or pNIPAm, which was prepared as described above, with different concentration ratio in deionized water.

2.2.8 Absorption Assay

1.0 mg/mL of the conjugate solution in 100 mM sodium phosphate buffer (pH 7.0) was prepared and the UV absorbance at 280 nm was recorded by UV-VIS spectrometer. CT concentration (wt%) of the conjugate was determined by comparison of the absorbance to the standard curve. Standard curve was obtained from mixture of native CT and free pDMAPS or pNIPAm, which was prepared separately, with different concentration ratio in 100 mM sodium phosphate buffer (pH 7.0).

2.2.9 Gel Permeation Chromatography

For GPC conjugate MW determination, 12 polymer chains were assumed to be attached for each CT conjugate. M_n values determined by GPC were multiplied by 12 and added to the MW of native CT (25,500 Da) to yield CT-polymer conjugate MW. Number and weight average molecular weights (M_n and M_w) and the polydispersity index (M_w / M_n) were estimated by gel permeation chromatography (GPC). For pDMAPS, analysis was conducted on a Water 2695 Series with a data processor, using 80 % 100mM sodium phosphate buffer(pH=9.0)/20 % Acetonitrile with 0.01 volume % NaN_3 as an eluent at a flow rate 1 mL/min, with detection by a refractive index (RI) detector. Polystyrene sulfonate standards were used for calibration. For pNIPAm, analysis was conducted using dimethylformamide (DMF) with 50 mM LiBr at a flow rate of 1 mL/min and 50 °C, with detection by an RI detector. Poly(ethylene oxide) standards were used for calibration and diphenylethylene was used as a flow marker.

2.2.10 Cloud Point Curves for CT Conjugates

CT-pDMAPS and CT-pNIPAm (2-3 mg polymer/mL each) were dissolved in 0.1 M phosphate buffer (pH 8.0). CT-pNIPAm samples were heated from 20 to 35 °C and CT-pDMAPS samples were cooled from 30 to 5 °C at ±1 °C/min. The absorbance at 490 nm was measured and LCST/UCST temperature was calculated from the inflection point on the temperature versus absorbance curves.

2.2.11 Dynamic Light Scattering

CT-pDMAPS (3 mg/mL) and CT-pNIPAm (0.5 mg/mL) samples were dissolved in 0.1 M phosphate buffer (pH 8.0) and then filtered using a 0.45 μM cellulose filter. A Malvern Zetasizer nano-ZS was used to measure hydrodynamic diameter (D_h). Each sample was measured in triplicate or greater at each specified temperature.

2.2.12 CT and CT conjugate Biocatalytic Activity

N-succinyl-Ala-Ala-Pro-Phe p-nitroanilide was used as a substrate for enzyme bioactivity assays. In a 1 mL cuvette, 0.1M sodium phosphate buffer (810-990 μL, pH 8.0, incubated at 25 °C), substrate (0-180 μL, 6 mg/mL in DMSO (0-1.2 x 10^{-3} M)), and enzyme (10 μL, 0.1 mg enzyme/mL 0.1 M pH 8.0 sodium phosphate buffer (4 x 10^{-8} M)) were mixed. The rate of the hydrolysis was determined by recording the increase in absorbance at 412 nm for the first 30 seconds after mixing. K_M and k_{cat} values were calculated using EnzFitter software when plotting substrate concentration versus initial rate.

2.2.13 Enzyme Stability

Native CT and CT-conjugates (1 mg enzyme/mL) were dissolved in 0.1 M sodium phosphate buffer (pH 8.0) and incubated in a water bath at either 25 °C or 40 °C. At various time

points, aliquots were removed and diluted to 0.1 mg enzyme/mL using 0.1 M phosphate buffer (pH 8.0). Residual activity was calculated as the percentage of activity remaining relative to the activity at time zero. Substrate (Suc-AAPF-pNA) concentration was kept constant at 288 μM for each sample and time point.

2.2.14 Cycling of CT Conjugates Above and Below UCST and LCST

Both CT-pDMAPS and CT-pNIPAm conjugates were cycled in and out of their immiscible phases by temperature manipulation. Both conjugate and native CT samples (1 mg enzyme/mL) were dissolved in 0.1 M phosphate buffer (pH=8.0). For CT-pDMAPS, one cycle was defined as incubating conjugate sample at 4 °C (on ice) for 10 minutes, followed by incubation at room temperature for 10 minutes, then 50 μL of sample was removed for residual activity assay. For CT-pNIPAm one cycle was defined as incubation at 33 °C in water bath for 10 minutes, followed by incubation at room temperature for 10 minutes, then 50 μL of sample was removed for residual activity assay. For each sample, visual inspection (turbidity of solution) was used to confirm changing of immiscible/miscible CT-conjugate phases above and below responsive temperatures. 50 μL aliquots removed from incubated samples were diluted with 450 μL 0.1 M phosphate buffer (pH=8.0) to yield 0.1 mg/mL samples for activity assay. Residual activity assay was done at 25 °C with 288 μM substrate (*N*-succinyl-Ala-Ala-Pro-Phe-p-nitroanilide) for each sample. Residual activity was calculated as: initial rate for each sample after cycle "x"/initial rate for each sample before cycle one. Native CT controls were separate for each conjugate as the cycling conditions were different for the two conjugates.

2.3 Results and Discussion

2.3.1 Reaction Between the ATRP initiator and Chymotrypsin

In order to generate highly modified enzyme-polymer conjugates, we have designed and synthesized a water-soluble protein-reactive ATRP initiator[107]. To determine the efficiency of reaction between the enzyme (chymotrypsin) and the initiator we measured the increase in molecular weight using MALDI-TOF-MS (**Figure 2.1d**). On average, 12 ATRP initiating moieties were attached to each CT molecule, through the reaction of an NHS-ester on the initiator molecule with primary amine groups, either on surface accessible lysine residues or the *N*-terminus. Consequently, for each CT molecule there were 12 different sites from which polymer chains could be grown. Following conjugate synthesis (**Figure 2.2**), acid hydrolysis was used to cleave both pDMAPS and pNIPAm from the surface of CT molecules for polymer molecular weight determination.

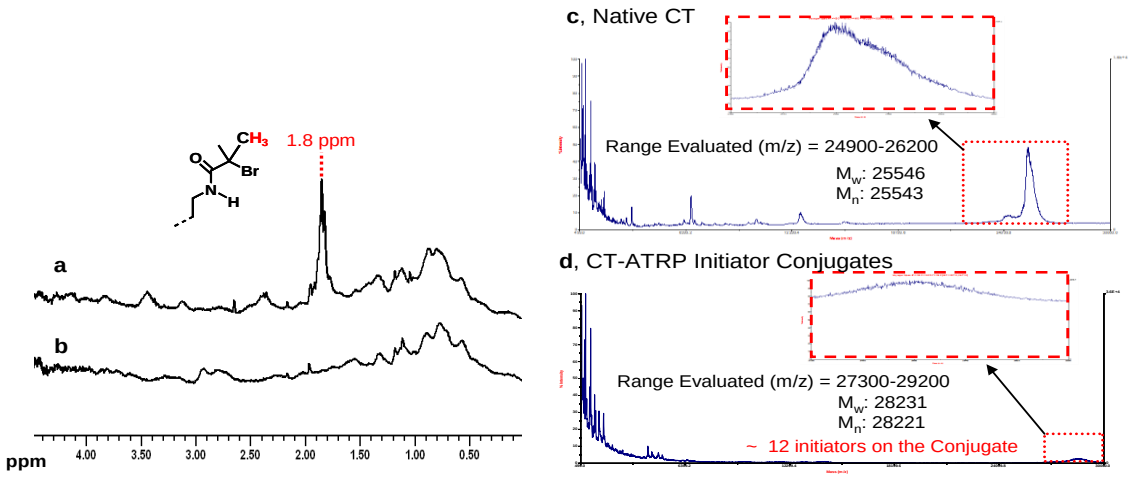

Figure 2.1 ^{1}H NMR and MALDI TOF MS spectra of native CT and CT-ATRP initiator conjugate. (**a**) ^{1}H NMR of CT Initiator conjugate in D_2O, (**b**) native CT in D_2O, (**c**) MALDI-TOF-MS spectrum of native CT, and (**d**) CT Initiator MALDI-TOF MS spectrum.

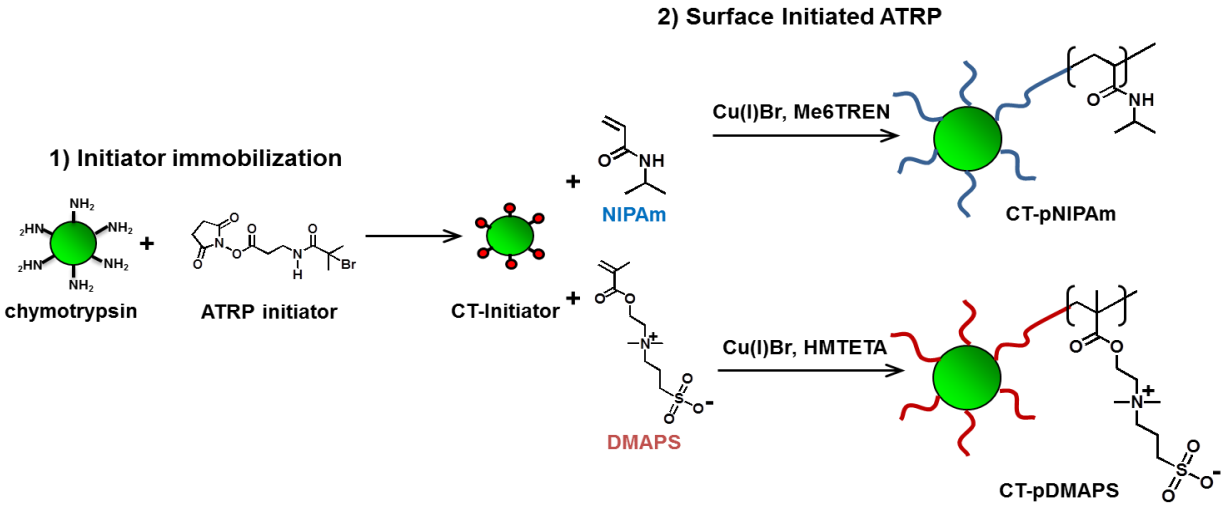

Figure 2.2 Schematic representation of polymer-based protein engineering used in this study. (1) Initiator immobilization onto CT surface and (2) "grafting from" ATRP reaction to produce CT-pDMAPS and CT-pNIPAm conjugates.

Subsequent GPC analysis yielded number average molecular weight values (M_n) of 10.3 kDa for pDMAPS and 9.2 kD for pNIPAm. From these M_n values, conjugate molecular weights were calculated to be 148 kDa for CT-pDMAPS and 135 kDa for CT-pNIPAm (Table 2.1). Now that we had ensured that chymotrypsin could be modified through the high density attachment of thermo-responsive grown-from polymers, we were in a position to explore the temperature dependence of bioconjugate structure and function.

Table 2.1: CT bioconjugate molar mass characterization

	Cleaved Polymer			CT Conjugate MW		
Sample	M_n	PDI (M_w/M_n)	Degree of Polymerization	BCA	Absorption	GPC
CT-pDMAPS	10259 Da	1.51	37	117 kDa	119 kDa	148 kDa
CT-pNIPAm	9151 Da	1.71	82	166 kDa	171 kDa	135 kDa

Molar mass of the conjugates was determined by cleaving the polymer from the surface of the enzyme using acid hydrolysis and then estimating molecular weight using GPC. Molar mass of the conjugates was also estimated using BCA assay and protein absorption assay as described in the methods section.

2.3.2 Physical Properties of CT-pDMAPS and CT-pNIPAM conjugates

We first sought to determine the lower critical solution temperature (LCST) and upper critical solution temperature (UCST) behavior of the free polymers and CT bioconjugates. The polymer component of the bioconjugates clearly responded to changes in temperature in the same manner as the free polymer (**Figure 2.3**).

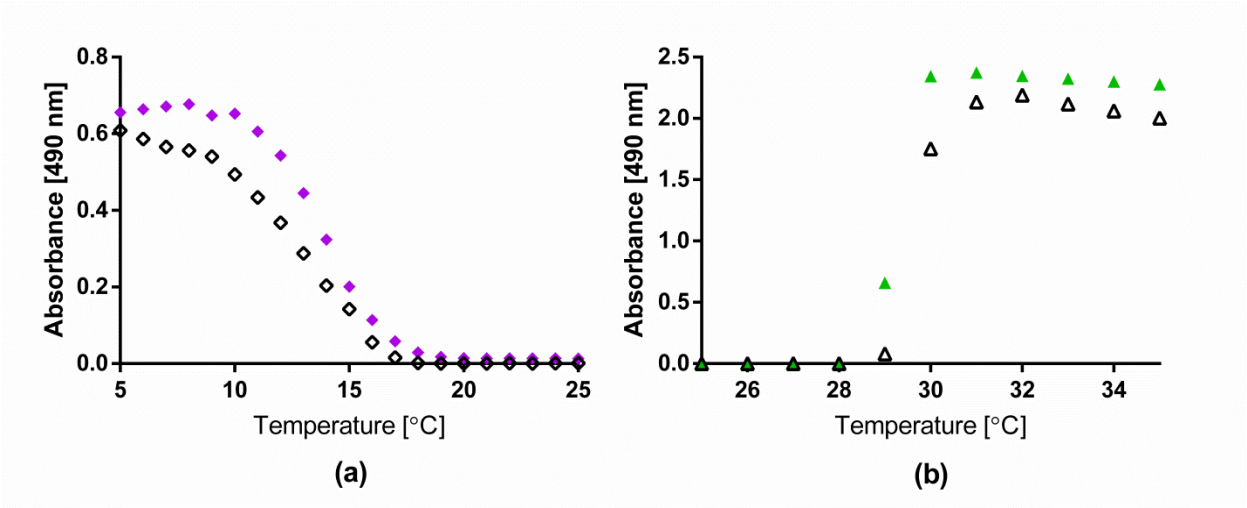

Figure 2.3 Cloud point curves for CT-pDMAPS and CT-pNIPAm conjugates and free polymer. Curve (a) corresponds to CT-pDMAPS (purple diamond) and free pDMAPS (open diamond) polymer (8100 Da). Curve (b) shows behavior for CT-pNIPAm (green triangle) and free pNIPAM (open triangle) polymer (9500 Da). Concentrations for each sample were 2-3 mg/mL with 0.1 M phosphate buffer (pH 8.0) as solvent. Absorbance at 490 nm was recorded as the samples were heated at 1 °C/min. The reported UCST and LCST cloud point temperatures were taken from the point of inflection on these cloud point curves.

For CT-pDMAPS, the UCST cloud point was 13 °C which compares well with the UCST cloud point for free pDMAPS polymer (12 °C). The LCST cloud point for the polymer component of CT-pNIPAm (~29.5 °C) was only slightly lower than the LCST cloud point for free pNIPAm (30 °C). LCST and UCST transitions for the free polymer are representative of polymer chain collapse, but the thermodynamics governing these behaviors are not the same[54].

Phase transition during LCST is an entropy driven process [101], while UCST events are generally governed by changes in enthalpy [54]. For each of the conjugates, the change from extended polymer to collapsed polymer occurred slightly more rapidly than for free polymer (note the difference in slope). It is possible that the protein-polymer interface was influencing the thermo-responsive behavior. Above a polymer's LCST, the polymer chains collapse and become insoluble in aqueous media, pushing water molecules to the outside of a newly formed hydrophobic polymer shell. This behavior is reversible; thus, as the sample is cooled back to a temperature below the LCST, the polymer chains rearrange, and are once again soluble in aqueous media. For a polymer that exhibits UCST behavior, the polymer chains are extended and water soluble above the UCST, and collapsed/insoluble below the UCST temperature in aqueous media. When translating this temperature sensitive behavior from free polymer to enzyme-polymer conjugates, we hypothesized that two different polymer conformations would be likely when temperature was varied above or below LCST/UCST temperature. Both above the LCST and below the UCST, the bioconjugates should have a collapsed, insoluble behavior. When below LCST and above UCST, an extended polymer component of the bioconjugate, with higher water solubility compared to the collapsed state, should be in existence.

We determined the cloud point curves for the bioconjugates and showed that there was phase separation and insolubility at the specific UCST and LCST temperatures for each of the CT-polymer conjugates. We therefore proceeded to examine the impact of temperature on bioconjugate size. The hydrodynamic diameter (D_h) for CT-pDMAPS and CT-pNIPAm conjugates, measured by dynamic light scattering (DLS) at temperatures of interest near the LCST and UCST, was temperature-dependent (**Figure 2.4**).

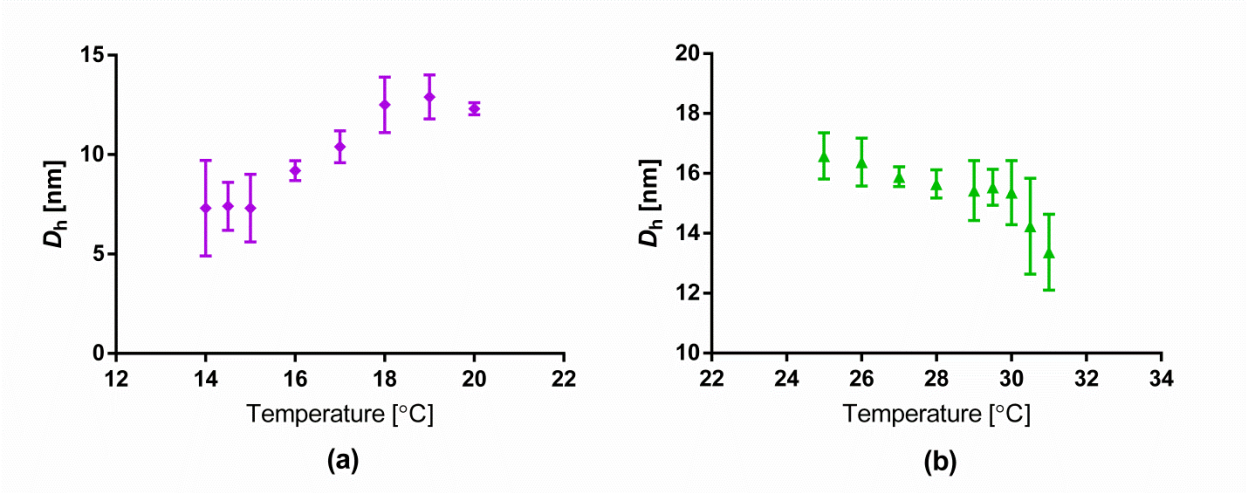

Figure 2.4 Temperature dependence of CT-conjugate hydrodynamic diameter (D_h). Number average D_h for (a) CT-pDMAPS conjugate (3 mg/mL) and (b) CT-pNIPAm conjugate (0.5 mg/mL).

As expected, owing to the longer polymer chain (Table 2.1), CT-pNIPAm conjugates had a larger extended state D_h of ~ 16 nm compared with ~13 nm for CT-pDMAPS. The hydrodynamic diameter decreased above the LCST for CT-pNIPAm and below the UCST for CT-pDMAPS as the polymers collapsed and became less hydrated. We hypothesized that as the polymers collapsed, they more fully covered the surface area of the protein rather than extending outward. The specific phase separation behavior for each conjugate exhibited in the cloud point curves was conserved in the D_h measurements. CT-pDMAPS UCST transition encompassed a larger temperature range when compared with CT-pNIPAm LCST transition. For CT-pDMAPS, a gradual decrease in D_h was seen from 18-15 °C, until D_h plateaued at ~7.5 nm around 15 °C. In comparison, CT-pNIPAm conjugates showed a more rapid phase transition with the D_h quickly decreasing from 30-31 °C. The quick formation of hydrophobic aggregates (high D_h) for each CT-polymer conjugate at extreme temperatures prevented the examination of the D_h at

temperatures further away from the UCST and LCST. We next completed an exhaustive analysis of the chymotrypsin bioconjugate activity and specificity as a function of temperature.

2.3.3 Bioconjugate Activity

Overall enzyme activity was retained during cycling of CT-pNIPAm and CT-pDMAPS conjugates above and below their respective LCST and UCST temperatures (**Figure 2.5**). As the polymers in the conjugate switched between a collapsed and extended state, no large decrease in conjugate residual activity was observed.

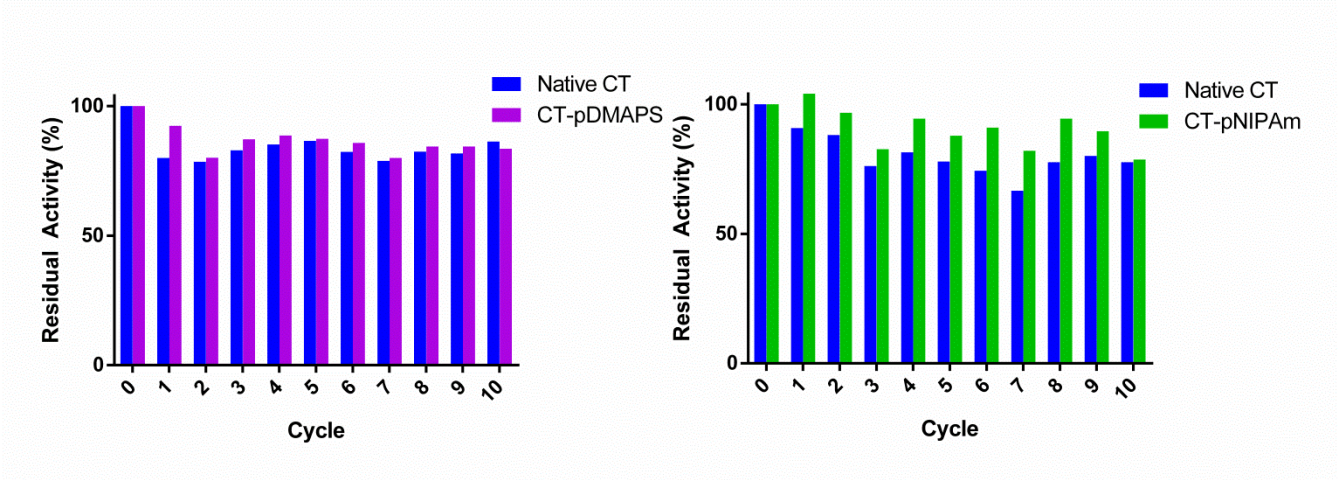

Figure 2.5 CT conjugates maintain activity after cycling above or below responsive temperatures. (a) CT-pDMAPS conjugates and (b) CT-pNIPAm conjugates over 10 UCST or LCST cycles. Cycling temperature for CT-pNIPAm was 33 °C and cycling temperature for CT-pDMAPS was 4°C.

The kinetic constants (k_{cat}, K_M, and k_{cat}/K_M) were determined at three different temperatures (5 °C, 25 °C, and 40 °C) for each of the conjugates and native CT, using Suc-AAPF-pNA as the model substrate. These temperatures were chosen so as to observe enzyme function above and below the measured UCST and LCST cloud points.

At 25 °C, both CT-pDMAPS and CT-pNIPAm polymers were in their polymer chain extended state. CT-pDMAPS conjugates showed similar k_{cat}/K_M values to native CT, while CT-

pNIPAm conjugates showed slightly lower k_{cat}/K_M values (**Table 2.2**). In addition, CT-Initiator conjugates showed increased k_{cat}/K_M values at each temperature. The ATRP initiator molecule was covalently coupled to the CT surface through the amine side group on lysine residues. Due to this attachment technique, CT surface charge was modified after initiator immobilization, and this modification could be responsible for the increase in bioactivity seen for the CT-Initiator conjugate at all three temperatures.

Table 2.2 Temperature dependence of chymotrypsin and bioconjugate activity, specificity and productivity for the hydrolysis of Suc-AAPF-pNA.

Sample	V_{max} [μM/sec]	K_M [μM]	k_{cat} [sec^{-1}]	k_{cat}/K_M [sec^{-1}/μM]	$(K_M)_x$ $(K_M)_{CT}$	$(k_{cat})_x$ $(k_{cat})_{CT}$	$(k_{cat}/K_M)_x$ $(k_{cat}/K_M)_{CT}$
5 °C							
Native CT	0.37 ± 0.03	70 ± 18	9.3 ± 0.68	0.13 ± 0.04	-	-	-
CT Initiator	0.34 ± 0.02	49 ± 14	8.6 ± 0.59	0.18 ± 0.05	0.69	0.92	1.33
CT-pDMAPS	0.27 ± 0.02	65 ± 17	6.8 ± 0.49	0.11 ± 0.03	0.93	0.73	0.79
CT-pNIPAm	0.26 ± 0.01	64 ± 13	6.6 ± 0.36	0.10 ± 0.02	0.92	0.70	0.77
25 °C							
Native CT	1.1 ± 0.05	75.2 ± 12.6	27 ± 1.3	0.36 ± 0.06	-	-	-
CT Initiator	1.1 ± 0.05	52.1 ± 8.99	29 ± 1.2	0.55 ± 0.10	0.69	1.04	1.50
CT-pDMAPS	0.82 ± 0.03	52.1 ± 7.13	21 ± 0.69	0.39 ± 0.06	0.69	0.75	1.08
CT-pNIPAm	0.87 ± 0.01	111 ± 5.16	22 ± 1.4	0.19 ± 0.02	1.48	0.79	0.53
40 °C							
Native CT	1.7 ± 0.05	87 ± 8.2	43 ± 1.2	0.49 ± 0.05	-	-	-
CT Initiator	2.0 ± 0.05	74 ± 6.5	50 ± 1.2	0.68 ± 0.06	0.84	1.16	1.38
CT-pDMAPS	1.3 ± 0.04	69 ± 7.6	33 ± 0.99	0.47 ± 0.05	0.79	0.76	0.96
CT-pNIPAm	0.6 ± 0.06	230 ± 53	14 ± 1.4	0.06 ± 0.01	2.70	0.32	0.12

Michaelis-Menten kinetic parameters were calculated at 5 °C, 25 °C, and 40 °C for native CT, CT-I, and each of the CT-polymer conjugates. K_M and V_{max} were calculated using EnzFitter software. k_{cat} was calculated by dividing V_{max} by the initial enzyme concentration.

We observed several interesting trends when closely examining the temperature dependence of k_{cat} and K_M for the CT-pDMAPS and CT-pNIPAm conjugates. For each temperature, the relative k_{cat} ratio for CT-pDMAPS stayed constant at ~0.75. At all three

temperatures, for CT-pDMAPS conjugates, K_M was lower when compared with native CT, meaning there was higher substrate affinity with the CT-pDMAPS conjugate than native CT. It has been hypothesized that reduced K_M values for CT-zwitterionic polymer conjugates resulted from the interaction of the model substrate with zwitterionic polymer [43]. Taking a similar approach we hypothesized that the model hydrophobic substrate for CT used in this study interacted with the hydrophilic pDMAPS polymer surrounding CT, increasing the local concentration of the substrate near the hydrophobic substrate binding pocket, thereby lowering K_M for CT-pDMAPS. As shown in the relative K_M values, this higher affinity was seen at each temperature, but was reduced, perhaps by the collapsed nature of pDMAPS, below the UCST. At 5 °C, the relative K_M value for CT-pDMAPS was higher when compared to relative K_M values at 25 °C and 40 °C. At temperatures below the UCST of CT-pDMAPS (13 °C), the polymer was in its collapsed state. It is not unreasonable to presume that once pDMAPS was in a collapsed state it would have restricted the access of the substrate to the active site via steric hindrance.

At 40 °C, a sharp decrease in CT-pNIPAm bioactivity was seen with a relative k_{cat}/K_M value of 0.12. At this temperature pNIPAm was in its collapsed, hydrophobic state, and K_M likely increased due to steric hindrance. In addition, since pNIPAm is more hydrophobic than pDMAPS, pNIPAM would have a stronger association with the hydrophobic model substrate. It was likely, then, that the long and dense pNIPAm molecules could partition the substrate in the polymer phase, thereby increasing K_M. The interaction of pNIPAm with the substrate, which was indicated by the increase in K_M at 25 °C, was also exhibited at other temperatures. For CT-pNIPAm conjugates, relative k_{cat} values were similar at both 5 °C and 25 °C, and only slightly lower than native CT. At 40 °C, the first order rate constant (k_{cat}) was much lower for CT-pNIPAm conjugates when compared to native CT, and we hypothesized that k_{cat} decreased

because of a decrease in water availability at the active site. CT catalyzes peptide bond hydrolysis through a charge stabilizing amino acid triad, and consequently, water is needed for the reaction to occur. As pNIPAm polymer chains surrounding CT collapse above the LCST, the polymer would be expected to alter the mobility of enzyme bound water molecules. Changes in water mobility at the CT-pNIPAm active site above pNIPAm LCST would be observed in a reduced k_{cat}, as observed. We surmised that these two factors caused a lower bioactivity for CT-pNIPAm conjugates at 40 °C. Next we assessed the impact of the polymer-based protein engineering on enzyme stability.

2.3.4 Polymer-Based Protein Engineering of Enzyme Stability

A first order inactivation model was used to examine the irreversible thermal inactivation of native CT and the bioconjugates at both 25 °C and 40 °C [111]. At both 25 °C and 40 °C the CT-pNIPAm and CT-pDMAPS conjugates showed dramatically enhanced stability compared to native CT and initiator modified CT (**Figure 2.6**).

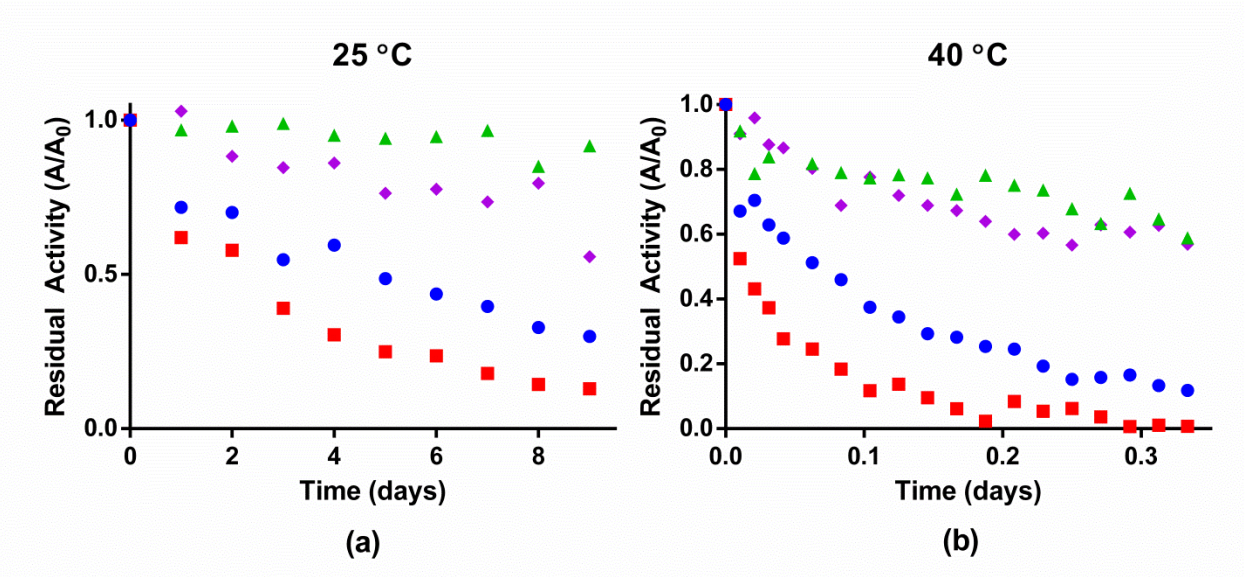

Figure 2.6 Irreversible thermal inactivation of chymotrypsin. Native CT (blue circle), CT-Br (red square), CT-pNIPAm (green triangle), and CT-pDMAPS (purple diamond) at (a) 25 °C and (b) 40 °C. Residual activity was determined relative to the activity at time zero for each conjugate.

While CT-conjugate stability was higher at both temperatures, the deactivation mechanisms at these temperatures are likely to differ. At 25 °C, CT inactivation is due mostly to autolysis [112] whereas at 40 °C both protein structure denaturation and autolysis contribute to the irreversible inactivation of CT. In addition, the stabilization mechanisms for pNIPAm and pDMAPS were likely different. We expected that pNIPAm would dampen the structural dynamics of CT thereby preventing structural unfolding in a manner similar to that observed after protein PEGylation [113, 114]. In contrast, pDMAPS likely formed charge interactions between the polymer and protein given its zwitterionic structure thereby stabilizing the protein[113]. While different, both mechanisms dramatically increased stability of CT-polymer conjugates at both 25 °C and 40 °C (Table 2.3). The half-lives of the bioconjugates were orders of magnitude greater than the native chymotrypsin. In addition to higher general conjugate

stability than native CT stability, at both experimental temperatures (25 °C and 40 °C), the stability of CT-pNIPAm conjugates was higher compared to CT-pDMAPS conjugates. At 25 °C, both CT-pNIPAm and CT-pDMAPS polymers were in their extended state. We attributed the higher stability of CT-pNIPAm to the lower activity values seen in **Table 2.2**. Since autolysis was the main contributor to CT denaturation at 25 °C, the lower activity values seen as this temperature corresponded to a higher stability. At 40 °C, CT-pNIPAm was in its collapsed state, which likely caused a decrease in autolysis by blocking CT molecules access to the active site. At 40 °C, CT-pDMAPS was in its extended state, and still provided increased stability compared to native CT through steric hindrances and structural stabilization, but to a lower degree than CT-pNIPAm conjugates.

Table 2.3: Temperature dependence of first order inactivation rate constants and half - lives for chymotrypsin and polymer-based protein engineered chymotrypsin.

Sample	25 °C		40 °C	
	k_{inact} (days^{-1})	$t_{1/2}$ (days)	k_{inact} (days^{-1})	$t_{1/2}$ (days)
Native CT	$0.13 \pm 1.2 \times 10^{-2}$	5.4 ± 0.51	6.6 ± 0.47	$0.10 \pm 7.5 \times 10^{-3}$
CT-Initiator	$0.26 \pm 2.0 \times 10^{-2}$	2.7 ± 0.21	24 ± 3.1	$0.03 \pm 3.8 \times 10^{-3}$
CT-pDMAPS	$0.05 \pm 8.3 \times 10^{-3}$	14 ± 2.4	1.7 ± 0.16	$0.41 \pm 3.9 \times 10^{-2}$
CT-pNIPAm	$0.01 \pm 3.4 \times 10^{-3}$	61 ± 19	1.0 ± 0.14	$0.66 \pm 8.8 \times 10^{-2}$

Stabilities of native CT and CT conjugates were determined by incubating 1 mg enzyme/mL. The inactivation constants (k_{inact}) and half-lives ($t_{1/2}$) were calculated by fitting a first order decay to the data.

2.4 Conclusion

We used polymer-based protein engineering to predictably alter the temperature dependence of relative enzyme activity, stability, and substrate affinity. LCST behavior in pNIPAm and UCST behavior in pDMAPS polymers were conserved in the enzyme-polymer bioconjugates grown from the surface of chymotrypsin. In addition, enzyme bioactivity was conserved when activity assays were conducted at temperatures where the conjugates were in

both their extended and collapsed states. Interactions between the model substrate and the polymer surrounding the protein core influenced changes in relative substrate affinity (K_M), although pDMAPS and pNIPAM showed opposing behavior (**Figure 2.7**). Relative substrate affinity was increased in CT-pDMAPS conjugates (lower K_M), but decreased (higher K_M) in CT-pNIPAm conjugates. When above the LCST and below the UCST (polymer collapsed state), relative activity of the conjugates was maintained, though slightly reduced, while increasing CT stability to autolysis and denaturation. CT conjugate stability was also higher compared to native CT at 25 °C, where the polymer was in its extended conformation. In summary, we showed that our water-soluble protein-reactive ATRP initiator could be used as the foundation of a polymer-based protein engineering strategy designed to tailor the temperature dependence of enzyme stability, activity and specificity. We are now exploring the utility of rational polymer-based protein engineering as an alternative to molecular biology dependent protein design.

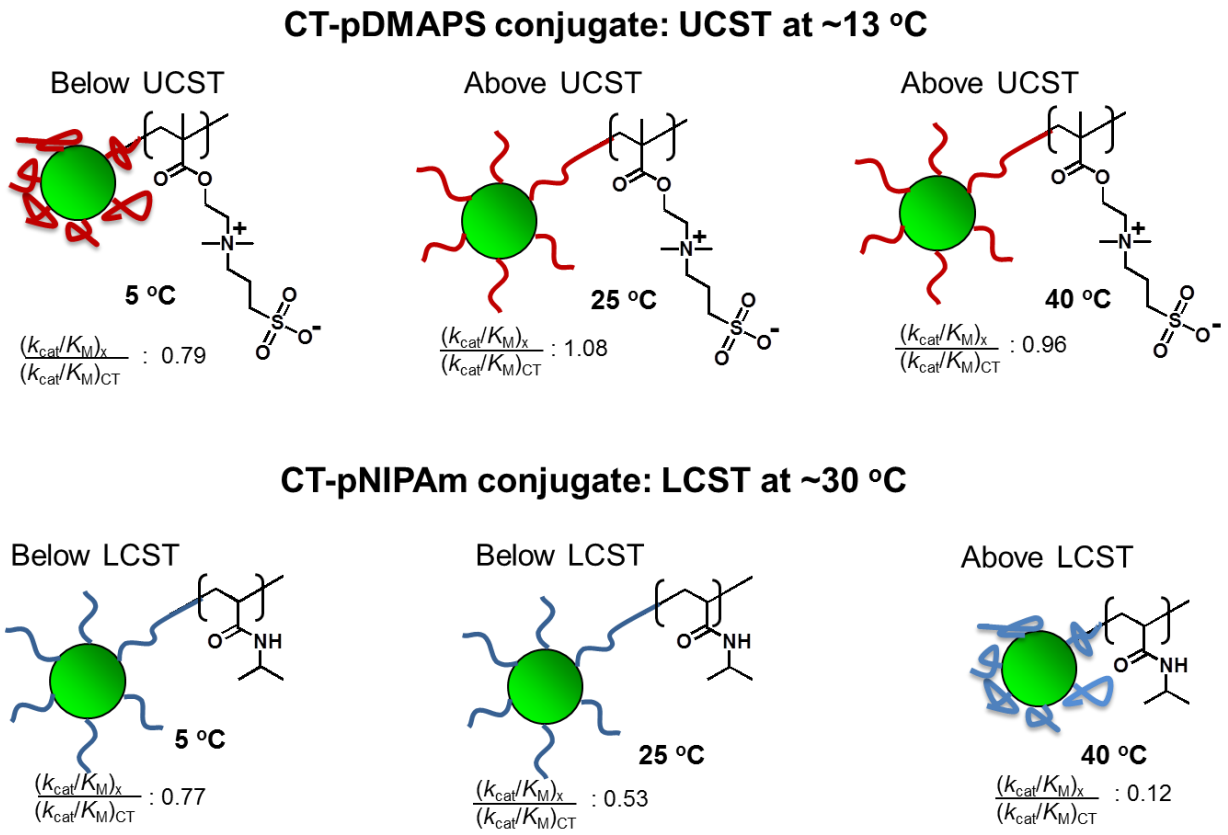

Figure 2.7 Schematic of bioconjugate conformation and its impact on k_{cat}/K_M as a function of temperature. At 5 °C, the polymer component of CT-pDMAPS was in a collapsed, hydrophobic state. At 40 °C, the polymer component of CT-pNIPAm was also collapsed and hydrophobic. At 25 °C, both CT-pDMAPS and CT-pNIPAm polymers were in their extended and hydrophilic state. Polymer length and density not drawn to scale, simplified for clarity.

Chapter 3 : Dramatically Increased pH and Temperature Stability of Chymotrypsin using Dual Block Polymer-Based Protein Engineering

3.1 Introduction

Techniques to synthesize protein-polymer conjugates have developed rapidly in recent years due to advancements in both protein and polymer science. One of the first, and still most common polymers to attach to proteins is poly(ethylene glycol) (PEG),[36] which imparts stealth properties on the protein by reducing immunogenicity and increases *in vivo* stability by slowing renal clearance and degradation. However, this polymer does not add specific functionality to the protein and often results in reduced activity.[97] More recently, different polymers have been utilized to synthesize "smart conjugates"[115] that respond to external stimuli such as pH[116-118] or temperature[119]. In addition, specific polymer choices for tailored applications, such as increased substrate affinity[43], enhanced activity in the GI tract[120], or higher activity at non-native pH[121], are becoming more common as knowledge about polymer and protein interactions progresses. Polymer-based protein engineering refers to these tailored polymer conjugation applications that target problems that previously could only potentially be solved with molecular biology-dependent techniques.

Poly(sulfobetaine methacrylamide) (pSBAm) and poly(*N*-isopropylacrylamide) (pNIPAm) are two polymers that have been investigated for a wide range of chemical and biological applications. Specifically, pNIPAm is used in applications for cardiac repair[122], protein drug release[52], and biomolecule separations[123]. pSBAm is used frequently for non-fouling surface modification[124, 125]. Both pSBAm and pNIPAm respond to changes in temperature by predictable alterations in polymer folding. pNIPAm has a lower critical solution temperature (LCST), where above ~32 °C in deionized water the polymer experiences a reversible collapse, in which it becomes hydrophobic and dehydrated[101]. pSBAm exhibits a

similar, but opposite behavior known as upper critical solution temperature (UCST) phase transition. pSBAm UCST values are more dependent on molecular weight than the LCST of pNIPAm, but below a given temperature polymer chains collapse from a coil to globule orientation as they phase separate and become insoluble in aqueous media[102]. Free block copolymers with both UCST and LCST properties have been reported previously[126, 127], but protein-polymer conjugates are most often only synthesized with single temperature responsiveness imparted by homopolymer conjugation[128, 129]. While block copolymers are sometimes conjugated to proteins with the "grafting to" approach, there are few reports of block copolymers being grown from proteins using "grafting from." Previously, Sumerlin and coworkers used "grafting from" to synthesize a block copolymer using two consecutive RAFT polymerizations from lysozyme[130] and bovine serum albumin[131]. Kulkarni *et al.* synthesized a block copolymer with modified temperature sensitivity, but used the "grafting to" process for protein conjugation[132].

Herein, we describe the "grafting from" synthesis of a block copolymer incorporating temperature sensitive polymers pSBAm and pNIPAm using two consecutive ATRP reactions from the surface of chymotrypsin (CT). CT is a serine protease that acts in the small intestine, and was selected in this study due to the large amount of information available on enzyme activity and stability at a wide range of pH and temperature.[108, 133] In addition, chymotrypsin based protein-polymer conjugates could be used to treat exocrine pancreatic insufficiency, but the enzyme would have to first survive passage through the stomach and into the small intestine. Previously, β-galactosidase[134] (for lactose intolerance) and proline specific endopeptidases[120] (for coeliac disease) have been modified with polymers to stabilize proteins with varying success. These reports suggest that the polymer choice is crucial in predicting

efficacy of polymer conjugation for stabilization in the GI tract. It is expected that the results seen in this study are applicable towards chymotrypsin as well as almost all other enzymes; the only requirement for this process being accessible surface lysines to couple the initiator molecule. pSBAm and pNIPAm were chosen to study the effect of phase transitions at both high and low temperature on CT bioactivity. The LCST temperature of pNIPAm is between room temperature and body temperature. Thus, it is a good candidate to incorporate into materials that need to be synthesized in aqueous solution at room temperature, but then change behavior once in the body, such as an enzyme targeted to fat tissue where it would likely need to be hydrophobic. Attaching a UCST polymer to an enzyme can potentially increase stability at low temperature, and increase long term storage time before use. A protein-polymer conjugate incorporating both of these polymers, which is described herein, could serve both purposes. In addition, the unique geometry of both UCST and LCST containing polymers in the same chain allowed for the examination of the interaction between each polymer block and CT at different phase transition temperatures. Stimuli responsive protein-polymer conjugates that respond to one stimulus often show slightly different behavior than free polymer because of interactions with or shielding by the protein. We hypothesized that temperature responsive properties could be altered by the enzyme as well as another polymer block that doesn't respond to stimuli (similar to PNIPAAm-b-PAA[132]) or that responds to a different stimulus. Thus, we designed a chymotrypsin protein-polymer conjugate to easily examine this hypothesis as well as the effect of polymer conjugation of enzyme bioactivity at multiple stimuli (high and low temperature).

3.2 Materials and Methods

3.2.1 Materials

α-Chymotrypsin (CT) from bovine pancreas (type II), pepsin from porcine stomach mucosa, copper (I) chloride, *p*-toluene sulfonic acid, 1,1,4,7,10,10-Hexamethyltriethylenetetramine (HMTETA) , *N*-succinyl-L-Alanine-L-Alanine-L-Proline-L-Phenylalanine-*p*-nitroanilide (Suc-AAPF-*p*NA), and [2-(Methacryloylamino)ethyl]dimethyl-(3-sulfopropyl) ammonium hydroxide) (sulfobetaine methacrylamide), were purchased from Sigma Aldrich (St Louis, MO) and used without further purification. *N*-isopropylacrylamide was purchased from Sigma Aldrich (St. Louis, MO) and purified by recrystallization using hexane. Me6TREN was synthesized as described previously by Ciampolini and Nardi[110]. Dialysis tubing (molecular weight cut off, 25-, 15- and 1.0-kDa, Spectra/Por®, Spectrum Laboratories Inc., CA) for conjugate isolation was purchased from Fisher Scientific (Pittsburgh, PA).

3.2.2 Reaction Between the ATRP Initiator and Chymotrypsin

Synthesis of the ATRP initiating molecules was carried out as described in Supplementary Information (Scheme 1). Following synthesis, initiator molecule (194 mg, 0.7 mmol) and CT (500 mg, 0.02 mmol protein, 0.32 mmol primary amine) were dissolved in 0.1 M sodium phosphate buffer (pH 8.0). The solution was stirred at 4 °C for 4 hours, and then dialyzed against deionized water, using dialysis tubing with a molecular weight cut off of 15 kDa, for 24 hours at 4 °C and then lyophilized.

3.2.3 Surface Initiated ATRP from CT-Cl

To synthesize CT-pSBAm-*block*-pNIPAm conjugates, first the CT-Cl initiator complex (50 mg, 0.029 mmol initiator) and SBAm [335 mg(1.2 mmol), 525 mg (1.8 mmol), 701 mg(2.4 mmol)] were dissolved in 0.1 M sodium phosphate buffer (20 mL, pH 6.0) with 35 mg NaCl (30

mM). In a separate flask, Me6TREN (33 µL, 0.12 mmol) was dissolved in deionized water (5 mL) and bubbled with argon for 10 min. Cu(I)Cl (17 mg, 0.12 mmol) was added to the Me6TREN solution and Argon was bubbled for an additional 50 minutes prior to addition of the copper catalyst solution to the monomer solution. After combining the two solutions, the reaction mixture was stirred for 5 h at 25 °C until the reaction was stopped by exposing the solution to air. Lastly, the solution was purified using dialysis tubing with a molecular weight cutoff (MwCO) of 25 kDa for 48 hours against deionized water at 4 °C and then lyophilized.

Following initial synthesis of CT-pSBAm conjugates of different chain lengths, pNIPAm was grown from CT-pSBAm using chain extension to yield CT-pSBAm-*block*-pNIPAm conjugates. CT-pSBAm conjugates [200 mg of CT-35 (0.02 mmol initiator), 280 mg of CT-50 (0.02 mmol initiator), 350 mg of CT-90 (0.01 mmol initiator)] and NIPAm [108 mg (0.96 mmol), 163 mg (1.44 mmol), 135 mg (1.2 mmol)] were dissolved in 0.1 M sodium phosphate buffer (20 mL, pH 6.0) with 35 mg NaCl (30 mM) and bubbled with argon. In a separate flask Me6TREN [10.7 µL (0.05 mmol), 10.7 µL (0.05 mmol), 6.4 µL (0.03 mmol)] was dissolved in deionized water (5 mL) and bubbled with Argon for 10 min. Cu(I)Cl (4 mg (0.04 mmol), 4 mg (0.04 mmol), 2.4 mg (0.03 mmol)) was added to the Me6TREN solution and argon was bubbled for an additional 50 minutes. The Me6TREN/CuCl solution was quickly transferred to the CT-pSBAm/NIPAm solution and reaction was allowed to proceed for 5 h at 25 °C. The reaction was stopped by quenching with air and the reaction mixture was purified using dialysis tubing with MwCO 25 kDa for 48 h against deionized water at 4 °C, and then lyophilized.

3.2.4 Polymer Cleavage from CT Surface

Both pSBAm and pSBAm-*block*-pNIPAm were cleaved from the surface of CT-polymer conjugates using acid hydrolysis. CT-pSBAm conjugates were incubated (15 mg/mL) in 6N HCl

at 110 °C under vacuum for 24 hours. CT-pSBAm-*block*-pNIPAm (20 mg/mL) conjugates were incubated in 4.5N *p*-toluene sulfonic acid at 80 °C under vacuum for 72 hours. Following incubation, cleaved polymers were isolated from CT using dialysis tubing (MwCO 1K Da) for 48 hours and then lyophilized.

3.2.5 Characterization of Cleaved Polymers

Number and weight average molecular weights (M_n and M_w) and the polydispersity index (M_w / M_n) were estimated by gel permeation chromatography (GPC) for pSBAm polymers cleaved from CT. Analysis was conducted on a Water 2695 Series with a data processor, using 80/20 mixture of 0.1 M sodium phosphate buffer (pH 9.0) and acetonitrile with 0.01 volume % NaN_3 as an eluent at a flow rate 1 mL/min, with detection by a refractive index (RI) detector. Polystyrene sulfonate standards were used for calibration. M_n was calculated for pSBAm-*block*-pNIPAm cleaved from CT by quantitatively comparing NMR peaks (integration of peaks) of copolymer to cleaved first block pSBAm NMR spectra.

3.2.6 Cloud Point Curves

CT-pSBAm-*block*-pNIPAm conjugates (2-3 mg polymer/mL) were dissolved in 0.1 M phosphate buffer (pH 8.0) in quartz cuvette. Conjugates were cooled from 25 °C to 1 °C and then heated up to 40 °C at ± 0.5 °C/min. The absorbance at 490 nm was measured in 1 °C increments and LCST/UCST cloud points were calculated from the inflection point in the turbidity curves.

3.2.7 CT and CT conjugate Biocatalytic Activity

N-succinyl-L-Ala-L-Ala-L-Pro-L-Phe-*p*-nitroanilide was used as a substrate for enzyme bioactivity assays. In a cuvette, 0.1 M sodium phosphate buffer (2820-2970 µL, pH 8.0), substrate (0-150 µL, 6 mg/mL in DMSO (0-500 µM)), and enzyme (30 µL, 0.1 mg enzyme/mL

0.1 M pH 8.0 sodium phosphate buffer (0.04 μM)) were mixed. The rate of the hydrolysis was determined by recording the increase in absorbance at 412 nm for the first 30 seconds after mixing. K_M and k_{cat} values were calculated using EnzFitter software when plotting substrate concentration versus initial hydrolysis velocity.

3.2.8 Thermal Stability

Native CT and CT-conjugates (40 μM) were dissolved in 0.1 M sodium phosphate buffer (pH 8.0) and incubated in a water bath in 50 μL aliquots at 37 °C. At specified time points, aliquots were removed and diluted to 4 μM using 0.1 M sodium phosphate buffer (pH 8.0). Residual activity, measured in 0.1 M sodium phosphate buffer (pH 8.0) at 25 ° C, was calculated as the ratio of activity remaining relative to the activity at time zero. Substrate (Suc-AAPF-*p*NA) concentration was kept constant at 288 μM for each sample and time point. Native CT and conjugate activities were measured in duplicate at each time point.

3.2.9 *In Vitro* Gastric Acid Stability

Native CT and CT-conjugates were incubated at 4 μM in 167 mM HCl at 37 ° C in 50 μL aliquots. Aliquots were removed at specified time points and residual activity was measured at 25 °C in 0.1 M sodium phosphate buffer (pH 8.0) with Suc-AAPF-*p*NA as substrate (288 μM). Each time point was measured in duplicate and residual activity was calculated as the ratio of activity remaining from time zero.

3.2.10 Stability to Pepsin Degradation

Native CT and CT-conjugates (4 μM) were incubated in 167 mM HCl with 16 nM pepsin at 37 °C in 50 μL aliquots. Samples were retrieved at specified time points and residual activity was measured in 0.1 M sodium phosphate buffer (pH 8.0) at 25 ° C with Suc-AAPF-*p*NA as

substrate (288 μM). Each time point was measured in duplicate and residual activity was calculated as the ratio of activity remaining from time zero. As a control, pepsin (16 nM) bioactivity towards Suc-AAPF-*p*NA was measured at pH 8.0 and no product formation was observed.

3.2.11 Size Measurements During 167 mM HCl (pH 1) Incubation

CT conjugates (4 μM) and native CT (29 μM) passed through a 0.2 μM cellulose filter were incubated in 167 mM HCl at 37 °C in 1 mL aliquots. Aliquots were removed from incubation at each specified time point. Hydrodynamic diameter was then determined using a Malvern zetasizer nano-ZS at 25 °C. Intensity PSD measurements, averaged over five sample runs at each time point, were used to calculate hydrodynamic diameter (D_h).

3.3 Results and Discussion

3.3.1 Conjugate Synthesis and Polymer Characterization

To test our hypothesis that separate stimuli responsive blocks in a protein-polymer conjugate influence stimuli responsive behavior of the other block, we decided to grow a block copolymer with both UCST and LCST responsive blocks from chymotrypsin. Previously, we synthesized separate CT-pDMAPS and CT-pNIPAm conjugates with temperature responsiveness by “grafting from” a water soluble bromine functionalized ATRP initiator coupled to chymotrypsin(CT-Br)[119]. In this study, a similar water soluble initiating molecule (Ini-Cl), functionalized with chlorine rather than bromine, was conjugated to chymotrypsin to yield the chymotrypsin ATRP macroinitiator (CT-Cl) (**Figure 3.1**).

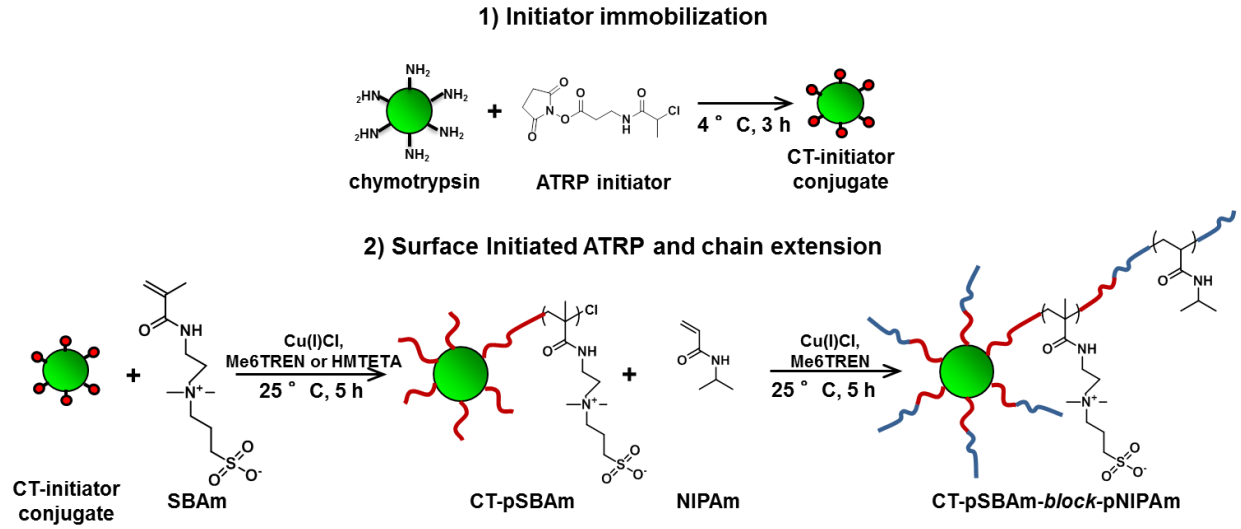

Figure 3.1 Synthesis of CT-pSBAm-*block*-pNIPAm diblock conjugates. Number of initiators and polymer chains per enzyme not drawn to scale. Fourteen initiators were estimated to be on each molecule as determined by MALDI-TOF-MS (**Figure 3.2**).

Similar to CT-Br, CT-Cl was functionalized with an NHS-ester to react with primary amines on surface lysines and the *N*-terminus of CT. After immobilization of the ATRP initiator, it was determined using MALDI-TOF-MS that there were an average of 15 initiating molecules per enzyme molecule (**Figure 3.2**). Calculated *m/z* values were 25493 Da for native CT and 28534 Da for CT-initiator-Cl. From these values, we calculated that there were 15 initiating sites for every chymotrypsin molecule. The presence of fifteen initiating sites per chymotrypsin molecule indicates that all of the 14 lysines on CT as well as the *N*-terminus were modified using this technique. From the MALDI spectra, two peaks were seen for native CT (one large intensity peak and one lower intensity) and this shape is conserved in the CT-initiator-Cl molecule as well. However, the peak for CT-initiator-Cl is broader than native CT, indicating the macroinitiator molecules are not completely monodisperse. Thus, we estimated that each chymotrypsin molecule had between 13-15 initiating molecules. The figures used in the manuscript contain 14 polymers per enzyme molecule to reflect this data.

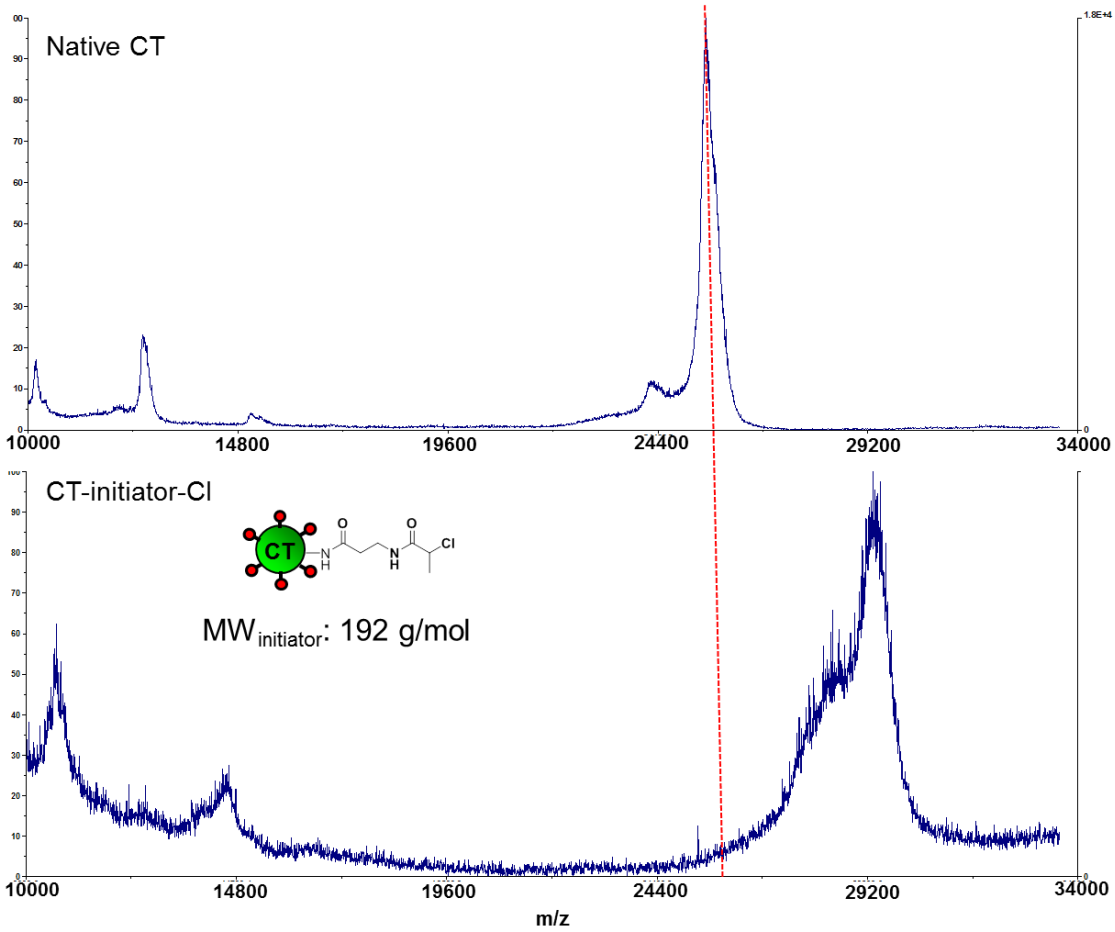

Figure 3.2 MALDI-TOF-MS spectra for native chymotrypsin (top) and ATRP initiator modified chymotrypsin (bottom).

Following synthesis of the CT-Cl macroinitiator, pSBAm was first grown from each of the 14 initiating sites on the surface of CT with three different molecular weights, yielding three conjugates with UCST behavior (CT-pSBAm$_{35}$, CT-pSBAm$_{50}$, CT-pSBAm$_{90}$). From GPC chromatograms, it was determined no residual free chymotrypsin was left after first block synthesis (**Figure 3.3 top**). We explored the synthesis of CT-pNIPAm-*block*-pSBAm conjugates, but sequential ATRP reactions in this order were not possible without optimization. After purification of CT-pSBAm conjugates, chain extension with pNIPAm was completed to yield

three CT-pSBAm-*block*-pNIPAm conjugates with three different molecular weights that showed both UCST and LCST behavior (CT-35/39, CT-50/67, CT-90/100).

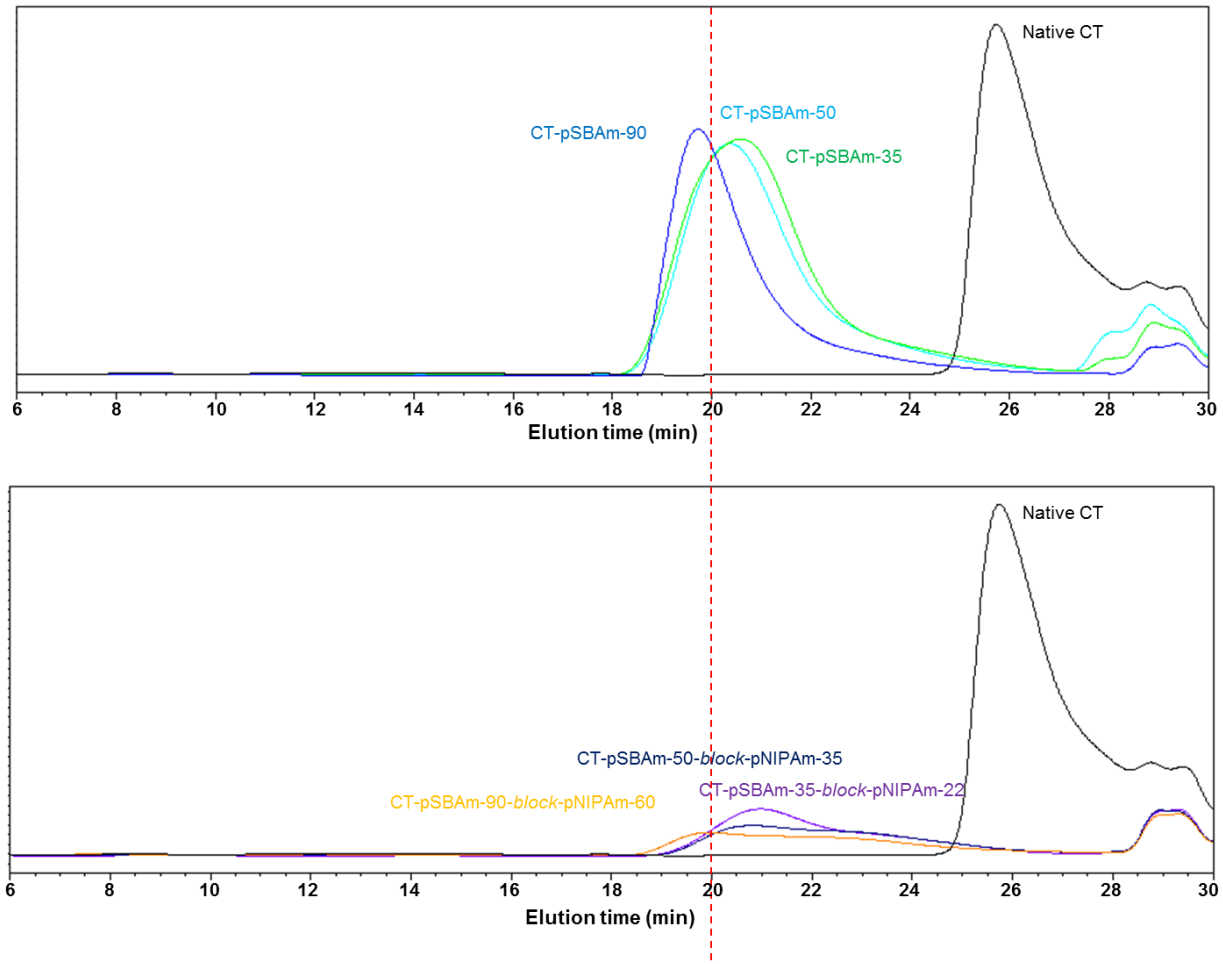

Figure 3.3 GPC chromatograms were acquired for CT-pSBAm homopolymer conjugates (top), CT-pSBAm-*block*-pNIPAm diblock conjugates (bottom),and native chymotrypsin using 100 mM sodium phosphate buffer (pH 7) with 0.01 % NaN_3 as the mobile phase with a flow rate of 1 mL/min. Instrumentation included a Waters 2695 Separations module with three aqueous columns and detection by a Water 2410 refractive index detector.

From GPC traces of block copolymer conjugates (**Figure 3.3 bottom**), it was evident that no native chymotrypsin was left after first block synthesis of pSBAm or second block chain extension of pNIPAm. The small peaks seen from 29-30 minutes correspond to the solvent eluting from the column ("ghost peak") and not native chymotrypsin. Since chymotrypsin is such

a small molecule in its native structure, the last fractions elute at the same time as solvent. Interestingly, the CT-pSBAm-*block*-pNIPAm diblock conjugates did not elute from the column using the conditions described above. The small peaks seen in the chromatograms corresponded to small amounts of residual CT-pSBAm homopolymer conjugate that was not successfully chain extended (<10 %). It was not expected that the diblock conjugates would elute from the column using an aqueous buffer. pNIPAm is an amphiphilic molecule, and dimethylformamide (DMF) is almost exclusively used as the mobile phase when determining molecular weight for free polymers[135] or protein-polymer conjugates[119] involving pNIPAm. Conversely pSBAm is a very hydrophilic molecule and does not have good compatibility with DMF GPC systems. Also, due to the contrasting size of pNIPAm and pSBAm (pSBAm monomer unit is much larger than that of pNIPAm), there was not an appropriate standard for GPC analysis. Thus, M_w and M_n for pSBAm-*block*-pNIPAm polymers could not be calculated using GPC techniques. Instead of GPC, we chose to determine M_n values for chain extended second block pNIPAm using relative ratios of peaks in NMR spectra.

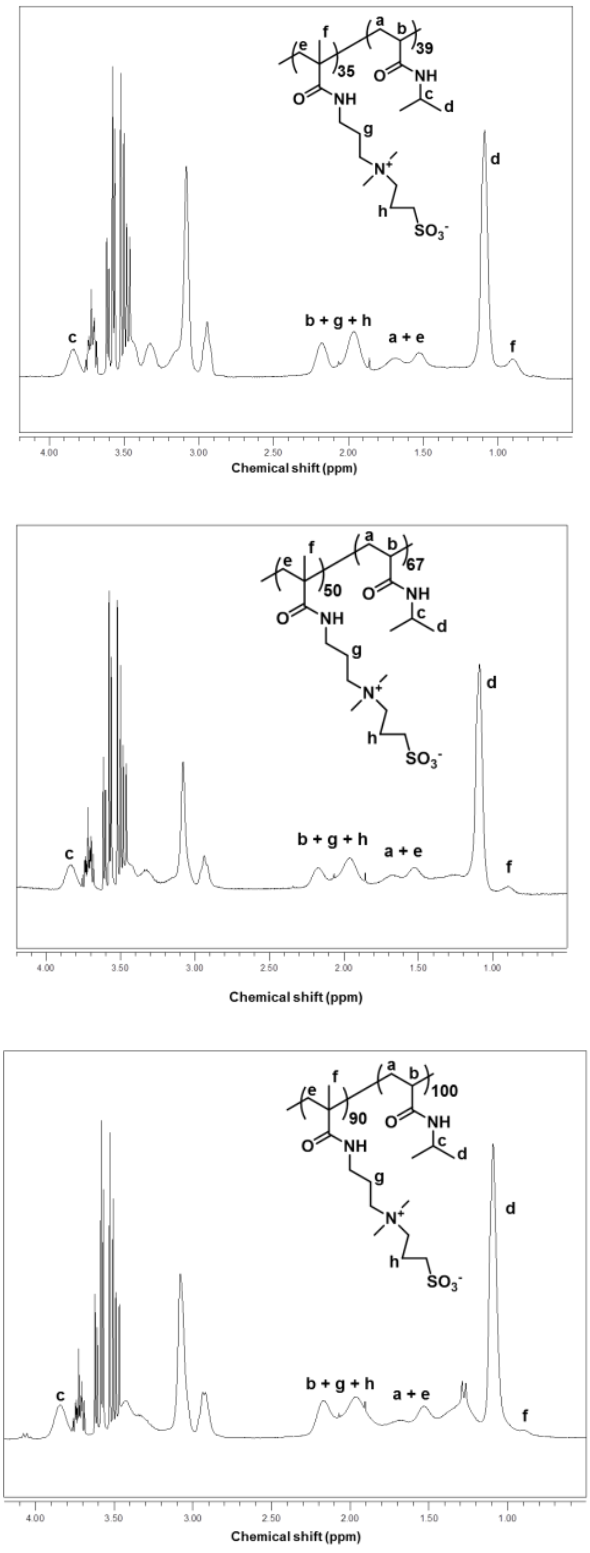

Figure 3.4 NMR spectra for acid hydrolyzed pSBAm-*b*-pNIPAm in D_2O. Relative intensity of characteristic peaks were used to calculate second block M_n.

M_n values for each of the second block pNIPAm segments were estimated using the NMR spectra of diblock polymers cleaved from chymotrypsin (**Figure 3.4**). To do this, the relative intensity from peak c (3.8-4.0 ppm), corresponding to one proton in the pNIPAm block was compared with the broad signal complex from 0.8-2.3 ppm (signals a + b + d + e + f + g + h) corresponding to 18 total protons in both the pNIPAm and pSBAm blocks. From these ratios, the M_n of the pNIPAm block was calculated when comparing to the M_n for pSBAm calculated from GPC analysis. This procedure is similar to the procedure used by Arotcarena *et al.*[126], who previously synthesized this same polymer using RAFT polymerization.

The nomenclature used for each of the conjugates corresponds to degree of polymerization of each polymer block in the conjugate based on GPC and NMR analysis of cleaved polymers. The first number corresponds to the pSBAM block and the second number refers to the chain extended pNIPAm block. The use of Ini-Cl/Cu(I)Cl, the addition of NaCl to the polymerization solution, and short polymerization time helped to lower the PDI of polymers grown from the surface of CT in this study (Table 3.1). It is also likely the reaction conditions reduced growing chain termination and ligand/catalyst degradation, which conserved the living nature of the polymer chain to allow chain extension of pNIPAm from CT-pSBAm.[136, 137] Minimal amounts (<10%) of CT-pSBAm conjugates did remain after chain extension indicating some chain termination might have occurred during first block synthesis.

Table 3.1 Molecular weight and hydrodynamic diameter of CT-pSBAm-*block*-pNIPAm conjugates

	Cleaved Polymer		CT Conjugate Molar Mass		Size (D_h) [nm]
	M_n (kDa)	PDI (M_w/M_n)	BCA (kDa)	GPC/NMR (kDa)	
CT-pSBAm$_{35}$	10.2	1.59	173	171	24.2 ± 2.5
CT-pSBAm$_{50}$	15.7	1.43	248	248	22.7 ± 1.9
CT-pSBAm$_{90}$	26.2	1.86	362	395	23.3 ± 1.0
CT-pSBAm$_{35}$-*block*-pNIPAm$_{39}$	14.6	-	302	232	46.1 ± 4.5
CT-pSBAm$_{50}$-*block*-pNIPAm$_{67}$	23.3	-	427	354	47.6 ± 8.7
CT-pSBAm$_{90}$-*block*-pNIPAm$_{100}$	37.5	-	475	553	64.1 ± 4.5

3.3.2 Phase Transition Temperatures of CT-pSPAm-*block*-pNIPAm Conjugates

UCST and LCST cloud points for each of the three molecular weight conjugates (CT-35/39, CT-50/67, and CT-90/100) were determined by measuring solution turbidity (absorbance at 490 nm) at temperatures from 0-40 °C. Each of the conjugates displayed both LCST and UCST behavior, but the specific phase change temperature was dependent upon the polymer chain length (**Figure 3.5**).

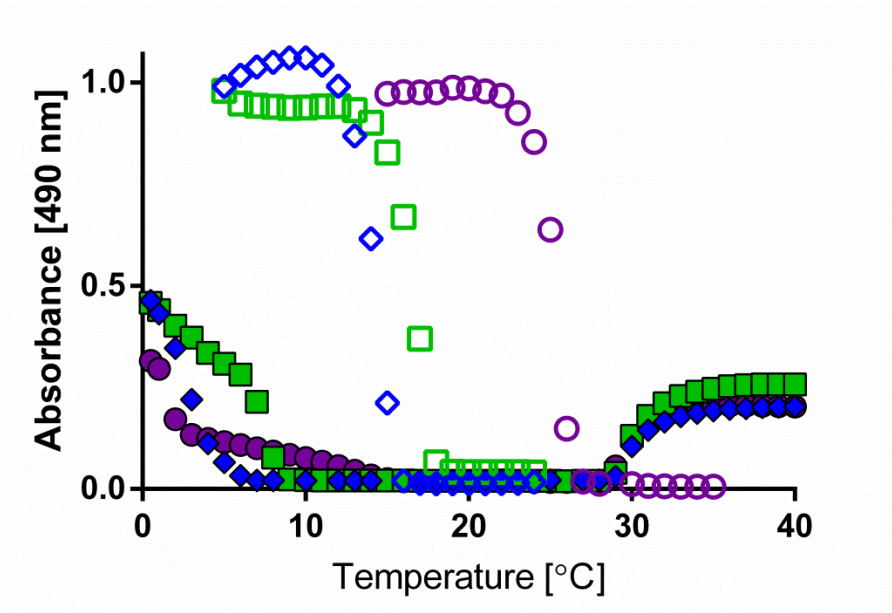

Figure 3.5 Cloud point curves for CT-pSBAm-*block*-pNIPAm conjugates. Chymotrypsin dual block conjugates (CT-35/39-blue filled diamond, CT-50/67-green filled square, CT-90/100-purple filled circle) and CT-pSBAm homopolymer conjugates (CT-35-blue open diamond, CT-50-green open square, CT-90-purple open circle) were incubated at 3 mg/mL in 0.1 M sodium phosphate buffer (pH=8.0), heated/cooled at ±0.5 °C/min, and absorbance at 490 nm was recorded.

Each of the dual block conjugates showed LCST behavior at 29 °C in 0.1 M phosphate buffer (pH=8.0). As previously reported, linear pNIPAm LCST is independent of molecular weight when the molecular weight is not ultra-high[101], so this result was not unexpected. LCST phase transition at 29 °C was slightly lower than previously reported LCST values for pNIPAm, but the lowered value is consistent with LCST behavior in salt buffers compared to deionized water[138]. The LCST also agreed well with the LCST temperature determined in our previous study for CT-pNIPAm conjugates[119]. The turbidity of these solutions (0.2-0.25 AU) was also lower than CT-pNIPAM conjugates. When above the LCST, pNIPAm polymer chains are insoluble in aqueous solutions and thermodynamically prefer to minimize interactions with water. Thus, as each of the conjugates reached temperatures above 29 °C, the pNIPAm

component of the bioconjugate collapsed. For free pNIPAm in solution, large aggregates form; greatly increasing turbidity. However, for CT-pSBAm-*block*-pNIPAm, hydrophilic CT and pSBAm components, even at temperatures above the LCST, prevented more extreme aggregation, which caused turbidity measurements above the LCST to plateau at a lower value than free pNIPAM or CT-pNIPAm conjugates.

When comparing CT-pSBAm-*block*-pNIPAm cloud point curves with CT-pSBAm curves (**Figure 3.5**), it was clear that the pNIPAm block influenced the UCST behavior of the pSBAm component in the final bioconjugate. A lower temperature was required for the CT-pSBAm-*block*-pNIPAm conjugates to show collapsed, insoluble behavior compared with CT-pSBAm conjugates. At low temperature, pSBAm was hydrophobic, but the pNIPAm and CT components of the conjugate were still hydrophilic and influenced the overall behavior of the conjugate. In addition to polymer collapse, aggregation of hydrophobic pSBAm polymer blocks between different CT molecules contributed to the turbidity seen in the cloud point curves. The pNIPAm block, located on the outside of the CT conjugates, likely sterically hindered pSBAm association between CT molecules, which could lower the transition temperature onset as determined by cloud point curves. The UCST behavior for CT-90/100, the longest chain conjugate, did not show a sharp increase in absorbance at a specific temperature. Instead, turbidity measurements for CT-90/100 increased linearly when decreasing temperature from 15 - 3 °C, and ultimately showed a sharp increase in absorbance around 2 °C. As with CT-35/39 and CT-50/67, we hypothesized that this effect was due to steric hindrance of pNIPAm and the hydrophilicity of CT and pNIPAm at this temperature range. However, the long chain length of pNIPAm on the outside of CT-90/100 prevented a sharp increase in turbidity at the temperature where insolubility was initially observed.

3.3.3 Effect of Double Shelled Polymer-Based Protein Engineering on CT Bioactivity

CT conjugate kinetics were examined at a variety of temperatures (2.5 °C, 7 °C, 16.5 °C, 24.5 °C, 33 °C, and 37.5 °C) to determine the effect of polymer UCST and LCST phase transitions and molecular weight on enzyme kinetics (**Table 3.2**). The rate of hydrolysis of *N*-succinyl-L-Ala-L-Ala-L-Pro-L-Phe-*p*-nitroanilide by CT and CT conjugates in 0.1 M sodium phosphate buffer (pH 8.0) was used to determine the impact of doubled-shelled PBPE on CT bioactivity.

Table 3.2 Michelis-Menten kinetics for CT and CT conjugate catalyzed hydrolysis of *N*S-AAPF-*p*NA from zero to 37.5 °C.

Sample	K_M [μM]	k_{cat} [sec^{-1}]	k_{cat}/K_M [sec^{-1}/μM]	$(K_M)_x$ $(K_M)_{CT}$	$(k_{cat})_x$ $(k_{cat})_{CT}$	$(k_{cat}/K_M)_x$ $(k_{cat}/K_M)_{CT}$
			2.5 °C			
Native CT	30 ± 5.1	8.9 ± 0.4	0.33 ± 0.06	-	-	-
CT-35/39	47 ± 7.5	6.3 ± 0.5	0.14 ± 0.02	1.59	0.71	0.42
CT-50/67	49 ± 7.7	6.8 ± 0.2	0.14 ± 0.02	1.65	0.76	0.42
CT-90/100	49 ± 10	4.5 ± 0.4	0.08 ± 0.02	1.66	0.51	0.24
			7 °C			
Native CT	29 ± 6.9	9.7 ± 0.5	0.34 ± 0.09	-	-	-
CT-35/39	41 ± 9.6	7.8 ± 0.5	0.19 ± 0.05	1.42	0.80	0.57
CT-50/67	41 ± 7.3	8.7 ± 0.5	0.21 ± 0.06	1.45	0.90	0.62
CT-90/100	45 ± 9.6	6.5 ± 0.4	0.15 ± 0.03	1.58	0.67	0.43
			16.5 °C			
Native CT	37 ± 8.6	16 ± 0.9	0.43 ± 0.10	-	-	-
CT-35/39	41 ± 6.8	13 ± 0.5	0.31 ± 0.05	1.09	0.79	0.72
CT-50/67	39 ± 5.6	14 ± 0.5	0.36 ± 0.05	1.04	0.87	0.84
CT-90/100	43 ± 7.1	10 ± 0.5	0.24 ± 0.04	1.16	0.64	0.56
			24.5 °C			
Native CT	51 ± 8.7	25 ± 1.3	0.50 ± 0.10	-	-	-
CT-35/39	50 ± 10	22 ± 0.9	0.43 ± 0.08	0.98	0.86	0.87
CT-50/67	53 ± 7.3	21 ± 0.9	0.41 ± 0.06	1.03	0.82	0.92
CT-90/100	50 ± 7.8	16 ± 0.7	0.31 ± 0.05	0.97	0.62	0.63
			33 °C			
Native CT	57 ± 5.0	36 ±1.3	0.64 ± 0.08	-	-	-
CT-35/39	67 ± 5.3	32 ± 0.9	0.47 ± 0.04	1.18	0.88	0.75
CT-50/67	65 ± 7.2	33 ± 1.4	0.51 ± 0.07	1.14	0.90	0.80
CT-90/100	75 ± 6.9	25 ± 0.7	0.33 ± 0.03	1.32	0.68	0.51
			37.5 °C			
Native CT	59 ± 6.9	47 ± 1.7	0.80 ± 0.10	-	-	-
CT-35/39	71 ± 6.7	43 ± 1.4	0.61 ± 0.06	1.19	0.92	0.77
CT-50/67	71 ± 6.3	43 ± 1.3	0.61 ± 0.06	1.21	0.92	0.76
CT-90/100	75 ± 11	32 ± 1.6	0.43 ± 0.07	1.27	0.69	0.54

CT conjugate bioactivity was temperature dependent after conjugation of pSBAm-*block*-pNIPAm (**Figure 3.6**). Relative K_M and k_{cat} values for CT-35/39, CT-50/67, and CT-90/100 were all modified after conjugation, but only relative K_M values were dependent upon temperature. For CT-35/39 and CT-50/67, relative k_{cat} values were between 0.8 and 0.9 at each of the tested temperatures. Relative k_{cat} values for CT-90/100 were slightly lower than CT-35/39 and CT-50/67 conjugates, but similarly, enzyme activity was conserved and was independent of temperature. In past studies, long chain polymer conjugation has decreased k_{cat} values due to limited structural flexibility[121], which likely contributed to decreased k_{cat} values in this study as well[114].

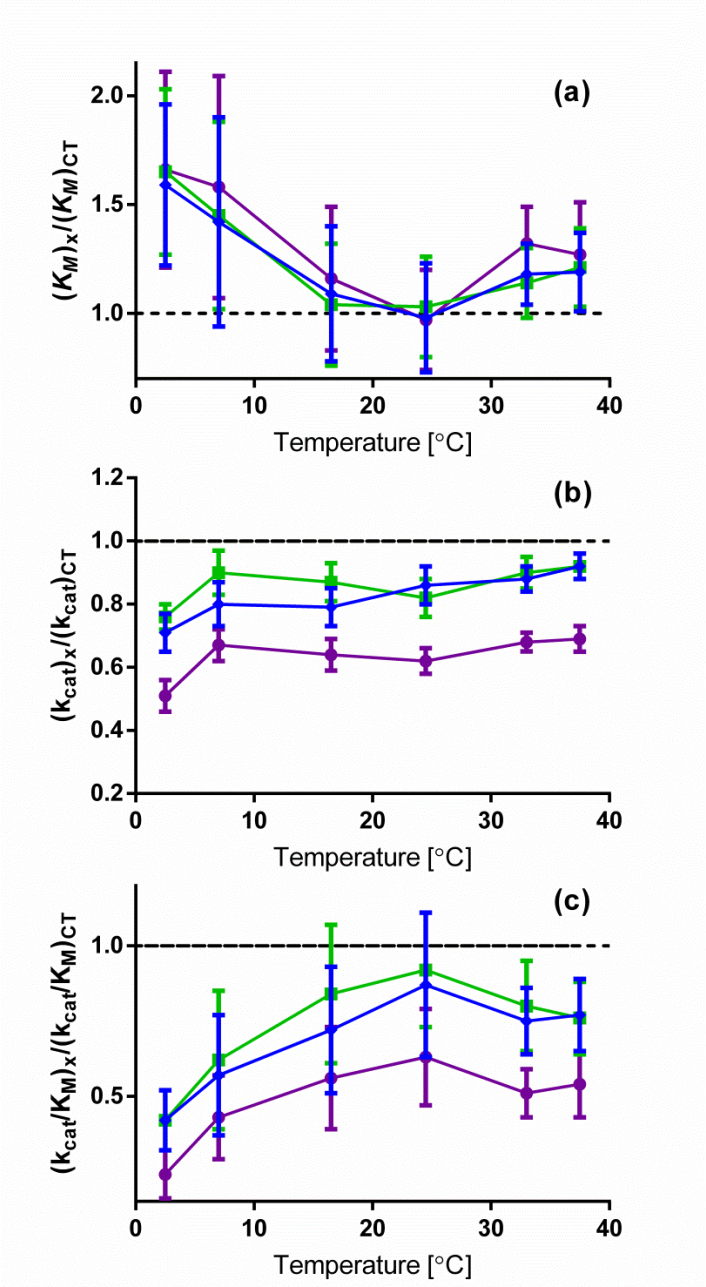

Figure 3.6 Temperature dependence of chymotrypsin catalytic constants. (a) specificity (K_M), (b) activity (k_{cat}), and (c) productivity (k_{cat}/K_M) relative values for the hydrolysis of *NS*-AAPF-*p*NA by CT-pSBAm-*block*-pNIPAm conjugates (CT-35/39-blue diamond, CT-50/67-green square, CT-90/100-purple circle) relative to native CT in 0.1 M sodium phosphate buffer (pH=8.0). Exact values for native chymotrypsin at each temperature are shown in Table 3.2.

While k_{cat} values were independent of temperature, relative K_M values for CT-pSBAm-*block*-pNIPAm bioconjugates showed a significant dependence to both low and high temperatures. At 25 °C, each of the conjugates calculated K_M values were similar to native CT. However, at temperatures both higher and lower than 25 °C, relative K_M values increased significantly for each of the conjugates. At low temperatures the increase in relative K_M was more extreme than the K_M increase at high temperature. At assay temperatures below 25°C, relative K_M values increased until reaching a maximum (~1.6-1.7 for each of the conjugates) at 2.5 °C. At 40 °C, relative K_M for each of the conjugates was approximately 1.2, indicating lower substrate infinity for the conjugates compared to native CT at this temperature. For CT-35/39 and CT-50/67, relative K_M values were slightly lower at 35 °C than K_M values at 40 °C. CT-90/100 relative K_M values were only slightly higher at 35 °C than 40 °C.

We hypothesized that the increase in K_M values at both high and low temperature was a result of restricted access to the active site for the model substrate due to steric hindrance caused by polymer collapse during both UCST and LCST phase transitions. Figure 3.8 shows our hypothesis of how polymer collapse impacted substrate access to the enzyme active site, drawn to the scale of each polymer block approximated from dynamic light scattering data (Table 3.1).

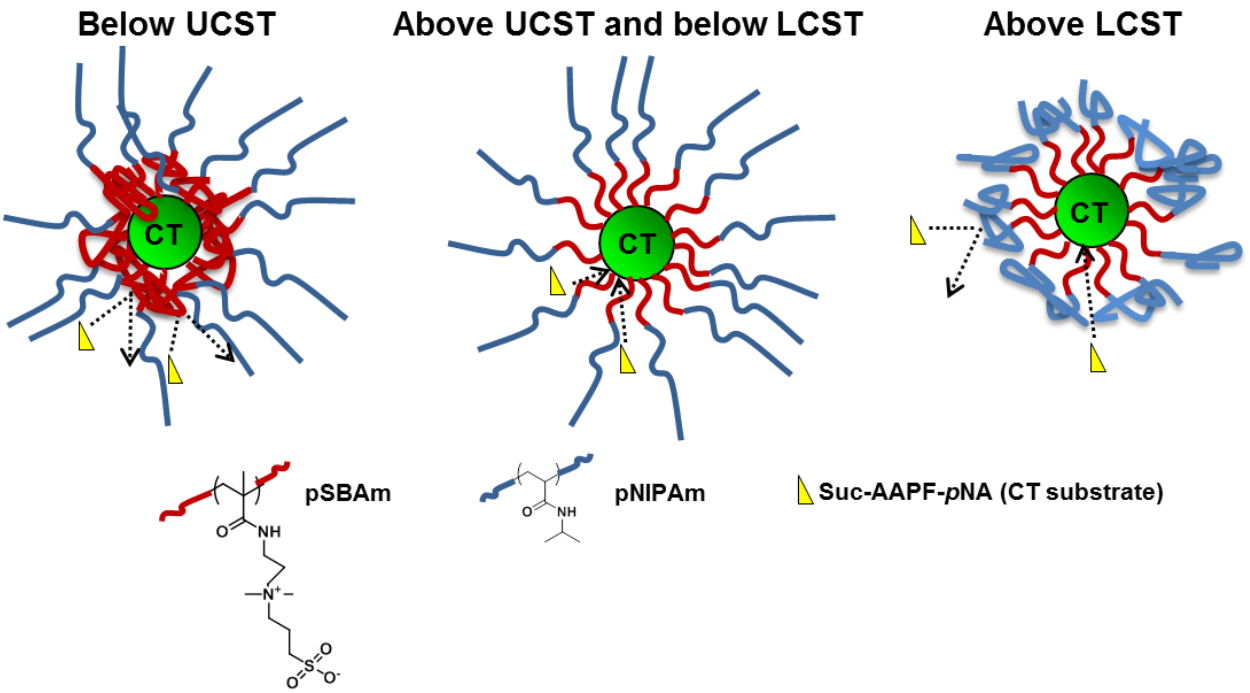

Figure 3.7 Schematic of the hypothesized effect of pSBAm and pNIPAm polymer collapse on substrate affinity (K_M). At 25 °C, both pSBAm and pNIPAm were in their extended conformation and allowed Suc-AAPF-*p*NA access to CT active site. At temperatures below pSBAm UCST and above pNIPAm LCST, polymer collapse inhibited access to the active site for Suc-AAPF-*p*NA due to steric blocking. At temperatures below pSBAm UCST, this effect is hypothesized to be more pronounced than at temperatures above pNIPAm LCST, because the pSBAm block was closer to the enzyme core than the pNIPAm block.

At temperatures above 29 °C, as determined by cloud point curves, the pNIPAm block of the polymer was collapsed upon itself to minimize its interaction with water. As the pNIPAm polymers collapsed, a more compact shell existed compared to pNIPAm orientation at 25 °C, which likely restricted the model substrate's ability to reach the active site. At low temperature, we hypothesized that the increase in relative K_M was also due to steric hindrance from polymer collapse, except the pSBAm polymer block collapsed at low temperature rather than pNIPAm. As seen from the cloud point curves, CT-90/100 UCST polymer collapse began at 16 °C, so it was not surprising to see the highest relative K_M increase of the three conjugates at this assay

temperature. As temperature decreased, the UCST induced polymer collapse appeared to continue to increase as evidenced by the increase in turbidity measurements in cloud points curves. The increase seen in relative K_M values at lower temperatures was most likely due to this increase in polymer collapse and dehydration. Once the substrate reached the active site, the rate of the reaction was similar at each temperature measured, as shown by the lack of dependence of relative k_{cat} values on temperature.

Chain length of the polymers did not appear to have a large effect on the relative K_M values. While CT-90/100 conjugates did have slightly higher relative K_M values than CT-35/39 and CT-50/67, a clear trend between the three conjugates was not noticeable. It is also important to notice the difference in relative K_M values with respect to the location of the collapsed polymer in the conjugate. Since the pSBAm block was synthesized first, this polymer was closer to the core of the conjugate, while the pNIPAm block was on the outside of the conjugates. We surmised that, due to this orientation, polymer collapse and turbidity increases were seen at both high and low temperatures, but the specific geometry of the overall collapsed conjugate was different. We hypothesized that the pSBAm collapse showed higher relative K_M values due to its location closer to the core of the conjugate (closest to the active site). In addition, while pNIPAm collapse at high temperature also induced increased relative K_M values, the effect was not as pronounced due to its location on the outside of the conjugate.

Relative productivity (k_{cat}/K_M) ratios for each of the CT-pSBAm-*block*-pNIPAm conjugates were also dependent upon temperature. Relative productivity values for CT-35/39 and CT-50/67 were similar to native CT at 25 °C, and CT-90/100 was slightly reduced due to lower k_{cat} values at this temperature. For each temperature tested other than 25 ° C, k_{cat}/K_M values were decreased, mostly as a result of the increased relative K_M values seen after phase transitions. The

largest decrease in productivity ratios was seen at 2.5 ° C, where relative K_M values were the highest and a slight decrease in k_{cat} values was seen for each conjugate.

3.3.4 CT Conjugate Stability

We have explored in detail the thermal stability, pH stability, and protease degradation stability conditions of the CT-pSBAm-*block*-pNIPAm conjugates. CT conjugates of each molecular weight had higher stability than native CT to (a) incubation at 37 °C, (b) incubation in 167 mM HCl (pH 1), and (c) incubation with pepsin (**Figure 3.8**). Specifically, maintaining stability of proteins as they are subjected to extreme pH and protease degradation (as would be seen in the GI tract) is a large challenge. Most studies on oral peptide delivery technologies have focused on transport through the intestinal membrane[139] or pharmacokinetics/biodistribution,[140] but do not examine stability of the protein in the GI tract.

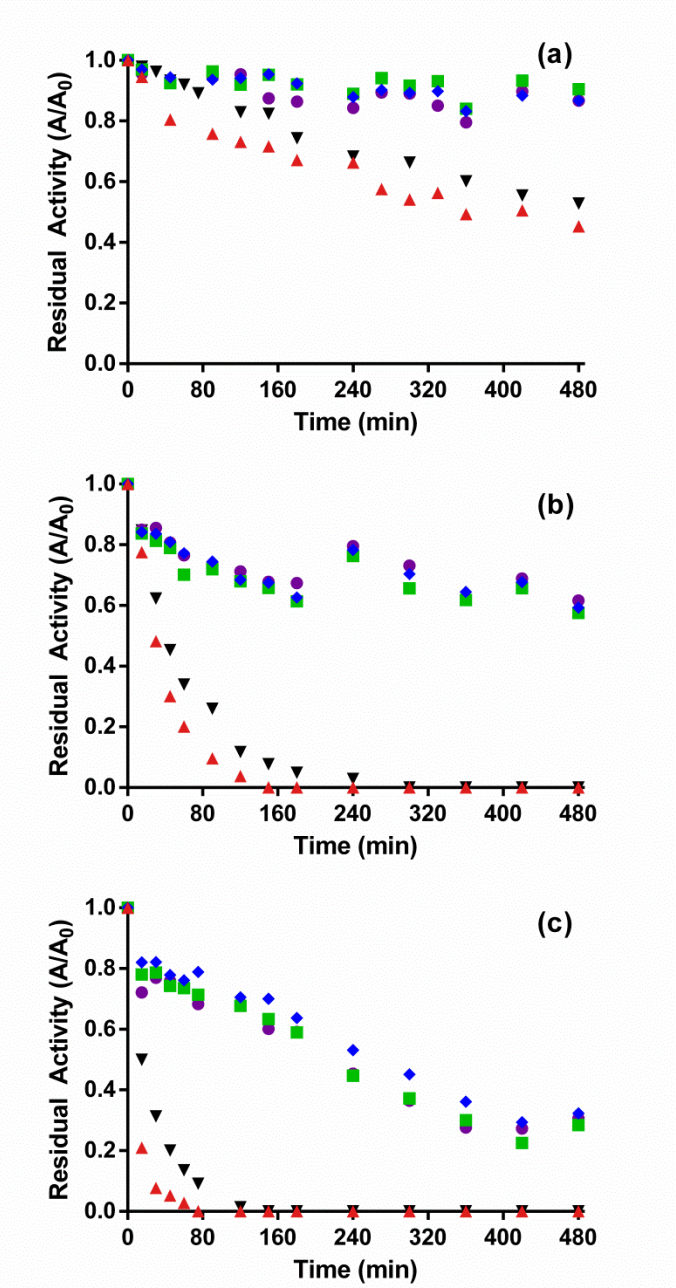

Figure 3.8 Rate of irreversible inactivation for chymotrypsin. CT-pSBAm-*block*-pNIPAm conjugates (CT-35/39-blue diamond, CT-50/67-green square, and CT-90/100-purple circle), native CT (red diamond), and native CT with pSBAm-*block*-pNIPAm in solution (black triangle) at were incubated at 37 °C in (a) 0.1 M sodium phosphate buffer (pH=8.0), (b) 167 mM HCl (pH=1), and (c) 167 mM HCl with 19 nM pepsin. Residual activity was calculated as the activity remaining from t=0. All assays were conducted at 25 °C.

3.3.5 Stability at Ambient Temperature and Neutral pH

CT conjugates lost only 10 % of their activity after 8 hours incubation at 40 μM in 0.1 M sodium phosphate buffer (pH 8.0), while native CT lost half of its activity over the same time period (Figure 3.9a). At 37 °C and pH 8, CT was still active and, consequently, one contributor to irreversible inactivation at this temperature and pH was autolysis. As a protease, CT hydrolyzes peptide bonds to break down proteins, and CT inactivates itself due to self-digestion of unfolded CT in solution. As a result of the polymer density around CT conjugates, steric hindrance limited CT molecules access to each other, decreasing autolysis and increasing stability. Previously, PEGylation of protein molecules has been shown to reduce structural dynamics[114], and charged polymers have increased the stability of CT after conjugation due to charge effects[43, 141]. Increased stability imparted by CT-pSBAm-*block*-pNIPAM conjugates was likely due to a combination of both effects as the pSBAm block contained protein stabilizing ions and pNIPAm chemical structure was similar to PEG.

3.3.6 Stability at Extremes of pH

Interestingly, CT conjugates also showed increased to stability to low pH. Native CT and CT conjugates were incubated in 167 mM HCl (pH 1) at 37 °C for 3 hours to mimic gastric acid. *In vivo*, gastric acid promotes unfolding of proteins to increase access of pepsin to cleavable amino acid sequences. Each of the CT conjugates maintained at least 60 % of activity after incubation in 167 mM HCl for 3 hours, compared to complete activity loss for native CT after the same time period (Figure 3.9b). In 167 mM HCl, (pH 1), native CT unfolds due to disruption of hydrogen bonding. One can imagine two mechanisms through which PBPE might stabilize CT to such a dramatic extent. First, the polymer stabilized the structure of CT, which reduced unfolding. Second, as some CT molecules unfolded, access to cleavage sites by autolysis was

restricted by steric hindrance of polymer as seen at 37 °C and pH 8.0. However, at pH 1 the enzyme should be inactive, and autolysis cannot contribute to CT inactivation. We therefore measured activity of CT and CT-conjugates at pH 1.0 and no product formation was observed with large excess of substrate (data not shown). Thus, protein unfolding without autolysis was the main mechanism for CT inactivation in 167 mM HCl. To further develop our mechanistic understanding, we used dynamic light scattering to examine native CT and CT conjugate hydrodynamic diameter during incubation at pH 1(**Figure 3.9**).

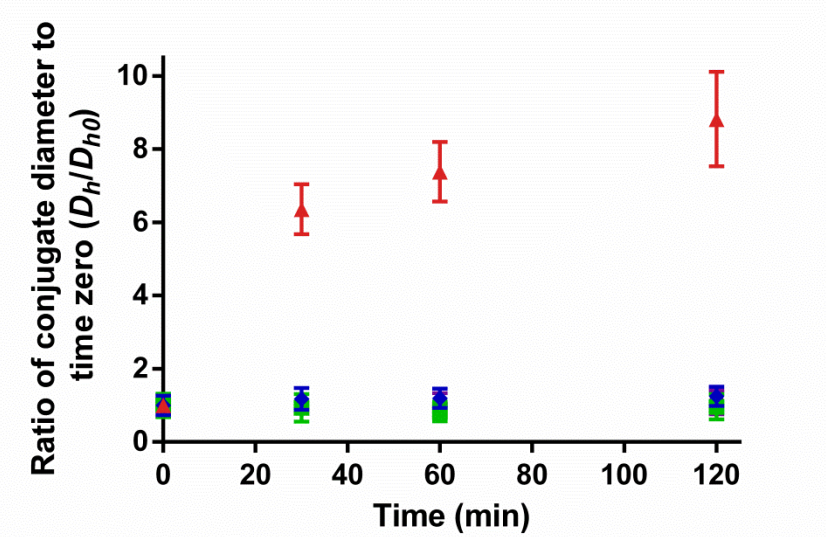

Figure 3.9 Dependence of native and CT conjugate hydrodynamic diameter during incubation in 167 mM HCl (pH 1) at 37 °C. Size values are presented as ratios of each samples size at time zero. Increased hydrodynamic diameter (D_h) indicates protein unfolding. D_h values at time zero were: native CT (red triangle)-6.3 ± 0.5 nm, CT-35/39 (blue diamond)-51 ± 9.7 nm, CT-50/67 (green square)-63 ± 14 nm, CT-90/100 (purple triangle)-72 ± 12 nm.

After 2 hours, the hydrodynamic diameter (D_h) for native CT increased 9-fold, while CT conjugate size increased less than 20 %. After incubation at low pH in 167 mM HCl, hydrogen bonding and other forces that maintain globular structure of proteins were likely disrupted for native CT. The disruption of forces led to protein unfolding, causing the protein to transition

from a globular conformation to a more linear structure, which increased D_h measurements for native CT. While very small increases in D_h were seen for CT conjugates, the magnitude was much lower due to the structural stabilization provided by the conjugated polymers that maintained CT globular structure. In a control experiment, we also showed that free pSBAm-*block*-pNIPAm in solution had a small effect on structural stabilization of native CT at pH 1 (**Figure 3.8b**). We surmised that structure stabilizing ions in the pSBAm block (ammonium and sulfonate) of the free polymer slightly increased solution total salt concentration to stabilize CT tertiary structure. While stabilization was increased a small amount with free polymer in solution, polymer conjugation to the protein was superior for structural stabilization due to the high local concentration of the polymer near the enzyme surface.

We next decided to explore the stability of CT conjugates to pepsin degradation in acid. CT bioconjugates were stable to pepsin incubation at 37 °C in 167 mM HCl (**Figure 3.8c**). Native CT lost all activity after only 75 minutes, while CT conjugates maintained approximately 70% residual activity after the same time period and still had 30% of initial activity after 7 hours. For pepsin to cleave proteins through hydrolysis, pepsin molecules must have access to their preferred amino acid sequence on chymotrypsin. Due to the high density polymer shell around CT-pSBAm-*block*-pNIPAm conjugates of each molecular weight, access for pepsin was inhibited. In addition, due to the low pH conditions, unfolding occurred for native CT, which increased access for pepsin degradation.

Multi-stimuli responsive polymers represent a new class of protein-polymer conjugates that respond to two stimuli through separate responses from each block. Temperature responsive polymer conjugation has previously been utilized for separation purposes upon heating[142], and the conjugate described herein could be used for separations of the covalently coupled protein at

both high and low temperature, which could be driven by the need to conserve energy required for high temperatures or prevent protein denaturation. In addition, protein-polymer conjugates with both UCST and LCST behavior show that other protein-polymer conjugates with separate blocks of pH and temperature responsive behavior can be synthesized as well. Still, polymer incompatibility between the two distinct blocks could cause some responsive polymers to not be able to be synthesized in a block copolymer. UCST and LCST are just two of the multitude of responsive properties that can be incorporated into block copolymers. A dual block conjugate with pH and temperature sensitive behavior could see applications in treating cancer by responding to lower pH[143] that is common in a tumor mass, as well as responding to targeted external heating at the tumor[144]. The dual block system lets scientists design the pH and temperature triggers more specifically than could be done for a single polymer block with dual responsiveness. Lastly, this approach shows that smart polymer functionality can be implemented with equal success on the inside or outside block of a dual block polymer shell. Since the polymer blocks must sometimes be synthesized in a specific order due to compatibility between each block, the success of implementing specific responsive functionality on the inside or outside could be hindered.

3.4 Conclusion

In this study, dual temperature responsive CT-pSBAm-*block*-pNIPAm conjugates with different polymer chain lengths and molecular weights were synthesized using a "grafting from" approach with two successive ATRP reactions. Chain extension of the pNIPAm block from homopolymer CT-pSBAm conjugate was utilized to grow the block copolymer from the surface of CT. From cloud point curves, we showed that CT-35/39, CT-50/67, CT-90/100 conjugates each had both UCST and LCST phase transition behavior. LCST behavior was due to the

pNIPAm polymer block and was not affected by chain length. The pSBAm polymer block imparted UCST behavior on each of the conjugates, but the specific transition temperature and behavior was dependent upon the chain length of attached polymers. Polymer conjugation to CT affected both enzyme turnover number (k_{cat}) and substrate affinity (K_M) values, but only relative K_M values were dependent upon temperature. Relative productivity (k_{cat}/K_M) ratios were also dependent upon temperature, mostly due to observed effects of relative K_M values. Stability of CT-pSBAm-*block*-pNIPAm conjugates was dramatically higher than native CT. We believe that the polymers reduced protein unfolding and restricted access of proteases thru steric hindrance for a variety of incubation conditions including thermal, low pH, and protease degradation. We have generated a protein that would be expected to survive passage through the stomach and are now in a position to modify a variety of proteins with responsive polymers that first protect enzymes from this environment and then respond to stimuli as needed.

Chapter 4 : Low pH Structural Stability of Chymotrypsin-Polymer Conjugates is Dependent on Polymer Chemical Structure

4.1 Introduction

Chymotrypsin is one of the most commonly used proteins when modifying proteins with polymers[145-147]. The frequent use of chymotrypsin is likely due to the extensive information available on chymotrypsin molecular properties and structure, including its amino acid sequence[148], crystal structure[149], and substrate preference[150, 151] for many different species of the enzyme. In addition, it is inherently stable to many conditions that other proteins may not be stable to including wide pH changes[152] or organic solvents[153, 154].

One of the most useful applications, and certainly the most therapeutically relevant application of chymotrypsin, is as an enzyme replacement therapy[155]. In humans, chymotrypsin natively works in the small intestine, where it breaks down proteins after secretion from the pancreas, and chymotrypsin replacement therapy is used to treat diseases where chymotrypsin insufficiency is a symptom[156]. Exogenous chymotrypsin must be delivered orally as that is the only viable route of administration to the gastrointestinal (GI) tract. However, the GI tract, specifically acid in the stomach and proteases throughout, has evolved to breakdown foodstuff proteins in order to facilitate amino acid nutrient absorption into the bloodstream. Still, unmodified chymotrypsin has been investigated as an enzyme replacement therapy to treat autism[157], cystic fibrosis[158-160], and exocrine pancreatic insufficiency[161]. In addition, many other enzymes such as lactase[162-164], lipase[165, 166], and amylase[167] are used with varying modification to treat GI tract disorders. In order to overcome the tendency of the harsh conditions in the GI tract to break down proteins, some type of modification strategy, either chemical or biological, is often necessary for replacement enzyme therapies.

In order for an enzyme replacement therapy to be effective in the GI tract, it needs to (1) have bioactivity in conditions that are relevant to the GI tract; that is, in solutions with pH values ranging from 1-8. In addition to being active in the GI tract, the enzyme (2) must also be stable to acid degradation in the stomach. Lastly (3), an additional benefit for an enzyme-polymer replacement therapy would be mucoadhesion; [86, 168] which would extend the residence time of the enzyme in the location of action.

Since the native location of action for chymotrypsin is the small intestine, chymotrypsin is inherently active from pH 5-10[169], with its pH optimum at pH 8[170]. Still, a hyperactive enzyme-polymer conjugate, which has been observed in the presence of amines[171], could make an enzyme-polymer replacement therapy more effective than native enzyme. Contrasted with the beneficial pH profile of chymotrypsin bioactivity, chymotrypsin stability to acidic stomach conditions is low, because chymotrypsin is secreted directly into the small intestine from the pancreas, natively avoiding the harsh conditions in the stomach. Many strategies such as encapsulation in polymers[172], modifications to specific amino acid residues[173, 174], or polymer conjugation[175, 176] have been used in the past in order to stabilize proteins to digestive tract conditions. Since it has a balance of negative and positive surface charges, native chymotrypsin is also not mucoadhesive. Thus, there is an opportunity for polymer-based protein engineered chymotrypsin to be more effective than native chymotrypsin as an enzyme replacement therapy by having higher stability to low pH and increased residence time in the GI tract via mucoadhesion.

With these three design criteria and strategies previously used to enhance activity and stability in mind, we chose four different polymers for this study to grow directly from the surface of chymotrypsin using polymer-based protein engineering. The polymers,

poly(carboxybetaine acrylamide) (pCBAm(+-)), poly(oligoethylene glycol methacrylate) (pOEGMA), poly(quaternary ammonium methacrylate) (pQA(+)), and poly(sulfonate methacrylate) (pSMA(-)), were chosen to represent four distinct charge states of polymers-zwitterionic and neutrally charge, uncharged, positively charged, and negatively charged, respectively. These specific charged polymers were chosen due to the inclusion of charged groups in the polymers bearing similar chemical structures to ions (sulfonate anion, ammonium cation) generally considered to be kosmotropes (order-making/stabilizing) by the Hofmeister series.[141, 177] In addition, both positively and negatively charged polymers have been shown to possess mucoadhesive properties.[178, 179] While uncharged and determined to not be mucoadhesive, pOEGMA was selected due to the increase in protein stability to different stressors such as temperature,[180] protease degradation,[181] and lyophilization[182] after PEGylation. Since each polymer was chosen to be stabilizing, we hypothesized that each of the conjugates would be more stable than native chymotrypsin to low pH incubation while maintaining bioactivity and mucoadhesion at a range of pH values. The overall goal of the study was to determine which polymer conjugation could be most effective as an enzyme replacement therapy. Specifically, this study was designed to understand the effect of polymer chemical structure in chymotrypsin-polymer conjugates on conjugate mucoadhesion, enzyme bioactivity, and enzyme stability (both bioactivity stability and structural stability). To test the hypothesis, kinetic analysis of CT conjugates, *in vitro* mucoadhesion experiments at different pH values, and residual activity measurements during pH 1 incubation were completed. Additional intrinsic tryptophan fluorescence measurements were used to further examine the effect of polymer choice on the structural stability of chymotrypsin in protein-polymer conjugates.

4.2 Materials and Methods

4.2.1 Materials

All chemicals were purchased at Sigma-Aldrich (St. Louis, MO) and used as received unless otherwise indicated. Poly(ethylene glycol) methyl ether methacrylate (M_n=475) ($OEGMA_{475}$) was filtered through basic alumina column to remove inhibitor prior to use. Me6TREN was synthesized as described previously by Ciampolini and Nardi[110]. Dialysis tubing (molecular weight cut off, 15kDa, Spectra/Por®, Spectrum Laboratories Inc., CA) for conjugate isolation were purchased from Fisher Scientific (Pittsburgh, PA).

4.2.2 Initiator Immobilization onto Chymotrypsin

Synthesis of the ATRP initiating molecules was carried out as described previously[107]. Following synthesis, the initiator molecule (NHS-Br) (469 mg, 1.4 mmol) and CT (1.0 g, 0.04 mmol protein, 0.56 mmol -NH_2 group in lysine residues) were dissolved in sodium phosphate buffer (100 mL, 0.1 M NaPhos (pH 8)). The solution was stirred at 4 °C for 3 hours, and then dialyzed against deionized water, using dialysis tubing with a molecular weight cut off of 15 kDa, for 24 hours at 4 °C and then lyophilized. Initiator immobilization was quantified using matrix assisted laser desorption ionization-time of flight mass spectroscopy (MALDI-TOF-MS) on a PerSeptive Voyager STR MS with nitrogen laser (337 nm) and 20kV accelerating voltage located at the CMA, CMU, Pittsburgh, PA using sinapinic acid as the matrix and a gold sample plate. MALDI-TOF MS instrumentation was supported by NSF grant CHE-9808188.

4.2.3 Surface Initiated ATRP from CT-Br

Chymotrypsin-pOEGMA and chymotrypsin-pSMA were synthesized using CuCl/$CuCl_2$/bpy in deionized water. For CT-pOEGMA, 4.6 mL of a deoxygenated CuCl/$CuCl_2$/bpy stock solution (5mM/45mM/110mM) in DI water was added to 16.4 mL of a

CT-Br (50 mg, 1.4 mM initiator) and $OEGMA_{475}$ (2415 mg, 330 mM, targeted degree of polymerization 225) solution in deoxygenated DI water and allowed to react at 4 °C for 80 minutes. CT-pSMA was synthesized by adding 4.6 mL of stock $CuCl/CuCl_2$/bpy (5 mM/45mM/110 mM) in deoxygenated DI water to 16.4 mL of CT-Br (50 mg, 1.4 mM initiator) and SMA (1190 mg, 285 mM, targeted degree of polymerization 227) in deoxygenated 100 mM NaPhos (pH 7) and allowed to react for 65 minutes at 4 °C. CT-pQA was synthesized by adding 2 mL of CuBr (3.7 mg, 16 mM) and HMTETA (7.4 mg, 16 mM) in deoxygenated DI water to 25 mL of CT-Br (50 mg, 1.4 mM initiator) and QA monomer (405 mg, 64 mM) in 64 mM deoxygenated $NaSO_4$ solution and allowed to react at 25°C for 120 minutes. Lastly, CT-pCBAm was synthesized by adding 5 mL of CT-Br (50 mg, 1.4 mM initiator) and CBAm (348 mg, 332 mM) in deoxygenated 100 mM NaPhos (pH 7) buffer to 2 mL of CuCl (2.5 mg, 12 mM) and Me6TREN (5.5 mg, 12 mM) in deoxygenated DI water and allowed to react for 120 minutes at 4°C. All conjugates were purified using dialysis tubing (MWCO 25 kDa) against DI water for 48 hours at 4°C. Samples were lyophilized and chymotrypsin weight percent in each conjugate was determined using BCA assay.

4.2.4 Molecular Characterization of Conjugates and Polymers

All polymers were cleaved from the surface of CT-polymer conjugates using acid hydrolysis. CT conjugates (15 mg/mL) were incubated in 6N HCl at 110 °C under vacuum for 24 hours. Following incubation, cleaved polymers were isolated from CT using dialysis tubing (MwCO 1K Da) for 48 hours and then lyophilized. Number and weight average molecular weights (M_n and M_w) and the polydispersity index (M_w / M_n) were estimated by gel permeation chromatography (GPC) for polymers cleaved from CT. Analysis was conducted on a Waters 2695 Series with a data processor, using 0.1 M sodium phosphate buffer (pH 7.0) with 0.01

volume % NaN_3 (pOEGMA, pCBAM), 0.1 M sodium phosphate (pH 2.0) with 0.5 % TFA (pQA), or 80% sodium phosphate (pH 9.0)/20% acetonitrile (pSMA) as eluent with at a flow rate 1 mL/min, with detection by a refractive index (RI) detector, and PEG (pOEGMA, pCBAm, pQA) or polystyrene sulfonate (pSMA) narrow standards for calibration.

A Micromeritics (Norcross, GA) NanoPlus 3 dynamic light scattering (DLS) instrument was used to measure the intensity average hydrodynamic diameter (D_h) of each of the chymotrypsin conjugates at 2 mg/mL in 50 mM NaPhos (pH 7) buffer at 25 °C. Histograms of results were plotted after 70 accumulation times, and average D_h values were calculated from these runs.

4.2.5 Polymer *In Vitro* Mucoadhesion

Mucoadhesion of free polymers was evaluated using mucin protein in different buffer systems. Free polymers were synthesized by the same protocol as CT conjugates, but with small molecule initiator instead of chymotrypsin macroinitiator. Polymers were dissolved at 1 mg/mL in different buffers (167 mM HCl (pH 1), 50 mM ammonium acetate (pH 4.5), 50 mM NaPhos (pH 8)) and mixed with mucin protein (3 mg/mL in DI water) at different weight ratios. After mixing, solutions were incubated for 30 minutes at 37°C and absorbance at 400 nm (turbidity) was recorded. Turbidity measurements were plotted as relative ratios to the turbidity measurement at w/w ratio 0.0. For experiments with NaCl and ethanol, polymers were dissolved in buffer solutions with either 0.2 M NaCl, 0.5 M NaCl, or 10% v/v ethanol and then mixed with mucin.

Polymer zeta potential (ζ) measurements were made on a Micromeritics (NanoPlus 3) zetasizer instrument. Free polymers were dissolved at 2 mg/mL in specified buffer solution. Zeta potential values are averages of 4 repeat runs.

4.2.6 CT Conjugate Biocatalytic Activity

N-succinyl-L-Ala-L-Ala-L-Pro-L-Phe-*p*-nitroanilide was used as a substrate for enzyme bioactivity assays. In a cuvette, 0.1 M sodium phosphate buffer (930-990 µL, pH 6,7, or 8), substrate (0-60 µL, 6 mg/mL in DMSO), and enzyme (10 µL, 0.1 mg enzyme/mL 0.1 M pH 8.0 sodium phosphate buffer (4 µM)) were mixed at 37°C using circulating water bath. The rate of the hydrolysis was determined by recording the increase in absorbance at 412 nm for the first 30 seconds after mixing. K_M and k_{cat} values were calculated using Graphpad software with Michaelis-Menten curve fit when plotting substrate concentration versus initial hydrolysis velocity.

4.2.7 *In Vitro* Gastric Acid Stability

Native CT and CT-conjugates were incubated at 4 µM in 167 mM HCl at 37 ° C in 50 µL aliquots. Aliquots were removed at specified time points and residual activity was measured at 37 °C in 0.1 M sodium phosphate buffer (pH 8.0) with Suc-AAPF-*p*NA as substrate (288 µM). Each time point was measured in triplicate and residual activity was calculated as the ratio of activity remaining from time zero.

4.2.8 Intrinsic Tryptophan Fluorescence of CT Conjugates

CT conjugates were incubated at 37 °C in 167 mM HCl (pH 1) at 12 µM CT in 100 µL aliquots for each time point. At the specified time point, samples were diluted to 4 µM using 0.1 M NaPhos buffer (pH 8) and the intrinsic fluorescence was measured in triplicate at 37 °C. Spectrum emission from 300-400nm was measured for each sample after excitation at 270 nm. The wavelength values corresponding to the maximum emission intensity for each measurement were calculated and the average maximum wavelength (λ_{max}) was plotted for each sample.

4.3 Results and Discussion

4.3.1 CT Conjugate Synthesis and Polymer Characterization

To test our hypothesis, four distinct chymotrypsin-polymer biohybrid conjugates were synthesized using "grafting from" polymer-based protein engineering. Each of the four polymers, which represent a different charge state, pCBAm (+-)- zwitterionic with a net neutral charge, pOEGMA- uncharged and neutral, pQA(+)-positively charged, and pSMA(-)-negatively charged, were grown directly from the surface of chymotrypsin using atom transfer radical polymerization (ATRP) (**Figure 4.1**).

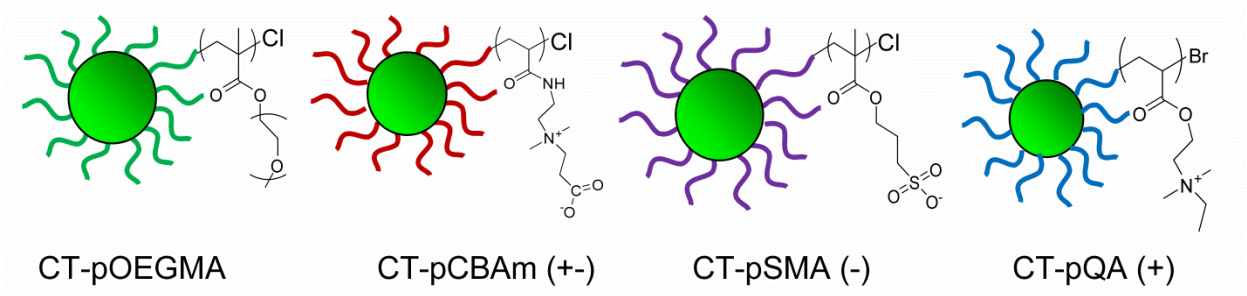

Figure 4.1 Chemical structure of conjugates used in this study CT-pOEGMA, CT-pCBAm (+-), CT-pSMA (-), and CT-pQA (+). Chemical structures of polymers shown at pH 7; when pH<4.5, the carboxylic acid in pCBAm is protonated and pCBAm has an overall positive charge. All other polymers have no pH dependence.

Polymers were grown from 12 ATRP initiators (as calculated by MALDI-TOF-MS, **Figure 2.1**) covalently attached to surface accessible lysines via NHS-ester/amine chemistry. Successful polymerization from chymotrypsin was confirmed using dynamic light scattering (DLS), and each chymotrypsin-polymer conjugate had a similar increase in hydrodynamic diameter (D_h) (**Figure 4.2**) compared to native chymotrypsin (5.7 ± 2 nm). To characterize polymers grown from chymotrypsin, the polymers were cleaved from the surface of chymotrypsin using acid hydrolysis in 6N HCl. Polymer molar mass was calculated using SE-

HPLC, and the molar mass values for polymer correlated well with hydrodynamic diameters measured by DLS. (Table 4.1)

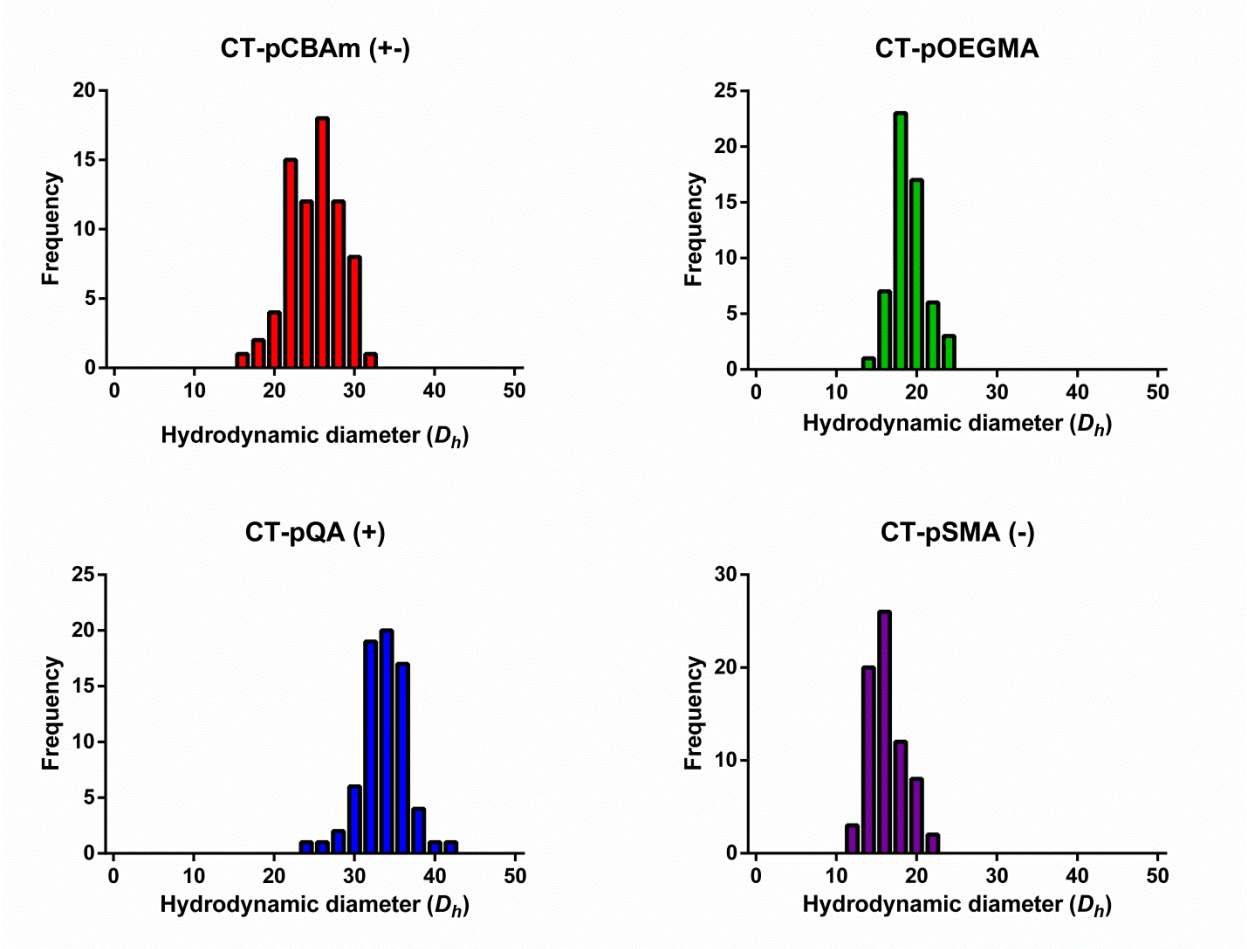

Figure 4.2 Chymotrypsin-polymer size increased compared to native CT after polymer modification. CT-pCBAm(+-) (26.3 ± 3.2 nm), CT-pOEGMA (20.1 ± 2.0 nm), CT-pQA(+) (34.5 ± 2.9 nm), and CT-pSMA (-) (17.2 ± 2.2 nm) hydrodynamic diameter values were measured by dynamic light scattering (DLS) in 50 mM sodium phosphate (pH 7.0, 25 °C). Each conjugate had a similar increase in D_h compared to native chymotrypsin D_h (5.7 ±2 nm).

Table 4.1 Molecular weight and hydrodynamic diameter of chymotrypsin conjugates

		Cleaved Polymer		Conjugate	
	Cu/Ligand Pair	**M_n (kDa)**	**PDI (M_w/M_n)**	**Molar Mass (kDa)**	**Size (D_h) [nm]**
CT-pCBAm (+-)	CuCl:Me6TREN	30.7	1.90	393	26.3 ± 3.2
CT-pOEGMA	CuCl:$CuCl_2$:bpy	11.6	1.46	165	20.1 ± 2.0
CT-pQA (+)	CuBr:HMTETA	19.1	2.10	254	34.5 ± 2.9
CT-pSMA(-)	CuCl:$CuCl_2$:bpy	9.6	1.43	140	17.2 ± 2.2

4.3.2 *In Vitro* Mucoadhesion of CT Conjugate Polymers

Polymer mucoadhesion is a facile way to increase residence time of drug delivery payloads in the GI tract. In order to examine the *in vitro* mucoadhesive properties of each of the polymers conjugated to chymotrypsin, the turbidities of solutions were measured after incubating polymers at different w/w ratios with mucin protein at 37 °C in 167 mM HCl (pH 1), 50 mM ammonium acetate (pH 4.5), and 50 mM sodium phosphate (pH 8), corresponding to the pH conditions seen along the GI tract. Increased turbidity was due to the increased size of mucin colloidal suspensions which was the result of polymer-mediated mucin particle crosslinking[88]. pQA (+) showed mucoadhesive properties at each of the tested pH values, pCBAm mucoadhesion was dependent on the pH, and pSMA (-) and pOEGMA were not mucoadhesive at any of the tested pH values (**Figure 4.3a-c**).

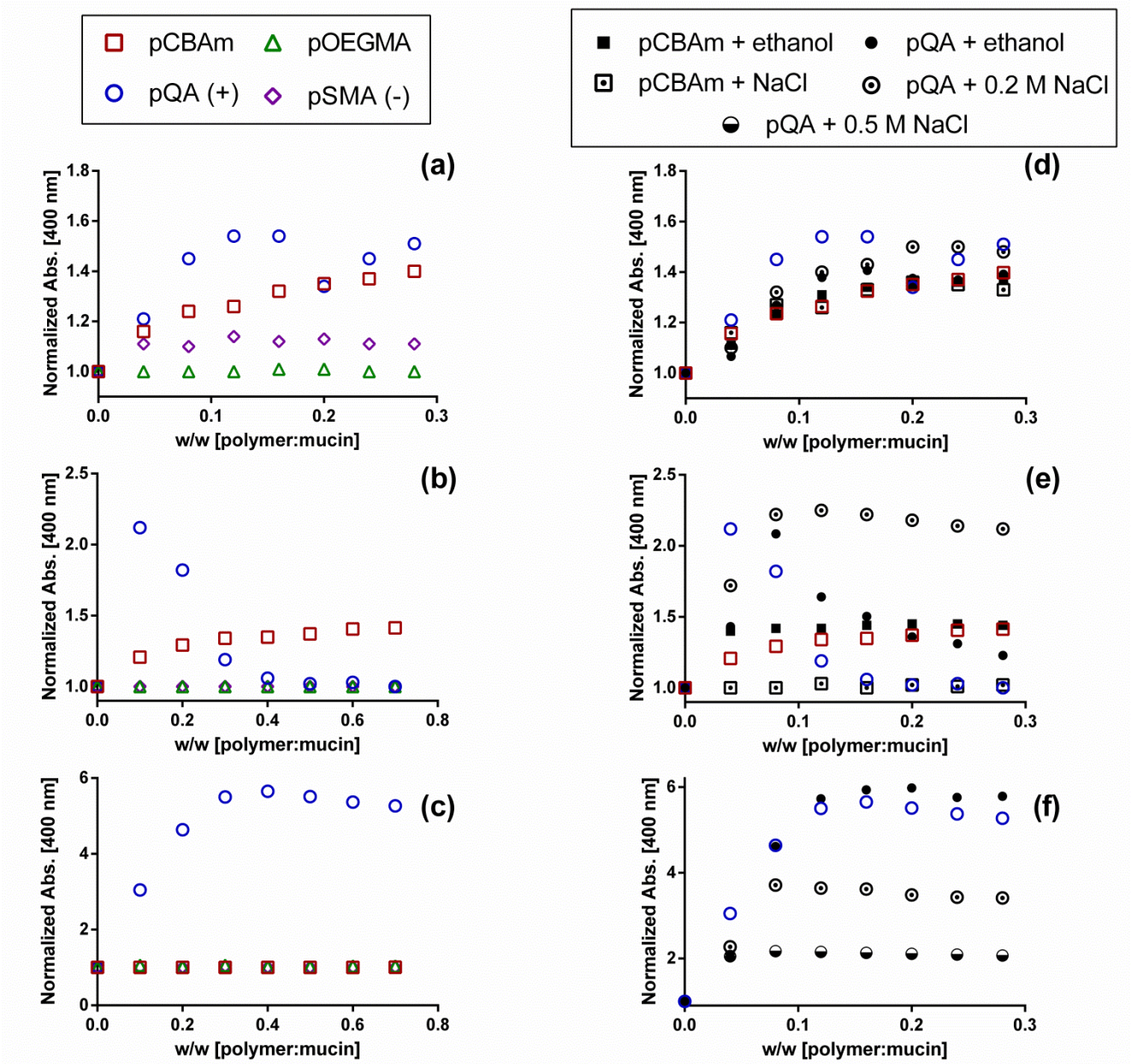

Figure 4.3 Mucoadhesion of polymers grown from CT was dependent on pH and polymer. (a) 167 mM HCl (pH 1), (b) 50 mM ammonium acetate (pH 4.5), (c) 50 mM sodium phosphate (pH 8), (d) 167 mM HCl with 10% ethanol or 0.2 M NaCl, (e) 50 mM ammonium acetate with ethanol or NaCl, and (f) 50 mM sodium phosphate with 10% ethanol, 0.2 M NaCl, or 0.5 M NaCl. Normalized absorbance at 400 nm (turbidity) at 37 °C was used as a marker for mucoadhesion between free polymer and mucin protein.

Driven by the association of polymeric materials with mucin protein secreted by goblet cells in the lining of the GI tract, mucoadhesion *in vivo* is classically thought of being due to electrostatic attractions, hydrogen bonding, or hydrophobic interactions.[86] Sialic acid, a major component in mucin, is a polysaccharide with carboxylic acid functionality giving mucin a net negative charge at neutral pH.[183] Since positively charged pQA (+) increased turbidity at each pH, we hypothesized that electrostatic interactions were the main driving force for pQA (+) mucoadhesion. To test the hypothesis, further turbidity experiments were completed for mucoadhesive polymers, but with the addition of NaCl or ethanol. If mucoadhesion was mainly caused by electrostatic attraction, then the turbidity profiles should be affected by the addition of NaCl, but if hydrophobic interactions were the main driving force, then doping with ethanol would induce a change in turbidity. Both pCBAm and pQA (+) mucoadhesion were unaffected by the addition of ethanol, but dependent on the introduction of NaCl (**Figure 4.3d-f**). From these results, it was clear, not surprisingly, that the mucoadhesion of pQA (+) (at every pH) and pCBAm (at low pH) polymers was due to electrostatic attraction of positively charged polymers with negatively charged mucin. In order to further confirm this hypothesis, the zeta potentials of free polymers and mucin were measured at each pH (**Table 4.2**). Indeed, the zeta potential values of each of the polymers correlated well with electrostatic interactions being responsible for the behavior seen in the *in vitro* mucoadhesion experiments. As an uncharged polymer, pOEGMA did not show mucoadhesive properties at any of the pH values tested. This result was not surprising, as pOEGMA is commonly shown as not having mucoadhesive properties.[88] Predictably, pSMA (-) was also not mucoadhesive, likely due to electrostatic repulsion of the negative charge in the polymer and negatively charged mucin.

Table 4.2 Zeta potential (ζ) measurements of free polymer in mucoadhesive relevant solutions

	Zeta potential (ζ) [mV]				
	Mucin	**pCBAm**	**pOEGMA**	**pQA (+)**	**pSMA (-)**
50 mM Citric acid (pH 2.3)	0.7 ± 0.4	15 ± 6	1.9 ± 0.6	34 ± 10	-22 ± 3.6
50 mM (NH_4^+) acetate (pH 4.5)	-3.6 ± 0.5	0.3 ± 0.4	2.9 ± 2.3	29 ± 5.9	-25 ± 2.6
50 mM NaPhos (pH 8.0)	-7.1 ± 0.7	-2.0 ± 1.8	1.2 ± 4.5	7.8 ± 4.0	-22 ± 5.1

While it was clear that pQA (+) and pCBAm did indeed have mucoadhesive properties, several unexpected and interesting trends resulted for these polymers. The pH responsive behavior of pCBAm was likely due to the ionization state of the carboxylic acid in the polymer at each of the test pH values. In highly acidic conditions (pH 1), protonation occurred in pCBAm, resulting in a net positive charge. However, at pH 4.5 and pH 8, no mucoadhesion was observed for pCBAm due to deprotonation and a net neutral charge. While pQA (+) was mucoadhesive at each pH tested, the normalized absorbance values after incubation for pQA (+) polymers were much higher at pH 8 compared to both pH 1 and pH 4.5. This result was likely due to the reduced number of negatively charged crosslinking sites in mucin at pH 1. As described earlier, carboxylic acid functionality is responsible for the negative charge in mucin, so it was not surprising to see less of a crosslinking effect at low pH values. Interestingly, at pH 4.5, pQA (+) normalized turbidity initially increased before returning to baseline levels at 0.3 w/w ratios. At this pH, it was likely that, at higher ratios of pQA (+), the polymer fully encapsulated mucin particles rather than crosslink between particles, resulting in solubilization and lower turbidity.

These results indicate that, as a potential chymotrypsin enzyme replacement therapy, strictly based on mucoadhesion, the CT-pQA (+) conjugates would be the best candidate of the four conjugates. Since the pH optimum for chymotrypsin activity is pH 8, the ideal situation

would see CT polymer conjugates with the longest residence time in the small intestine. While pCBAm polymers did increase turbidity in low pH solutions, chymotrypsin is unfortunately not active at this low pH, which makes CT-pCBAm a less attractive option compared to CT-pQA (+) when considering only mucoadhesive properties. Other properties to consider that may help to hypothesize which conjugate may be most useful as a complete enzyme replacement therapy include the activity and stability at a range of pH values.

4.3.3 Effect of Polymer Structure on Chymotrypsin Bioactivity

Bioactivity kinetic constants for CT conjugates were calculated using the small molecule substrate, *N*-succinyl-Ala-Ala-Pro-Phe-*p*-nitroanilide, in 100 mM sodium phosphate buffer (pH 6-8) at 37 °C. Conjugate activity was dependent on the covalently attached polymer in the protein-polymer biohybrid (**Figure 4.4**). Relative k_{cat} values for each conjugate were independent of pH, and were all decreased compared to native chymotrypsin. CT-pSMA (-) and CT-pOEGMA activity values were both less than half that of native chymotrypsin, while CT-pQA (+) and CT-pCBAm maintained approximately 70% of native chymotrypsin activity after modification. A reduction in k_{cat} is often seen for enzyme-polymer conjugates and has been hypothesized to be due to a structural stiffening of the enzyme.[114] This result was not surprising as a decrease in relative k_{cat} values was also seen for CT-pSBAm-*b*-pNIPAM conjugates (**Figure 3.6**). Still, the decrease in activity for CT-pSMA (-) and CT-pOEGMA was larger than expected and could be due to interactions between the polymers and chymotrypsin. A large increase in substrate affinity was seen for CT-pQA (+) conjugates, as evidenced by the decrease in K_M values. CT-pOEGMA showed slightly lower substrate affinity and CT-pCBAm showed similar substrate affinity to native chymotrypsin, but both conjugates displayed relative K_M values independent of pH. Interestingly, CT-pSMA (-) relative K_M values were dependent on

pH. Indeed, substrate affinity was greatly decreased at pH 6 for CT-pSMA (-), but was similar to native chymotrypsin at pH 7 and pH 8. The K_M effects for CT-pSMA (-) and CT-pQA (+) were most likely due to electrostatic repulsion and attraction, respectively, between the polymer coat around chymotrypsin and the substrate. As a negatively charged substrate molecule, the affinity of the substrate for chymotrypsin has previously been shown to be affected by polymer conjugation.[184] Mostly due to K_M effects, CT-pQA (+) exhibited higher productivity (k_{cat}/K_M) values than native chymotrypsin at each pH. Conversely, both CT-pSMA (-) and CT-pOEGMA productivities were lower than native chymotrypsin at each pH, and CT-pCBAm conjugates showed similar productivity to native chymotrypsin at each pH.

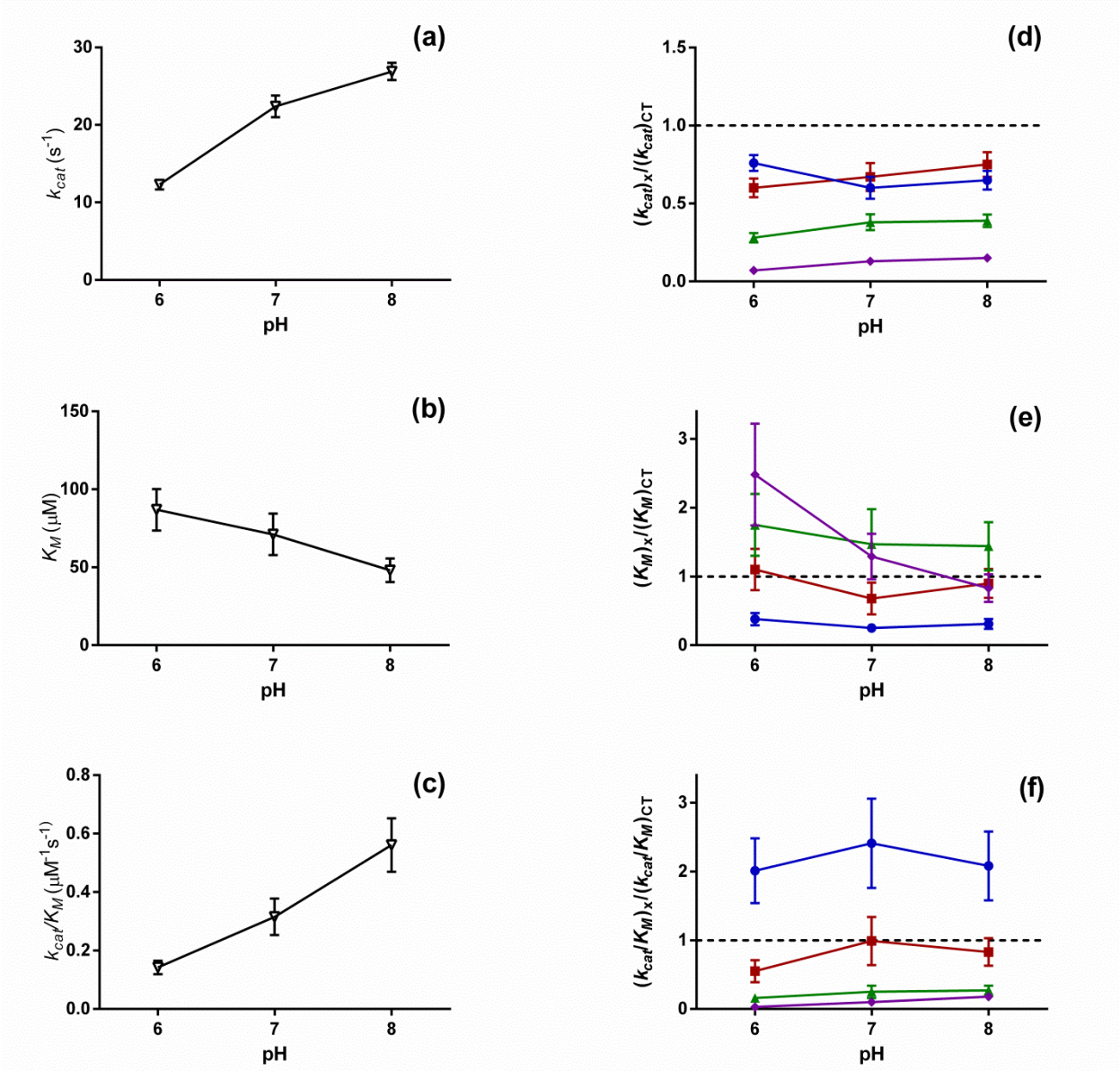

Figure 4.4 Dependence of chymotrypsin and chymotrypsin conjugate kinetic values on pH. Kinetic constants (a) k_{cat}, (b) K_M, and (c) k_{cat}/K_M were measured for native chymotrypsin (black open upside down triangle) from pH 6-8 at 37 °C in 100 mM sodium phosphate buffer. Relative kinetic constants (d) k_{cat}, (e) K_M, and (f) k_{cat}/K_M were calculated for CT-pSMA (purple diamond), CT-pOEGMA (green triangle), CT-pQA (blue circle), and CT-pCBAm (red square) in the same conditions and plotted relative to native chymotrypsin.

4.3.4 Effect of Polymer Chemical Structure on CT Low pH stability

The stability of the CT conjugates to low pH conditions was assessed by incubating conjugates in 167 mM HCl at 37 °C for one hour and measuring residual activity at specified time points. (**Figure 4.5a)** Similar to activity, the stability of CT conjugates was dependent on the polymer attached to chymotrypsin. Both CT-pCBAm (+, positive at low pH) and CT-pQA (+) were more stable than native chymotrypsin, with stability profiles similar to what was seen for previously reported CT-pSBAm[185] and CT-pQA conjugates[186]. However, CT-pOEGMA and CT-pSMA (-) both lost activity quicker than native chymotrypsin, indicating that both pOEGMA and pSMA (-) had a destabilizing effect on chymotrypsin. Interestingly, native chymotrypsin with free pQA (+) or pCBAm (+) polymers was not more stable than native chymotrypsin to pH 1 degradation, indicating that the covalent attachment of polymers is necessary for increased stability. (**Figure 4.5b)** Incubation of native chymotrypsin with pSMA (-) free polymers actually decreased activity compared to native chymotrypsin, confirming the destabilization effect of pSMA (-) towards chymotrypsin. Conversely, while CT-pOEGMA conjugates showed similar low stability to CT-pSMA (-) conjugates when incubated in 167 mM HCl, native chymotrypsin incubated with free pOEGMA had a similar stability profile to native chymotrypsin, chymotrypsin with pQA (+), and chymotrypsin with pCBAm (+). This result indicates that the mechanism of destabilization in CT-pOEGMA conjugates is likely different from CT-pSMA (-) conjugates. Indeed, it is possible that a much higher concentration of pOEGMA is needed to destabilize chymotrypsin compared to pSMA (-).

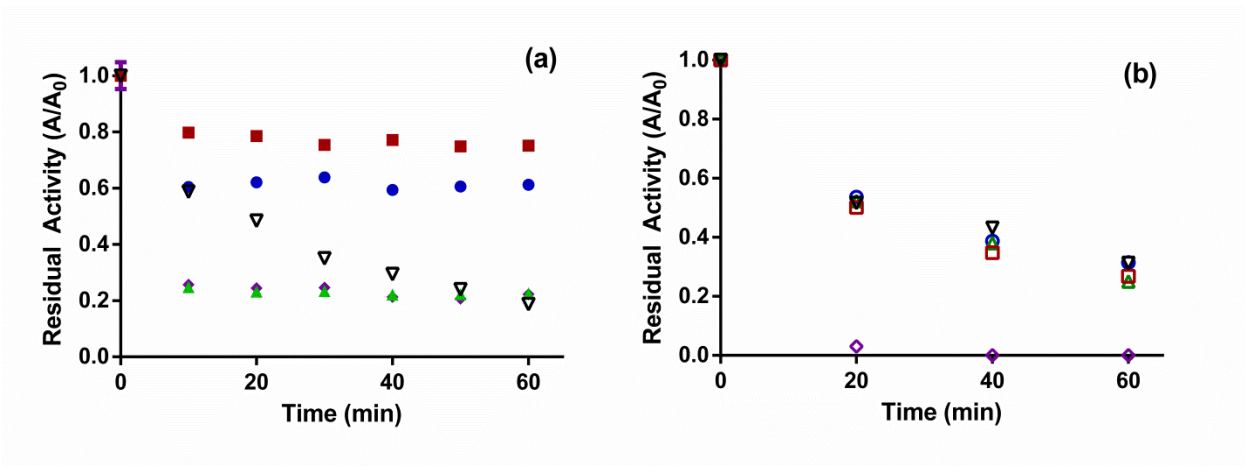

Figure 4.5 Dependence of chymotrypsin irreversible inactivation on polymer. (a) Native chymotrypsin (black upside down triangle), CT-pCBAm (red square), CT-pOEGMA (green triangle), CT-pQA (+) (blue circle), CT-pSMA (-) (purple diamond) were incubated in 167 mM HCl at 37 °C. (b) Native CT (black upside down triangle) was incubated with pOEGMA (green triangle), pCBAm (red square), pSMA (-) (purple diamond), and pQA (+) (blue circle) free polymers. Activity assays were completed using 288 µM substrate (*NS*-AAPF-pNA) in 100 mM sodium phosphate (pH 8.0) at 37 °C.

While different stability profiles were observed for each of the conjugates, it was still not clear whether the modified stability profiles were due to chymotrypsin structural changes or enzymes autolysis. In order to correlate residual activity values with protein structural data, intrinsic tryptophan fluorescence was measured for each of the conjugates. (**Figure 4.6**)

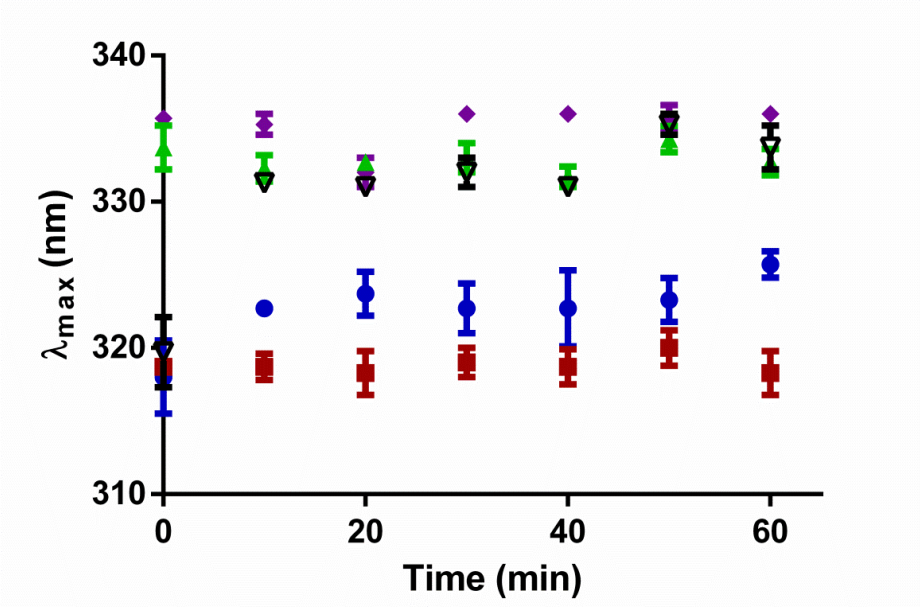

Figure 4.6 Dependence of chymotrypsin structural stability on polymer chemical structure in chymotrypsin-polymer conjugates. Tryptophan intrinsic fluorescence wavelength of maximum emission intensity values (λ_{max}) after incubation in 167 mM HCl (pH 1) at 37°C for native chymotrypsin (black upside down triangle) and chymotrypsin conjugates; CT-pCBAm (red square), CT-pOEGMA (green triangle), CT-pQA (+) (blue circle), CT-pSMA (-) (purple diamond). An increase in λ_{max} indicates protein unfolding.

The degree of protein unfolding was monitored by measuring maximum wavelength of fluorescence emission (λ_{max}) for each of the conjugates. Each CT conjugate was incubated in 167 mM HCl and fluorescence emission spectrum was measured from 300-400 nm after excitation at 270 nm. Native chymotrypsin λ_{max} increased from 320 nm prior to incubation up to 334 nm at 60 minutes. This result was expected as native chymotrypsin has been previously shown to structurally denature due to the low pH, and an increase in λ_{max} values is correlated with structural unfolding.[187, 188] Not surprisingly, both CT-pSMA (-) and CT-pOEGMA had increased lambda max values compared to native chymotrypsin starting at t=0 min. Conversely, CT-pQA (+) had increased λ_{max} values over the course of the experiment, but the increase was

not as large in magnitude as native chymotrypsin indicating more structural stability for CT-pQA (+). CT-pCBAm (+) conjugates showed the least amount of unfolding during this experiment as the λ_{max} remained almost unchanged during the course of the experiment. From this experiment, it was clear that the loss in activity for both CT-pOEGMA and CT-pSMA (-) conjugates was due to structural unfolding and not enzyme autolysis. The results of the intrinsic fluorescence experiments correlated well with residual activity measurements where both CT-pQA (+) and CT-pCBAm (+) were more stable than native chymotrypsin, but CT-pCBAm (+) had higher activity during the course of the experiment. In addition, both CT-pSMA (-) and CT-pOEGMA lost activity quickly during residual activity experiments, and this reduced activity coincided with a large increase in λ_{max} values during intrinsic fluorescence experiments.

While it was clear from both residual activity and intrinsic fluorescence experiments that chymotrypsin structural stability was dependent on the choice of polymer attached to the enzyme, it was still not clear why these polymers reduced the activity of chymotrypsin. Interestingly, anionic nanoparticles have previously been shown to inhibit the activity of chymotrypsin and promote structural unfolding.[189] In that work, it was hypothesized that the anionic nanoparticles selectively associated with a cationic core of amino acid residues around the chymotrypsin active site. In addition, the authors hypothesized the hydrophobic nature of the nanoparticles also led to detrimental effects on chymotrypsin stability and activity due to a region of hydrophobic residues also near the active site. Of course, of the destabilizing polymers used in this study, one was negatively charged (pSMA) (-) and the other was amphiphilic (pOEGMA). While the inhibition and destabilizing properties of negatively charged molecules seemed to be conserved in this study, the surface charge of initiator modified chymotrypsin (CT-Br) must be considered rather than native chymotrypsin. Indeed, a large amount of positive

surface area was lost when modifying ATRP initiator onto surface lysine residues, which commonly bear a positive charge in native chymotrypsin at neutral pH. However, from molecular dynamic simulations of CT-Br at pH 7, it was clear that there is still a region of positive charge near the active site which may be responsible for specific interactions with the conjugated polymers.(**Figure 4.7**) In addition, at pH 1 where the stability experiments were conducted for this study, CT-Br bore a global positive surface charge.

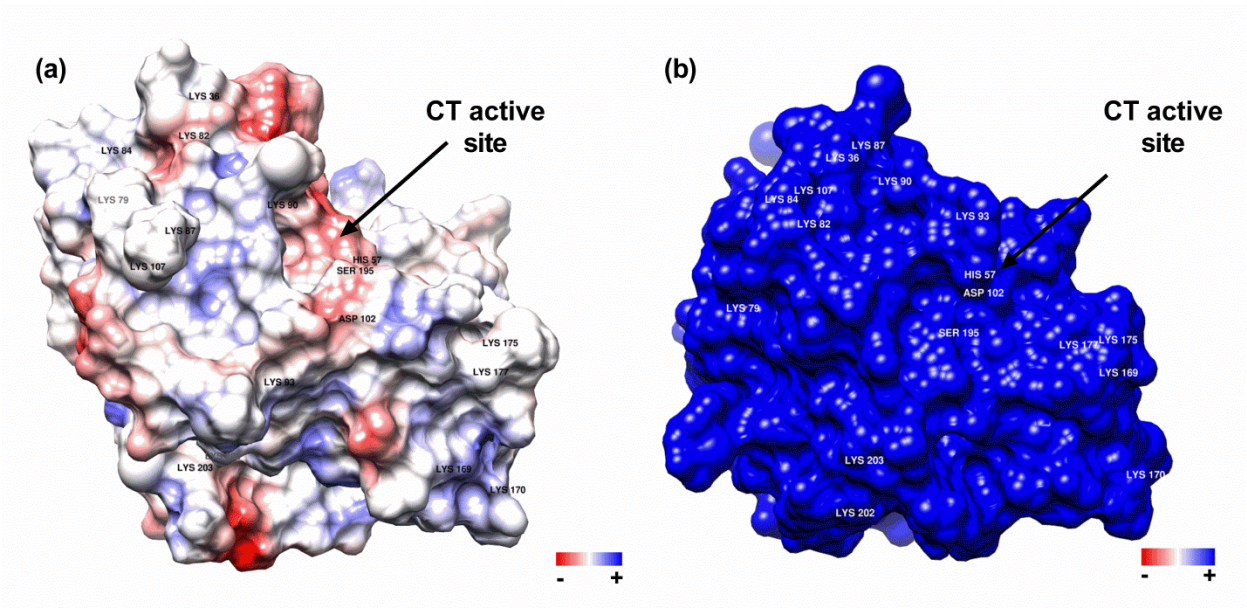

Figure 4.7 Electrostatic potential coulombic surface coloring for CT-Br. Molecular dynamic simulations were completed for CT-Br at (a) neutral pH and (b) pH 1. Molecular dynamics simulations were run and subsequent figures were made by Sheiliza Carmali, and graciously adapted for this dissertation.

Classically, it has been observed that denaturing osmolytes (urea, guanidine hydrochloride) preferentially accumulate at the protein surface, whereas stabilizing osmolytes (TMAO, betaine) are preferentially excluded from the surface.[190] This preferential accumulation or exclusion of osmolytes is due either to specific interactions of the osmolytes with the protein or a global change of water structure.[191] In any case, stabilizing osmolytes

result in a stronger hydration layer which strengthens protein structural stability, and denaturing osmolytes displace water molecules in the hydration layer causing lower stability.[192] In this work, we hypothesized that pQA (+) and pCBAM (+) stabilized chymotrypsin to low pH structural unfolding through preferential exclusion of the polymer from chymotrypsin surface. (**Figure 4.8**) Since polymer interactions with chymotrypsin were thermodynamically unfavorable, the water hydration layer was strengthened increasing structural stability. In addition, we hypothesized that pSMA (-) and pOEGMA destabilized chymotrypsin through preferential interaction. Indeed, we hypothesized the negatively charged and amphiphilic polymers interacted with chymotrypsin's surface resulting in displacement of water from the hydration layer, and lowering structural stability. The preferential exclusion was hypothesized to be due to electrostatic repulsion between positively charged polymers and the positive surface of chymotrypsin at low pH. Conversely, we hypothesized electrostatic attraction was responsible for pSMA (-) binding and hydrophobic effects contributed for pOEGMA. We are interested in the specific origins of these interactions (specific amino acid, protein backbone, etc.) and plan to determine the origin with future experimentation.

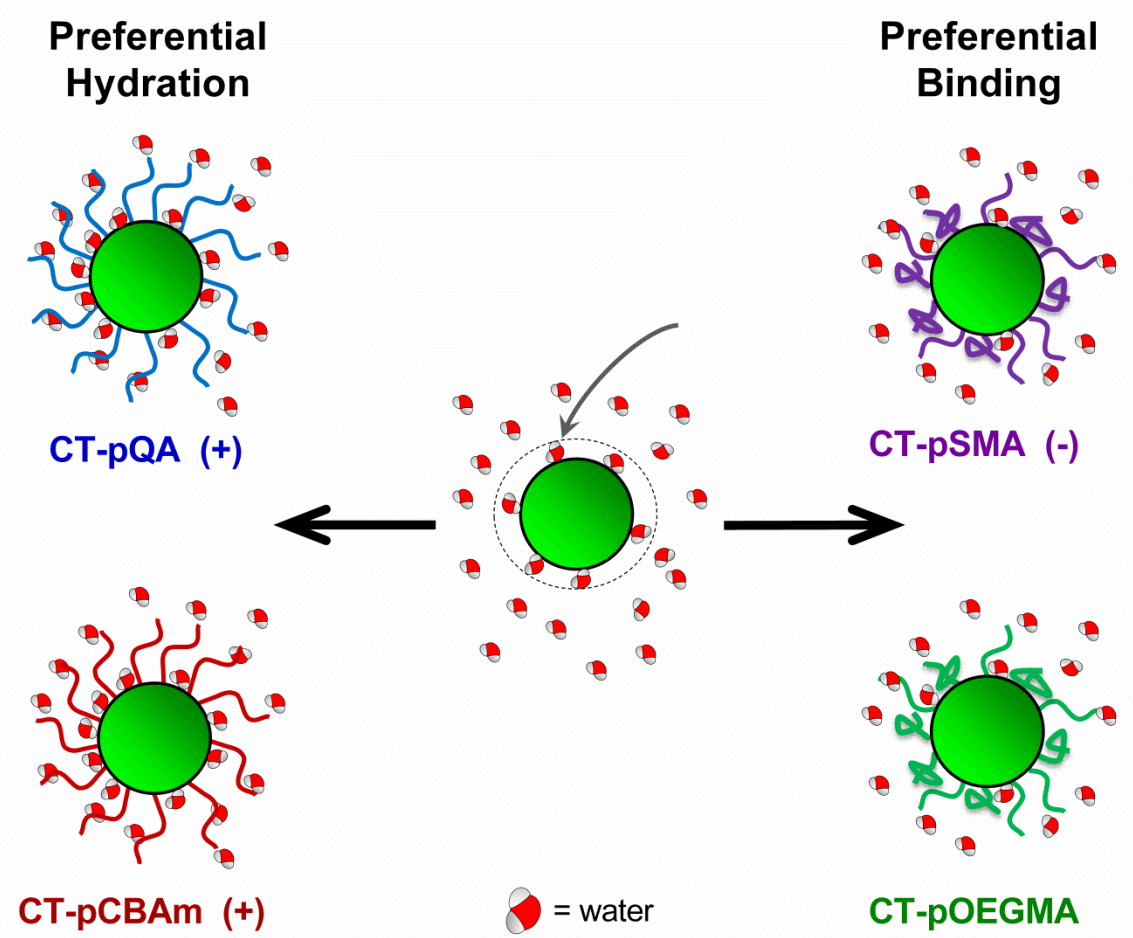

Figure 4.8 Hypothesized effect of polymer conjugation on hydration shell of chymotrypsin. For CT-pSMA(-) and CT-pOEGMA, the polymers interacted with chymotrypsin, displacing water molecules via preferential binding which resulted in a decrease in stability. Conversely, CT-pQA (+) and CT-pCBAm(+) were excluded from chymotrypsin due to unfavorable interactions between polymer and protein, resulting in preferential hydration which increased stability to strongly acidic conditions.

4.4 Conclusion

In this study, four different chymotrypsin-polymer conjugates were synthesized using surface initiated ATRP polymer-based protein engineering. The four conjugates, CT-pCBAm, CT-pOEGMA, CT-pQA (+), and CT-pSMA (-), each had different mucoadhesive, bioactivity, and stability profiles. CT-pQA (+) and CT-pCBAm conjugates were mucoadhesive and

maintained bioactivity at all pH values tested, whereas CT-pOEGMA and CT-pSMA (-) were not mucoadhesive and had reduced activity. Most importantly, CT-pQA (+) and CT-pCBAm conjugates stabilized chymotrypsin, whereas CT-pSMA (-) and CT-pOEGMA destabilized the enzyme to the low pH structural denaturation. We hypothesized that the different stabilization properties were due to preferential accumulation of the destabilizing polymers and preferential exclusion of the stabilizing polymers at the enzyme surface. This accumulation and exclusion likely influenced the integrity of the surface hydration layer which led to structural destabilization and stabilization, respectively. It was predicted but not proven that the stabilization profiles imparted by the polymer could be applicable for other enzymes in low pH as well. Due to their increased stability and maintained activity, CT-pCBAm and CT-pQA (+) would be better candidates than CT-pOEGMA or CT-pSMA (-) as an exogenous chymotrypsin enzyme replacement therapy.

Chapter 5 : Piperazine Modified Protein Conjugates Synthesized using Polymer-Based Protein Engineering Enable *in vitro* Protein Transport across Cell Monolayers

5.1 Introduction

Food and Drug Administration (FDA) approval of protein based therapeutics has steadily increased over the past 25 years due to the increased knowledge of protein's roles in biological pathways and increased protein production capacities.[193] As a result of these advancements, research and development of protein therapeutics is as common as ever. Indeed, hundreds of protein-based therapeutics are currently approved by the FDA[194, 195] and future approval of protein based drugs is expected to increase.[196] While promising, the requirement for parenteral delivery is the biggest drawback to protein therapeutics. Most commonly, protein therapeutics are delivered *via* subcutaneous or intravenous injection, routes of administration that both require needles. Alternative delivery routes that have been explored include pulmonary,[197] transdermal,[198] ocular,[199] rectal,[200] intranasal,[201] vaginal,[202] and buccal[203]. While some of these alternative approaches have had clinical success, the oral delivery route would be preferred due to its ease of administration and ability to treat conditions throughout the body. The most obvious benefit of orally delivered proteins would be patient compliance. With intravenous or subcutaneous delivery routes, the requirement for needles, acute injection site reactions, and hospital visits cause patient hesitation and medication nonadherence. However, the low absorption efficiency of biological macromolecules across the intestinal mucosa has largely prevented the development of successful oral delivery strategies for protein drugs.[204]

Some of the most commonly used strategies to increase the bioavailability of proteins delivered *via* the oral route include enteric coated capsules,[205, 206] mucoadhesive systems,[207] specific cell targeting,[208] and chemical permeation enhancers.[83] A wide variety of chemical permeation enhancers, including fatty acids,[209, 210] surfactants,[211] or

lipophilic small molecules,[212] have been shown previously to increase the permeation of protein macromolecules across epithelial barriers. Chemical permeation enhancers work by interacting with the cellular lining of epithelial barriers, and increase transport *via* the paracellular route, by modifying the integrity of the tight junctions between cells in the epithelial layer, or via the transcellular route, by disrupting the epithelial cell membrane.[213] Piperazines, which are six membered rings with two opposing nitrogen molecules, are a specific class of permeation enhancers that increase permeation of protein macromolecules across both intestinal and skin barriers.[214, 215] Specifically, 1-phenyl piperazine (PPZ) is a piperazine derivative that has previously been shown to be an effective chemical permeation enhancer.[216] At relevant concentrations, PPZ increased the transport of large marker molecules dextran and mannitol while not inducing cell toxicity. Recently, 1,4-substituted piperazine molecules were shown to be similarly effective at increasing permeability while not inducing cell toxicity.[217]

While effective, one large drawback to chemical permeation enhancers is the global effect they have on the epithelium. In order for chemical permeation enhancers to have low toxicity, their effect must be both transient and local. However, when used to enhance permeability, chemical permeation enhancers are often only in solution with the macromolecule of interest. Indeed, there is no association, non-covalent or covalent, between chemical permeation enhancer and macromolecule. Thus, the toxicity potential of chemical permeation enhancers is sometimes high, because there is no bias to what passes across disrupted membranes. While the permeation of the macromolecule increases, the permeation of unwanted molecules, both large and small, is also increased, which leads to acute toxicity. With that thought in mind, polymer-based protein engineering was used to synthesize protein-chemical permeation enhancer conjugates with increased transport across epithelial barriers with low cell

toxicity. A novel 1-phenyl piperazine acrylamide monomer (PPZ), able to be polymerized in aqueous conditions using atom transfer radical polymerization (ATRP), was synthesized to incorporate directly into the protein-polymer conjugate. Poly(phenyl piperazine acrylamide) (pPPZ) polymer was chain extended from bovine serum albumin-poly(oligo ethylene glycol methacrylate) (BSA-pOEGMA) homopolymer conjugates using "grafting from" ATRP. pOEGMA was chosen as it is generally considered to be biocompatible and possesses beneficial *in vivo* properties.[44] 1-Phenyl piperazine was chosen due to its favorable efficacy and toxicity profiles, and BSA was chosen as a macromolecule model that is as large (66kDa) as many therapeutically relevant proteins. We hypothesized that the covalent attachment of the chemical permeation enhancer directly to the protein of interest would result in a localized effect of permeability, which would lead to permeation of BSA across an *in vitro* model of the intestinal epithelium. To test the hypothesis, trans-epithelial electrical resistance (TEER) measurements with colorectal adenocarcinoma (Caco-2) monolayers on trans-well plates were used to quantify the permeability of monolayers incubated with BSA-pOEGMA-*b*-pPPZ conjugates. Calcein, a small molecule fluorescent marker, and FITC labeled conjugates were used to assess the permeation of small and large molecules, respectively, across the Caco-2 monolayers.

5.2 Materials and Methods

5.2.1 Materials

All chemicals were used as received unless otherwise indicated. Poly(ethylene glycol) methyl ether methacrylate (M_n=475) ($OEGMA_{475}$) was filtered through basic alumina column to remove inhibitor prior to use. Me6TREN was synthesized as described previously by Ciampolini and Nardi[110]. Dialysis tubing (molecular weight cut off, 15kDa, Spectra/Por®, Spectrum

Laboratories Inc., CA) for conjugate isolation were purchased from Fisher Scientific (Pittsburgh, PA).

5.2.2 Synthesis of BSA-pOEGMA-*b*-pPPZ

BSA-pOEGMA-*b*-pPPZ conjugates were synthesized using surface initiated dual block atom transfer radical polymerization (ATRP). Prior to polymerization, three different BSA-Br macroinitiator conjugates with different number of initiators per molecule were synthesized by mixing BSA (500 mg, 0.46 mmol $-NH_2$) with different ratios of NHS-Br (BSA_{40}-463 mg, 0.14 mmol; BSA_{25}-154 mg, 0.46 mmol; BSA19-92 mg, 0.28 mmol) for 3 hours at 25 ^{0}C in 100 mM NaPhos buffer (pH 8). Unreacted NHS-Br was removed using dialysis (MWCO 15kDa) against DI water, and the degree of initiator modification was quantified using matrix assisted laser desorption ionization time of flight mass spectrometry (MALDI-TOF-MS) for each of the BSA-Br macroinitiators. BSA nomenclature indicates the number of ATRP initiating molecules on BSA-Br macronitiator. To synthesize BSA-pOEGMA-Cl conjugates, a stock solution of 5mM CuCl/45 mM $CuCl_2$/110 mM bpy (7.6 mL for BSA_{19}, 8 mL for BSA_{25}, 7 mL for BSA_{40}) in deoxygenated deionized (DI) water was added to a BSA-Br macroinitiator (BSA_{19}-140 mg, BSA_{25}-115 mg, BSA_{40}-70 mg)/OEGMA475 (BSA_{19}-1.872 g, BSA_{25}-1.967 g, BSA_{40}-1.695 g,) solution in deoxygenated DI water (BSA_{19}-47 mL, BSA_{25}-40 mL, BSA_{40}-25 mL) and allowed to react for 45 minutes at 30 ºC. Molar concentrations of reactants, catalyst, and ligand were selected to have I:CuCl:$CuCl_2$:bpy:OEGMA molar ratios of 1:1:9:22:102 with a constant BSA concentration of 30 μM. Reaction time was selected to target an expected degree of polymerization of 25. At the end of the reaction, copper catalyst, ligand, and unreacted monomer were removed using dialysis against DI water at 25ºC for 48 hours and the BSA-pOEGMA-Cl

conjugate was lyophilized. Weight percent of BSA in the lyophilized BSA conjugate was measured using BCA assay.

Poly(phenyl piperazine acrylamide) pPPZ chain extension using ATRP from BSA-pOEGMA was completed by adding a deoxygenated BSA-pOEGMA(115 mg BSA_{19}, 88 BSA_{25}, 55 mg BSA_{40})/PPZ monomer (114 mg for BSA_{19}, 169 mg for BSA_{25}, 240 mg for BSA_{40}) solution in 50 mM sodium phosphate (pH 7.0) to 3 ml of deoxygenated CuCl (2.5 mg for BSA_{19}, 3.7 mg for BSA_{25}, 3.5 mg for BSA_{40}), $CuCl_2$(1.4 mg for BSA_{19}, 2 mg for BSA_{25}, 1.9 mg for BSA_{40}), and Me6TREN (9.5 µL BSA_{19}, 14.1 µL BSA_{25}, 13.3 µL BSA_{40}) and allowed to react for 18 hours at 4ºC. These reaction conditions were chosen to have a 1:1.2:0.5:1.7:20 molar ratio of initiator:CuCl:CuCl2:Me6TREN:monomer with a constant BSA concentration of 65 µM.[218] Unreacted monomer, catalyst, and ligand were removed using dialysis filtration (MWCO 15kDa) against DI water for 48 hours and BSA-pOEGMA-*b*-pPPZ was lyophilized. Weight percent of BSA in the lyophilized BSA conjugate was measured using BCA assay.

5.2.3 Analytical Characterization of Conjugates and Cleaved Polymers

BSA-pOEGMA-Cl homopolymer conjugates were analyzed using size exclusion high pressure liquid chromatography (SE-HPLC) using 0.1 M sodium phosphate (pH 7.0) as the eluent using UV absorbance at 280 nm to detect conjugates.

The pPPZ second block M_n was determined by measuring NMR spectra of BSA-pOEGMA-*b*-pPPZ on a 300 MHz Bruker Avance instrument in deuterium oxide. pPPZ M_n was calculated by comparing the integration of characteristic peaks for phenyl piperazines (~7.0 ppm) protons to the characteristic peaks in the pOEGMA block (~4.2 ppm). M_n for pOEGMA homopolymer was calculated from SE-HPLC after acid hydrolysis of pOEGMA block from BSA-pOEGMA. PEG narrow dispersity polymer standards were used as the calibration standard.

Hydrodynamic diameter (D_h) values for the BSA-pOEGMA homopolymer and BSA-pOEGMA-*b*-pPPZ conjugates were measured using a Micromeritics (Norcross, GA) Nanoplus 3. Samples were dissolved at 2 mg/mL in 100 mM sodium phosphate buffer (pH 7) for each measurement, and D_h values were reported as averages over 70 accumulation times.

5.2.4 Caco-2 Cell Culture

Caco-2 cells (ATCC HTB-337), derived from human colorectal adenocarcinoma, were cultured in DMEM (Dulbecco's Modified Eagle's Medium) media with 10% fetal bovine serum (FBS), 10 IU/mL of penicillin, amphotericin B and 0.1 mg/mL streptomycin. Cells were incubated in fully humid conditions at 37 ºC with 5% CO_2. Only cells between passages 25-60 were used for viability and TEER assays.

5.2.5 Cell Toxicity of BSA-pOEGMA-*b*-pPPZ using MTT Assay

Toxicity of BSA-pOEGMA-*b*-pPPZ block conjugates and 1-phenylpiperazine (PPZ) to Caco-2 cells was assessed using a methyl thiazole tetrazolium (MTT) assay. Caco-2 cells were seeded at 10^5 cells per well on 96 well plates and incubated overnight in DMEM media. PPZ samples were dissolved in DMEM media at different concentrations and added to the cells for 3 hours at 37 ºC. At the end of the 3 hour incubation, PPZ treatments were removed, 10 µL of MTT reagent with 100 µL DMEM media was added to the cells, and cells were incubated for 3 hours at 37 ºC. Cells were lysed with 100 µL of SDS detergent and incubated overnight at 25 ºC in the dark. Absorbance was read at 570 nm for each treatment, and equivalent MTT/detergent/PPZ solutions with no cells were subtracted from the background. Cell viability was calculated and plotted as the relative cell viability compared to cells with DMEM media only.

5.2.6 Transepithelial Electrical Resistance (TEER)

Transepithelial electrical resistance (TEER) values of Caco-2 monolayers on transwell plates were measured when incubated with PPZ solutions. Caco-2 cells were seeded on BiaCoaT HTS membrane supports at 2 x 10^5 cells per well in BSM (basal seeding medium: DMEM with MITO+ Serum Extender and amphotericin B) and incubated for 48 hours at 37ºC. Media was changed to EDM (enterocyte differentiation medium) and cells were incubated for 24-48 hours. Prior to adding PPZ treatments, cell monolayer integrity was confirmed by measuring resting TEER. Only cell monolayers with TEER values at least 200 Ω/cm^2 were used for TEER experiments. 300 µL of PPZ solutions in EDM media were added to the apical side of transwell plates. Monolayers were incubated for 3 hours at 37 ºC and TEER measurements were recorded at specified time points. At the end of three hours, PPZ solutions were removed from the apical side of the well, cells were washed with phosphate buffered saline (PBS, pH 7.4), 300 µL of EDM media was added to the wells, and cells were incubated for 24 hours at 37 ºC to allow monolayers integrity to reform. At the end of 24 hours, TEER values were measured.

5.2.7 Permeability Measurements

Calcein and FITC labeled BSA were used as fluorescent markers to quantify permeability of Caco-2 monolayers. BSA macroinitiators were labeled with FITC by adding NHS-FITC (10 mg/mL in DMSO) to BSA-Br (4 µM in 10 mL 50 mM NaPhos buffer (pH 8)) and incubating at 4ºC in dark for 2 hours. Unreacted FITC was removed by dialysis against DI water and BSA-FITC was lyophilized.

Fluorescent markers were dissolved in EDM media with PPZ solutions and added to the apical side of transwell plates. 100 µL of basolateral solutions were retrieved at each TEER measurement and fluorescence was measured at 495/515 nm (calcein) and 494/521 nm (FITC)

excitation and emission wavelengths. At each time point, 1 mL of fresh EDM media was added to the basolateral side of the membrane. Apparent permeability across monolayers was calculated using the formula $P_{app} = \frac{\Delta M}{C_a A \Delta t}$ where P_{app} is apparent permeability, ΔM is marker mass in basal compartment, C_a is apical fluorescent marker concentration, A is area of the monolayer, and Δt is the elapsed time between samples. Marker mass in the apical compartment was converted from fluorescence measurements using a calibration curve of known fluorescent molecule concentration.

5.3 Results and Discussion

5.3.1 Synthesis and Characterization of Piperazine Containing Conjugates

We hypothesized that the covalent attachment of a chemical permeation enhancing molecule directly to the protein of interest could enable direct transport of a protein macromolecule across the intestinal epithelium while not inducing cell toxicity. To test this hypothesis, piperazine containing conjugates were synthesized using "grafting from" polymer-based protein engineering. Prior to conjugate synthesis, ATRP initiator (NHS-Br) was covalently attached to surface lysines on BSA using NHS ester/primary amine chemistry. The degree of initiator immobilization was predictably tailored by modifying the molar ratios of NHS-Br initiator to BSA primary amine during initiator immobilization reaction. Not surprisingly, lower ratios of NHS-Br resulted in a lower number of initiator molecules on BSA as determined by MALDI-TOF-MS (**Figure 5.1**). Three distinct BSA-Br macroinitiators were synthesized with 19, 25, and 40 initiators per BSA molecule by completing the reaction with a NHS-Br to BSA primary amine molar ratio of 0.6:1, 1:1, and 3:1, respectively. BSA contains a total of sixty primary amines (lysine + *N*-terminus), but n=40 represented initiator saturation using this immobilization strategy.

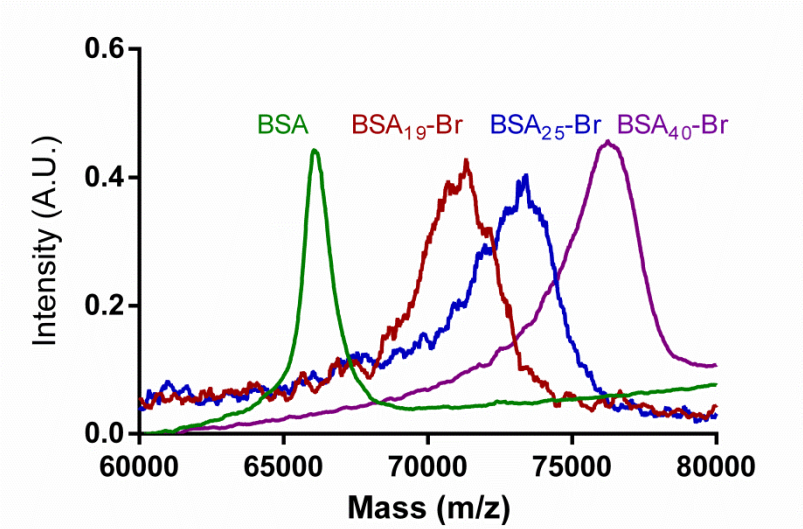

Figure 5.1 MALDI-TOF spectra of BSA-Br macroinitiators and native BSA. The number of ATRP initiators per BSA molecule was controlled by varying reactant ratios during initiator immobilization. The number of initiators for each macroinitiator was calculated by subtracting BSA-Br m/z values from native BSA m/z and dividing by the molecular weight of the initiator.

BSA-pOEGMA-*b*-pPPZ conjugates were synthesized by two sequential ATRP reactions directly from the surface of bovine serum albumin (BSA) (**Figure 5.2**). Polymerization of pOEGMA from BSA-Br was completed first using CuCl/$CuCl_2$/bpy as the copper catalyst/ligand pair.[25] The targeted degree of polymerization for the pOEGMA block as calculated by starting molar ratios of monomer to initiator was 102, but the reaction was stopped after only 45 minutes in order to yield shorter polymers while maintaining narrow dispersity.

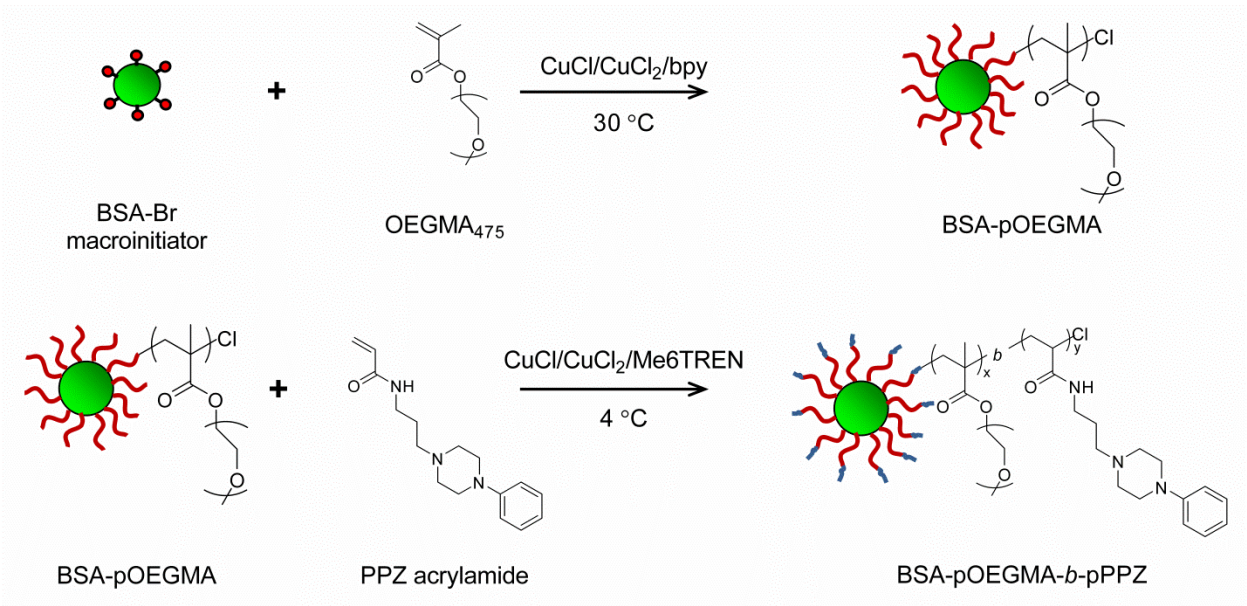

Figure 5.2 "Grafting from" atom transfer radical polymerization (ATRP) scheme used to synthesize BSA-pOEGMA-*b*-pPPZ conjugates.

In order to incorporate chemical permeation enhancement directly into the protein-polymer conjugates, a new phenyl piperazine acrylamide monomer was synthesized from 1-phenylpiperazine and *N*-(3-bromopropyl) acrylamide (**Figure 5.3a**) and characterized using ^{1}H NMR(**Figure 5.3b**). The three carbon spacer between acrylamide and phenyl piperazine was incorporated into the monomer after the first iteration of a phenyl piperazine monomer, which did not have the three carbon spacer, was insoluble in aqueous media following polymerization.

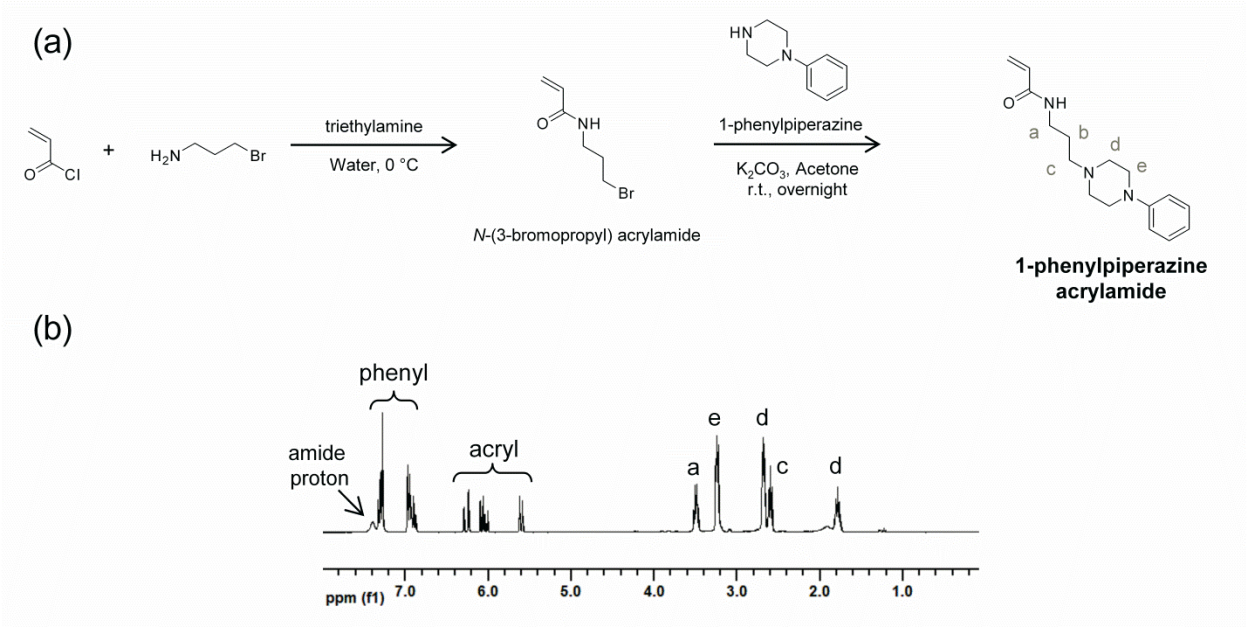

Figure 5.3 Synthesis of 1-phenylpiperazine acrylamide (a) Scheme for reaction of 1-phenylpiperazine acrylamide from *N*-(3-bromopropyl) acrylamide and 1-phenylpiperazine and (b) ^{1}H NMR spectra for 1-phenylpiperazine acrylamide. Initiator synthesis and characterization completed by Hironobu Murata.

Chain extension of poly(phenyl piperazine acrylamide) (pPPZ) from BSA-pOEGMA was completed using CuCl/$CuCl_2$/Me6TREN at 4 °C[218] and successful polymerization was confirmed using ^{1}H NMR (**Figure 5.4**). The characteristic peak at ~7.0 ppm corresponded to the phenyl protons (n=6) in the piperazine molecule and was not present for BSA-pOEGMA homopolymer conjugates. Degree of polymerization (DP) of the pPPZ chain extended block was estimated by comparing characteristic peaks of ester protons in pOEGMA (~4.2 ppm) to characteristic phenyl proton peaks in pPPZ.

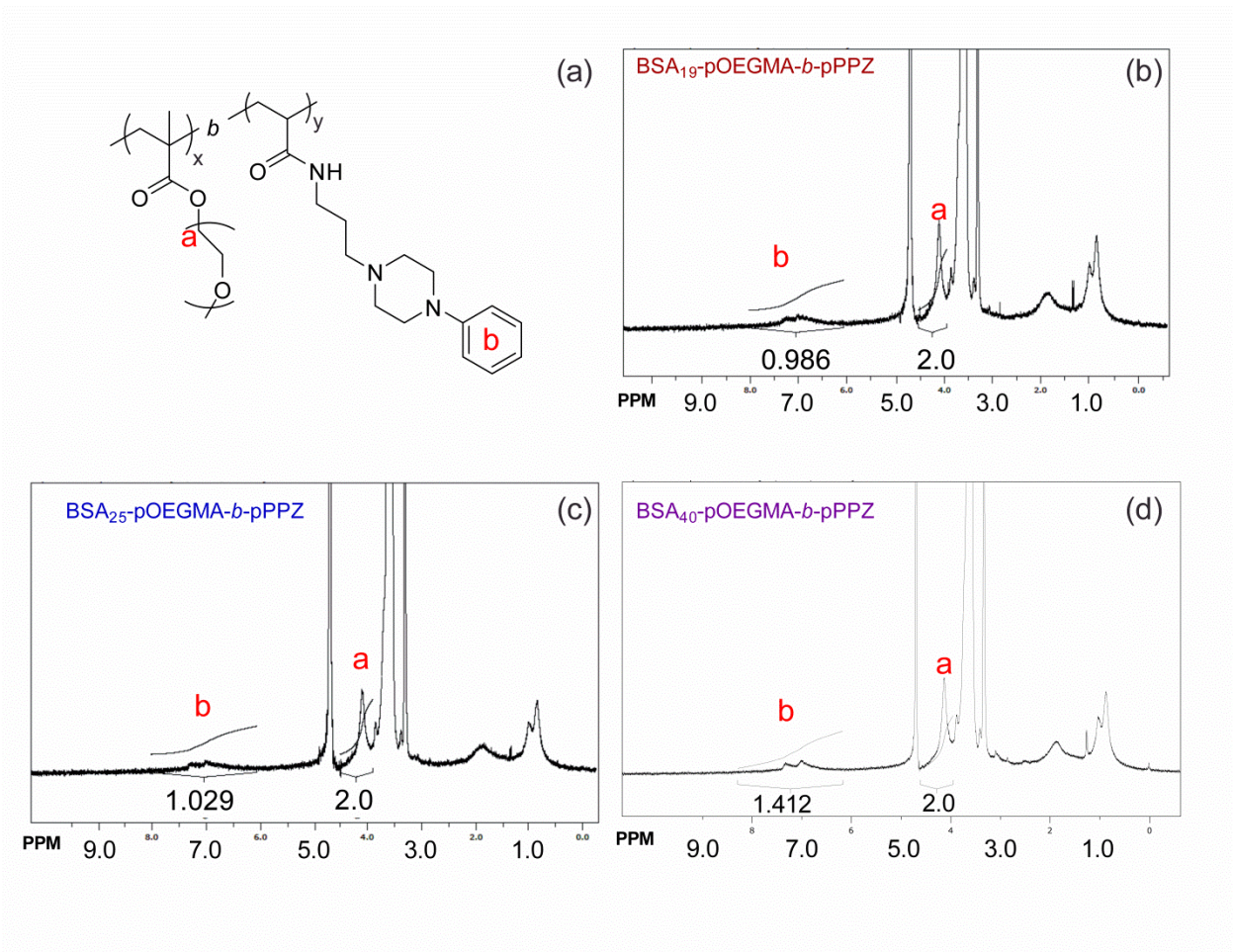

Figure 5.4 Incorporation of PPZ into BSA-pOEGMA-*b*-pPPZ was confirmed using ^{1}H NMR. (a) characteristic protons in pOEGMA (n=2 protons) and pPPZ (n=6 protons) used to calculate the pPPZ second block degree of polymerization and ^{1}H NMR spectra for (b) BSA_{19}-pOEGMA-*b*-pPPZ, (c) BSA_{25}-pOEGMA-*b*-pPPZ, and (d) BSA_{40}-pOEGMA-*b*-pPPZ block copolymer conjugates. The degree of polymerization for second block pPPZ was calculated by comparing integrations of characteristic peaks for each block, after normalizing the pOEGMA peak to n=2.

BSA-pOEGMA and BSA-pOEGMA-*b*-pPPZ conjugates were characterized using dynamic light scattering (DLS) and size exclusion-high pressure liquid chromatography (SE-HPLC). Hydrodynamic diameter measurements obtained using DLS confirmed the BSA-pOEGMA conjugates were larger than native BSA (**Figure 5.5a-c**), and BSA-pOEGMA

chromatograms (**Figure 5.5d**) indicated that no native BSA remained after polymerization. Due to the hydrophobic nature of the PPZ block, BSA-pOEGMA-*b*-pPPZ conjugates did not elute using aqueous SE-HPLC.

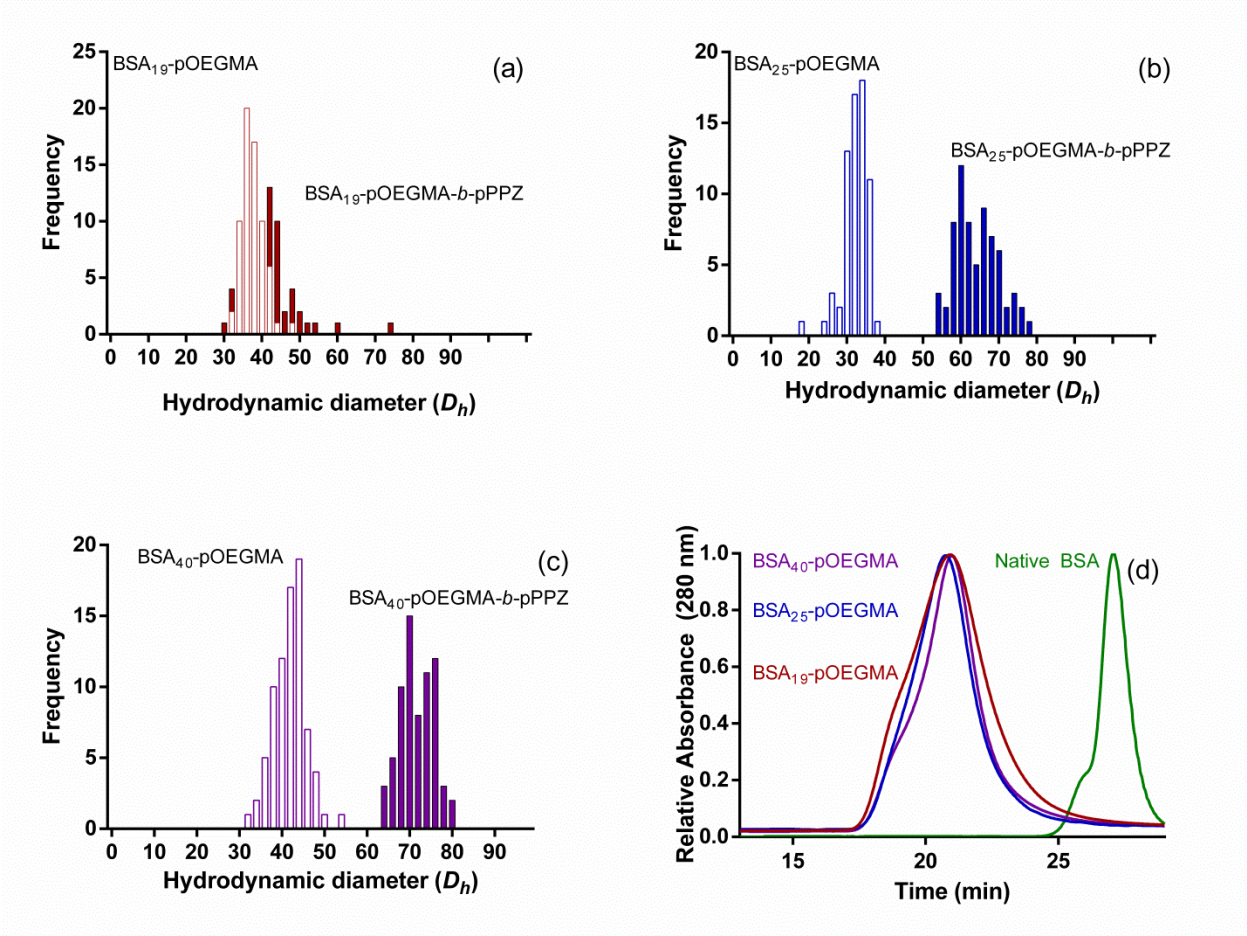

Figure 5.5 Size characterization of BSA-pOEGMA and BSA-pOEGMA-*b*-pPPZ conjugates. Hydrodynamic diameters (D_h) were measured using dynamic light scattering (DLS) for (a) BSA_{19}-pOEGMA and BSA_{19}-pOEGMA-*b*-pPPZ, (b) BSA_{25}-pOEGMA and BSA_{25}-pOEGMA-*b*-pPPZ and (c) BSA_{40}-pOEGMA and BSA_{40}-pOEGMA-*b*-pPPZ in 50 mM sodium phosphate buffer (pH 7.0). (d) SE-HPLC chromatograms for each BSA conjugate in 100 mM sodium phosphate (pH 7.0) indicated successful polymerization and the absence of native BSA.

Hydrodynamic diameter (D_h) measurements for the BSA-pOEGMA-*b*-pPPZ conjugates indicated large increases in size after pPPZ polymerization (**Figure 5.5a-c**). We surmised that

the conjugates slightly aggregated after the addition of pPPZ, which resulted in the large D_h values. The nomenclature used hereafter for each of the conjugates indicates the number of initiators per BSA molecule (BSA_{19}). While each of the conjugates had approximately the same degree of polymerization for both the pOEGMA and the pPPZ block (**Table 5.1**), each polymer block represented a different molar amount of the total conjugate, because the number of polymers per protein was intentionally not uniform across the three BSA-pOEGMA-*b*-pPPZ conjugates.

Table 5.1 Molecular characterization of BSA-pOEGMA-*b*-pPPZ

	Cleaved Polymer			Conjugate	
	M_n (kDa)	PDI (M_w/M_n)	DP[1]	Molar Mass (kDa)	Size (D_h) [nm]
BSA_{19}-pOEGMA	8.69	1.49	18	240	38.6 ± 2.9
BSA_{25}-pOEGMA	8.73	1.56	18	295	33.1 ± 3.2
BSA_{40}-pOEGMA	7.84	1.43	17	389	43.2 ± 3.7
BSA_{19}-pOEGMA-*b*-pPPZ	9.89	-	22 (4)	265	42.9 ± 6.7
BSA_{25}-pOEGMA-*b*-pPPZ	10.1	-	23 (5)	331	64.9 ± 5.7
BSA_{40}-pOEGMA-*b*-pPPZ	9.6	-	24 (7)	459	72.4 ± 3.9

[1]**DP indicates the degree of polymerization. DP values for the block copolymers correspond to total degree of polymerization with second block pPPZ DP in parentheses.**

5.3.2 Toxicity of BSA-pOEGMA-*b*-pPPZ

Prior to examining the permeability effects of BSA-pOEGMA-*b*-pPPZ conjugates on human colorectal adenocarcinoma (Caco-2) monolayers, their toxicity to Caco-2 cells was assessed using the methyl thiazole tetrazolium (MTT) assay (**Figure 5.6**).

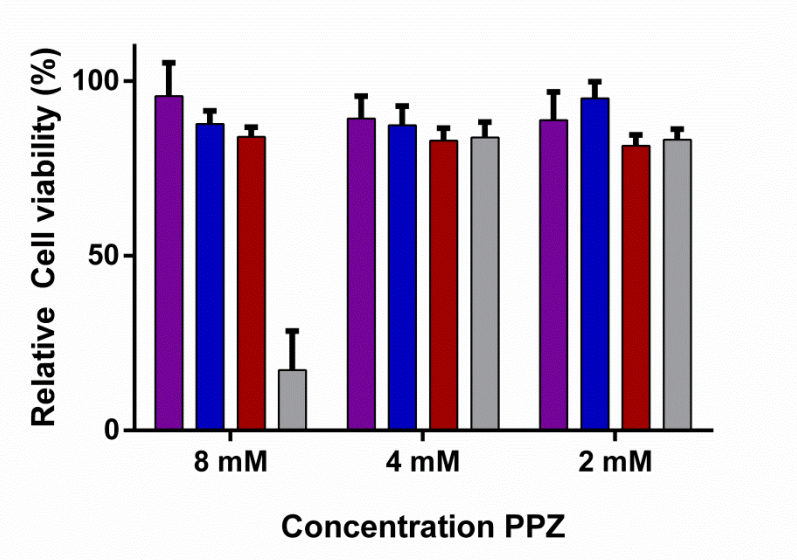

Figure 5.6 BSA-pOEGMA-b-pPPZ conjugates were not toxic to Caco-2 cells as quantified by MTT assy. Caco-2 cells were incubated with 1-phenylpiperazine (PPZ) (grey), BSA_{19}-pOEGMA-*b*-pPPZ (red), BSA_{25}-pOEGMA-*b*-pPPZ (blue), and BSA_{40}-pOEGMA-*b*-pPPZ (purple) for 3 hours at 37°C. Cell viability was assessed using MTT reagent and viability values were normalized to Caco-2 cells treated only with DMEM media.

BSA-pOEGMA-*b*-pPPZ conjugates and small molecule 1-phenylpiperazine (PPZ) were incubated with Caco-2 cells for 3 hours at 37 ºC and their cell toxicity was quantified in relation to Caco-2 cells treated only with DMEM media. PPZ had dose dependent toxicity profiles, while BSA-pOEGMA-*b*-pPPZ conjugates were relatively nontoxic at each of the concentrations tested. Interestingly, piperazines derivatives with only tertiary amines have previously been shown to be less toxic than piperazines with secondary amines.[217] Indeed, when synthesizing PPZ acrylamide from PPZ, the secondary amine is converted to a tertiary amine, so the cell toxicity results in this study agree well with the previous findings. BSA-pOEGMA homopolymer conjugates also had no toxicity towards Caco-2 cells (data not shown) indicating there were no toxic effects from either of the polymer blocks in the block copolymer conjugate. Concentrations

of BSA-pOEGMA-*b*-pPPZ with cell viability above 90% were determined to be safe in order to examine their permeability characteristics using TEER.

5.3.3 Permeability of Caco-2 Monolayers with PPZ

Caco-2 cells were seeded on transwell plates and allowed to form monolayers over 3 days.[219] By using appropriate differentiation media during monolayer formation, Caco-2 cells expressed the phenotype, including tight junctions and villi, for enterocytes in the small intestines.[220] In addition, Caco-2 monolayers are classically validated to have good correlation with absorption profiles of human small intestines.[221] Initial transepithelial electrical resistance (TEER) values across Caco-2 monolayers were measured prior to adding PPZ treatments, and structurally intact monolayers were confirmed by allowing only monolayers with TEER values above 200 Ω/cm^2 to be used. BSA-pOEGMA-*b*-pPPZ, BSA-pOEGMA homopolymer, and 1-phenyl piperazine solutions were incubated with Caco-2 monolayers at different molar concentrations of PPZ for 3 hours at 37°C. TEER measurements were taken at specific time points for each of the samples over the three hours (**Figure 5.7**). At the end of three hours, PPZ treatment was removed; cells were washed with phosphate buffered saline (PBS), replaced with EDM media, and incubated overnight at 37 °C. TEER measurements were recorded again at t=27 hr to examine the ability of the tight junctions to reform after removing PPZ treatment (**Figure 5.7**).

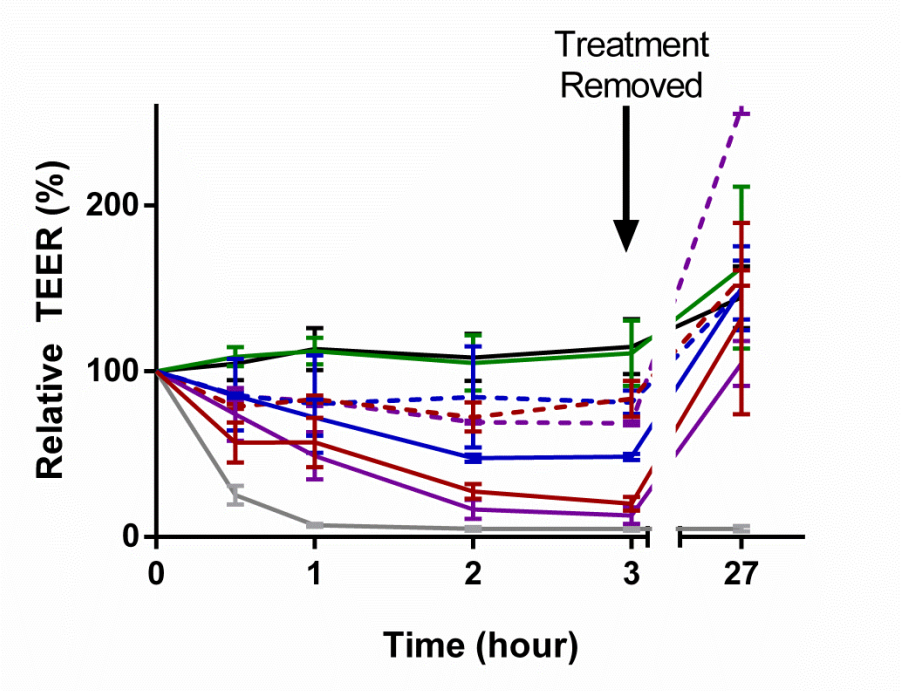

Figure 5.7 BSA-pOEGMA-*b*-pPPZ conjugates caused dose dependent drop in Caco-2 monolayer TEER. (a) Relative TEER values, normalized to t=0 hr for each sample, were assessed over 3 hours for Caco-2 monolayers incubated with 2 mM (dotted lines) and 4 mM (solid lines) PPZ; BSA_{19}-pOEGMA-*b*-pPPZ (red), BSA_{25}-pOEGMA-*b*-pPPZ (blue), BSA_{40}-pOEGMA-*b*-pPPZ (purple). Three controls, small molecule 1-phenylpiperazine (4 mM, grey), BSA-pOEGMA (green), and Caco-2 cells with EDM media only (black), were also examined. Relative TEER values for conjugates and control samples at were measured at t=27 hr after removing and washing experimental treatment at t=3 hr.

The flow of ions across Caco-2 monolayers, as measured by TEER, was used to assess the potential of PPZ treatments to transiently disrupt Caco-2 monolayers and enable paracelluar protein transport. Each of the BSA-pOEGMA-*b*-pPPZ conjugates showed a dose dependent drop in TEER over the course of the 3 hour experiment. Even though each of the conjugates contained different amounts of PPZ per molecule of BSA, it was clear from TEER experiments that the drop in TEER correlated with PPZ concentration and not BSA concentration, indicating PPZ was responsible for the TEER behavior. At 4 mM PPZ, BSA_{40}-pOEGMA-*b*-pPPZ was only 8 μM

BSA, BSA_{25}-pOEGMA-*b*-pPPZ was 16μM BSA, and BSA_{19}-pOEGMA-*b*-pPPZ was 20 μM BSA, but each had a relative TEER value of approximately 30 % at t=3 hr. BSA-pOEGMA homopolymer conjugates showed no drop in TEER indicating the PPZ block was responsible for the drop in TEER seen in BSA-pOEGMA-*b*-pPPZ conjugates. Measurements of TEER at t=27 hours for the BSA-pOEGMA-*b*-pPPZ conjugates indicated that the permeability effect was transient, and the integrity of monolayer tight junctions was restored after removing the PPZ treatment. TEER values for Caco-2 monolayers incubated with 1-phenylpiperazine dropped more rapidly than BSA-pOEGMA-*b*-pPPZ conjugates, but also did not recover at t=27 hr, indicating that PPZ was toxic to monolayer integrity at 4 mM.

In parallel to TEER measurements, permeability of monolayers was assessed using calcein, a fluorescent small molecule (**Figure 5.8a-c**). Permeation of calcein across the Caco-2 monolayers correlated well with the drop in TEER values seen for each of the treatments. Each conjugate induced higher calcein permeation the longer the treatment was added, and BSA_{40}-pOEGMA-*b*-pPPZ showed the largest increase in calcein permeation (approximately 10 times higher compared to control cells) of the conjugates. Yet again, permeation of calcein correlated well with PPZ concentration for BSA-pOEGMA-*b*-pPPZ conjugates rather than the BSA concentration, indicating the PPZ polymer block is crucial for permeation effects.

While it was clear that the conjugates caused a dose dependent drop in TEER, it was still necessary to confirm that the conjugates actually transported across Caco-2 monolayers. To confirm transport of BSA across the monolayer, BSA-pOEGMA-b-pPPZ conjugates were fluorescently labeled with NHS-Fluorescein (NHS-FITC). Initially, FITC labeling of BSA-pOEGMA-*b*-pPPZ conjugates was attempted after growing polymers from the surface of BSA. However, rather than covalently attaching to available lysines, NHS-FITC simply associated

non-covalently with the PPZ block in conjugates. To prevent non-specific association of FITC with piperazine, BSA-Br conjugates were covalently labeled with NHS-FITC prior to the "grafting from" ATRP of pOEGMA and pPPZ. Then pOEGMA and pPPZ were grown from BSA-FITC-Br macroinitiators using the same protocol described for unlabeled conjugates.

BSA-FITC-pOEGMA-*b*-pPPZ conjugates were incubated with Caco-2 monolayers at equivalent concentrations (2 mM PPZ, 4 mM PPZ) to unlabeled BSA-pOEGMA-*b*-pPPZ conjugates. Permeation of BSA-FITC-pOEGMA-*b*-pPPZ conjugates was calculated by measuring the fluorescence of solutions taken from the basolateral compartment at each time point (**Figure 5.8d-f).** Similar to calcein permeation measurements, the permeation of FITC labeled conjugates was PPZ dose dependent. Each of the BSA-pOEGMA-*b*-pPPZ conjugates showed increasing permeation over the course of the experiment, a result that was not surprising since the TEER values also reduced until removing the treatments at t=3 hours. Permeation of the conjugates during the third hour of treatment was 35 times higher for BSA_{19}-FITC-pOEGMA-*b*-pPPZ, 17 times higher for BSA_{25}-FITC-pOEGMA-*b*-pPPZ, and 27 times higher for BSA_{40}-FITC-pOEGMA-*b*-pPPZ (each at 4 mM) compared to native BSA-FITC incubated with media alone. Interestingly, each of the BSA_{25}-FITC-pOEGMA-*b*-pPPZ and BSA_{40}-FITC-pOEGMA-*b*-pPPZ conjugates had almost no increase in permeation at 2 mM concentrations. Conversely, even at 2 mM BSA_{19}-FITC-pOEGMA-*b*-pPPZ permeation in the third hour was 13 fold higher than control samples.

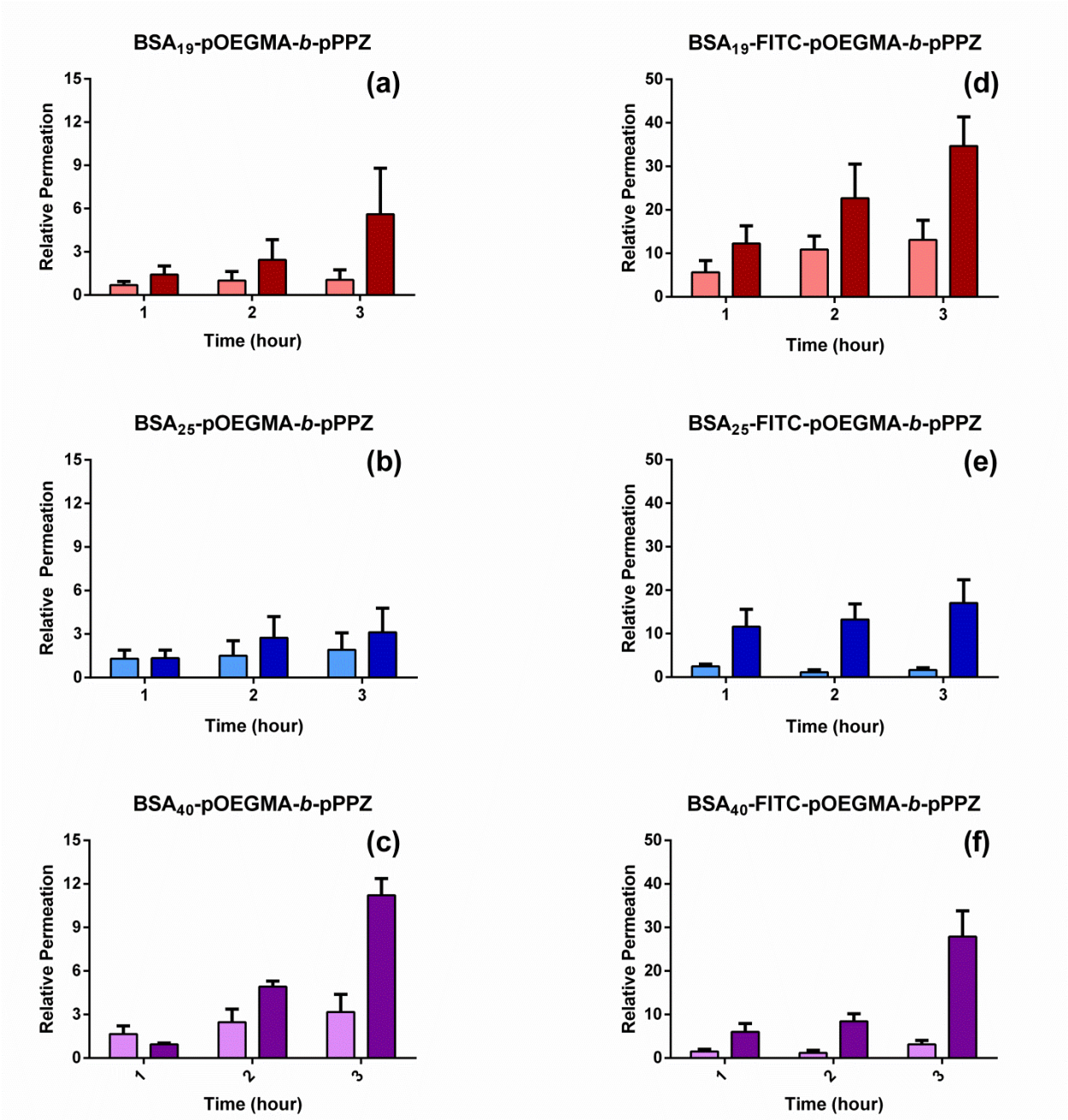

Figure 5.8 BSA-pOEGMA-*b*-pPPZ conjugates transported across cell monolayers. Caco-2 monolayers were incubated with BSA-pOEGMA-*b*-pPPZ conjugates at 37 °C for 3 hours. (a) Calcein was used as small molecule permeation marker for (a) BSA_{19}-pOEGMA-*b*-pPPZ, (b) BSA_{25}-pOEGMA-*b*-pPPZ, and (c) BSA_{40}-pOEGMA-*b*-pPPZ. FITC labeled conjugates were used to assess permeation of (d) BSA_{19}-FITC-pOEGMA-*b*-pPPZ, (e) BSA_{25}-FITC-pOEGMA-*b*-pPPZ, and (f) BSA_{40}-FITC-pOEGMA-*b*-pPPZ. Permeation was measured at 2 mM (light fill) and 4 mM (dark fill). Permeation values were normalized to both pre-treatment baseline permeation and control cells incubated with EDM only.

For protein therapeutic applications, the number of polymers attached to the protein may be limited by bioactivity considerations or number of surface accessible amino acid residues. Therefore it was important to determine that the permeation effect was conserved across different polymer architectures. To confirm that protein permeation was independent of polymer architecture, three conjugates with different polymer densities were synthesized. Indeed, each of the conjugates, with different molar ratios of PPZ units per protein unit exhibited similar decreases in TEER and increased permeability of Caco-2 monolayers. The drops in TEER seemed to be independent of polymer architecture; however, the relative permeation values for each of the conjugates were not the same. BSA_{19}-FITC-pOEGMA-*b*-pPPZ conjugates showed higher relative permeation values compared to BSA_{25}-FITC-pOEGMA-*b*-pPPZ and BSA_{40}-FITC-pOEGMA-*b*-pPPZ at equivalent doses of PPZ. Consequently, there may be a dependence of permeation on the organization of polymer around the protein core. Indeed, DLS measurements indicated that the BSA_{19}-pOEGMA-*b*-pPPZ conjugates aggregated less than the more densely modified conjugates, and this aggregation might affect protein permeation. It still must be determined if covalent attachment of PPZ directly to the protein of interest results in a localized effect of permeation. In order to minimize cell toxicity, the ideal situation would see small molecule permeation at low levels during protein permeation. While it was clear that the conjugates permeated across the monolayers, so did small molecule calcein. Thus, further experiments will be required to optimize the concentration of PPZ and polymer architecture that enables the lowest background permeation while maintaining protein permeation.

5.4 Conclusion

In this work, BSA-pOEGMA-*b*-pPPZ conjugates with the ability to transport across Caco-2 monolayers were synthesized and characterized. Conjugates were synthesized with a

high polymer density around the protein core by using two sequential "grafting from" ATRP reactions from BSA macroinitiators. The degree of initiator immobilization was easily modified by varying the initiator to protein molar ratios during the immobilization reaction. At equivalent doses of phenyl piperazine, BSA-pOEGMA-*b*-pPPZ conjugates showed lower toxicity to Caco-2 cells than small molecule 1-phenylpiperazine, as assessed by an MTT assay and recovery of Caco-2 monolayers after PPZ treatment. BSA-pOEGMA-*b*-pPPZ conjugates caused dose dependent and transient drops in TEER values during treatment. The fluorescent markers, calcein and FITC labeled BSA-pOEGMA-*b*-pPPZ conjugates, confirmed that both small molecule and proteins transported across *in vitro* Caco-2 monolayers, and the permeation enhancement correlated well with drops in TEER. The work in this study represents an exciting demonstration of permeation enhancing polymers covalently attached to protein enabling protein transport across typically impermeable membranes.

Chapter 6 : Conclusions, Implications and Future Directions

6.1 Conclusions

In this work, high density polymer modification of proteins was used in order to predictably tailor chymotrypsin structural stability, bioactivity, and substrate binding. A novel water soluble atom transfer radical polymerization (ATRP) initiator molecule was used in order to create highly modified chymotrypsin-polymer conjugates with low dispersity by growing polymer directly outward from the surface of chymotrypsin. The water soluble initiator was an improvement over previous protein reactive ATRP initiators in that it enabled a higher degree of polymer attachment to the protein. High density covalent polymer attachment enabled chymotrypsin-polymer conjugates to have temperature dependent kinetics and increased stability to extreme conditions including pH and temperature. Specifically, temperature responsiveness of the free polymers poly(sulfobetaine methacrylamide) (pSBAm) and poly(*N*-isopropyl acrylamide) (pNIPAM), at temperatures both above and below ambient temperature, was transferred to protein-polymer conjugates resulting in temperature dependent bioactivity. Block copolymer conjugates, with distinct pSBAm and pNIPAm blocks responsive to different stimuli, enabled enzyme bioactivity to be dependent on more than one stimulus. Interestingly, it was discovered that block copolymer conjugates were dramatically more stable than native chymotrypsin to low pH. Further experiments indicated the low pH stabilization was due to the first block, pSBAm, in the dual-block chymotrypsin conjugates. It was confirmed that the positively charged polymers, poly(quaternary ammonium methacrylate) (pQA) and poly(carboxybetaine acrylamide) (pCBAm), stabilized chymotrypsin at low pH, while the negatively charged polymer, poly(sulfonate methacrylate) (pSMA), and amphiphilic polymer, poly(oligoethylene methacrylate) (pOEGMA), destabilized chymotrypsin. We hypothesized that the stabilization profiles of chymotrypsin conjugates were due to the preferential exclusion

(positively charged polymer) or preferential binding (negatively charged and amphiphilic) of polymers from chymotrypsin. This exclusion or binding strengthened or displaced, respectively, the water hydration layer that is critical for protein stability. Lastly, bovine serum albumin-pOEGMA-*block*-poly(phenyl piperazine) (BSA-pOEGMA-*b*-pPPZ) conjugates decreased trans-epithelial electrical resistance (TEER) values and increased permeability of Caco-2 monolayers in a dose dependent manner. FITC labeled BSA-pOEGMA-*b*-pPPZ confirmed that protein conjugates transported across the monolayer rather than just reducing TEER and increasing permeation of a small molecule marker.

6.2 Implications

The findings in this work have increased the tools available to scientists looking to synthesize protein-polymer conjugates. Several new protocols for the synthesis of dual block protein-polymer conjugates were developed, and conjugates synthesized using a new water soluble protein reactive ATRP initiator were characterized. Temperature responsive conjugates showed temperature dependent aqueous solubility and bioactivity. Due to the temperature dependent solubility of chymotrypsin-polymer conjugates, the conjugates synthesized herein could be easily separated and recycled in industrial processes by simply varying the temperature. The dependence of chymotrypsin-polymer conjugate structural stability to low pH on the covalently attached polymer has not been reported before, but is important to consider when designing protein-polymer applications for varying applications. Indeed, acidic pH stable chymotrypsin conjugates could be used as an exogenous enzyme replacement therapy for diseases where chymotrypsin insufficiency is a symptom. Not surprisingly, stability results for chymotrypsin conjugates were consistent with the literature for small molecule stabilization and destabilization of proteins. Lastly, the covalent attachment of a permeation enhancing molecule

directly to a protein could be used for applications related to oral protein delivery. While not optimized in this study, it might be possible to promote protein permeation without background permeation.

6.3 Future Directions

In the future, it will be important to characterize the effect of high density polymer modification on the resulting properties of protein-polymer conjugates. For most of the applications in this dissertation, we synthesized conjugates with the maximum amount of polymers per protein. However, is it possible to modify the surface of proteins with only a few well-placed polymers and still have the same increase in stability? Conversely, does the high degree of modification for destabilizing polymers influence the resulting stability? Perhaps the destabilizing effect would be reduced if there were fewer polymers per protein molecule. In addition, it would be interesting if the stabilization effect was conserved for other proteins. While only tested on chymotrypsin in this study, we hypothesized the stabilization effect would be applicable to other proteins as well. Experiments from the literature with small molecule osmolytes indicate that the stabilization is conserved across many proteins, but the effect might be different for polymeric stabilizers. In addition, the specific molecular mechanism for stabilization is still not known for the polymer. While molecular mechanisms of small molecule osmolyte stabilization is still not known, isothermal titration calorimetry and molecular dynamic simulations are planned to examine interaction of chymotrypsin with the polymers.

The natural progression for permeation enhancing conjugates is to *in vivo* models. While the conjugates clearly enhance permeation *in vitro*, the fate of the conjugates *in vivo* is still unknown. Potential toxicity concerns include the degradation products of polymers and the effect of residual amounts of copper remaining in conjugates. It would also be interesting to further

optimize polymer architecture, PPZ concentration, and chemical structure of conjugates to yield the most effective and safe permeation enhancers. It would be interesting to test a library of polymers and a library of piperazine derivatives to determine which could be most efficacious.

References

[1] Carrigan, P. E., Ballar, P., and Tuzmen, S., 2011, "Site-Directed Mutagenesis," Disease Gene Identification: Methods and Protocols, K. J. DiStefano, ed., Humana Press, Totowa, NJ, pp. 107-124.

[2] Ho, S. N., Hunt, H. D., Horton, R. M., Pullen, J. K., and Pease, L. R., 1989, "Site-directed mutagenesis by overlap extension using the polymerase chain reaction," Gene, 77(1), pp. 51-59.

[3] Bornscheuer, U. T., and Pohl, M., 2001, "Improved biocatalysts by directed evolution and rational protein design," Curr. Opin. Chem. Biol., 5(2), pp. 137-143.

[4] Shu, J. Y., Panganiban, B., and Xu, T., 2013, "Peptide-Polymer Conjugates: From Fundamental Science to Application," Annu. Rev. Phys. Chem., 64(1), pp. 631-657.

[5] Roberts, M. J., Bentley, M. D., and Harris, J. M., 2012, "Chemistry for peptide and protein PEGylation," Advanced Drug Delivery Reviews, 64, Supplement, pp. 116-127.

[6] Kim, D., and Herr, A. E., 2013, "Protein immobilization techniques for microfluidic assays," Biomicrofluidics, 7(4), p. 041501.

[7] Abuchowski, A., van Es, T., Palczuk, N. C., and Davis, F. F., 1977, "Alteration of immunological properties of bovine serum albumin by covalent attachment of polyethylene glycol," J. Biol. Chem., 252(11), pp. 3578-3581.

[8] Abuchowski, A., Mccoy, J. R., Palczuk, N. C., Vanes, T., and Davis, F. F., 1977, "Effect of Covalent Attachment of Polyethylene-Glycol on Immunogenicity and Circulating Life of Bovine Liver Catalase," J. Biol. Chem., 252(11), pp. 3582-3586.

[9] Wu, Y. Z., Ng, D. Y. W., Kuan, S. L., and Weil, T., 2015, "Protein-polymer therapeutics: a macromolecular perspective," Biomater Sci-Uk, 3(2), pp. 214-230.

[10] Basak, S., Punetha, V. D., Bisht, G., Bisht, S. S., Sahoo, N. G., and Cho, J. W., 2015, "Recent Trends of Polymer-Protein Conjugate Application in Biocatalysis: A Review," Polymer Reviews, 55(1), pp. 163-198.

[11] Obermeyer, A. C., and Olsen, B. D., 2015, "Synthesis and Application of Protein-Containing Block Copolymers," Acs Macro Lett, 4(1), pp. 101-110.

[12] Li, M., Li, H., De, P., and Sumerlin, B. S., 2011, "Thermoresponsive Block Copolymer–Protein Conjugates Prepared by Grafting-from via RAFT Polymerization," Macromol. Rapid Commun., 32(4), pp. 354-359.

[13] Lele, B. S., Murata, H., Matyjaszewski, K., and Russell, A. J., 2005, "Synthesis of uniform protein-polymer conjugates," Biomacromolecules, 6(6), pp. 3380-3387.

[14] Heredia, K. L., Bontempo, D., Ly, T., Byers, J. T., Halstenberg, S., and Maynard, H. D., 2005, "In Situ Preparation of Protein−“Smart” Polymer Conjugates with Retention of Bioactivity," J. Am. Chem. Soc., 127(48), pp. 16955-16960.

[15] Gao, W., Liu, W., Mackay, J. A., Zalutsky, M. R., Toone, E. J., and Chilkoti, A., 2009, "In situ growth of a stoichiometric PEG-like conjugate at a protein's N-terminus with significantly improved pharmacokinetics," Proceedings of the National Academy of Sciences, 106(36), pp. 15231-15236.

[16] Hu, J., Zhao, W., Gao, Y., Sun, M., Wei, Y., Deng, H., and Gao, W., 2015, "Site-specific in situ growth of a cyclized protein-polymer conjugate with improved stability and tumor retention," Biomaterials, 47, pp. 13-19.

[17] Qi, Y., Amiram, M., Gao, W., McCafferty, D. G., and Chilkoti, A., 2013, "Sortase-Catalyzed Initiator Attachment Enables High Yield Growth of a Stealth Polymer from the C Terminus of a Protein," Macromol. Rapid Commun., 34(15), p. 10.1002/marc.201300460.
[18] Peeler, J. C., Woodman, B. F., Averick, S., Miyake-Stoner, S. J., Stokes, A. L., Hess, K. R., Matyjaszewski, K., and Mehl, R. A., 2010, "Genetically Encoded Initiator for Polymer Growth from Proteins," J. Am. Chem. Soc., 132(39), pp. 13575-13577.
[19] Matyjaszewski, K., and Tsarevsky, N. V., 2014, "Macromolecular Engineering by Atom Transfer Radical Polymerization," J. Am. Chem. Soc., 136(18), pp. 6513-6533.
[20] Konkolewicz, D., Magenau, A. J. D., Averick, S. E., Simakova, A., He, H., and Matyjaszewski, K., 2012, "ICAR ATRP with ppm Cu Catalyst in Water," Macromolecules, 45(11), pp. 4461-4468.
[21] McCormick, C. L., and Lowe, A. B., 2004, "Aqueous RAFT Polymerization: Recent Developments in Synthesis of Functional Water-Soluble (Co)polymers with Controlled Structures," Acc. Chem. Res., 37(5), pp. 312-325.
[22] De, P., Li, M., Gondi, S. R., and Sumerlin, B. S., 2008, "Temperature-Regulated Activity of Responsive Polymer−Protein Conjugates Prepared by Grafting-from via RAFT Polymerization," J. Am. Chem. Soc., 130(34), pp. 11288-11289.
[23] Li, H., Li, M., Yu, X., Bapat, A. P., and Sumerlin, B. S., 2011, "Block copolymer conjugates prepared by sequentially grafting from proteinsvia RAFT," Polymer Chemistry, 2(7), pp. 1531-1535.
[24] Liu, J., Bulmus, V., Herlambang, D. L., Barner-Kowollik, C., Stenzel, M. H., and Davis, T. P., 2007, "In Situ Formation of Protein–Polymer Conjugates through Reversible Addition Fragmentation Chain Transfer Polymerization," Angew. Chem. Int. Ed., 46(17), pp. 3099-3103.
[25] Averick, S., Simakova, A., Park, S., Konkolewicz, D., Magenau, A. J. D., Mehl, R. A., and Matyjaszewski, K., 2012, "ATRP under Biologically Relevant Conditions: Grafting from a Protein," Acs Macro Lett, 1(1), pp. 6-10.
[26] A.L. Lewis, S. W. L., 2011, "Conjugation reactions."
[27] Matyjaszewski, K., 2012, "Atom transfer radical polymerization (ATRP): current status and future perspectives," Macromolecules, 45(10), pp. 4015-4039.
[28] Siegwart, D. J., Oh, J. K., and Matyjaszewski, K., 2012, "ATRP in the design of functional materials for biomedical applications," Prog. Polym. Sci., 37(1), pp. 18-37.
[29] Cobo, I., Li, M., Sumerlin, B. S., and Perrier, S., 2015, "Smart hybrid materials by conjugation of responsive polymers to biomacromolecules," Nat. Mater., 14(2), pp. 143-159.
[30] Pelegri-O'Day, E. M., Lin, E.-W., and Maynard, H. D., 2014, "Therapeutic Protein–Polymer Conjugates: Advancing Beyond PEGylation," J. Am. Chem. Soc., 136(41), pp. 14323-14332.
[31] Xu, J., Jung, K., Corrigan, N. A., and Boyer, C., 2014, "Aqueous photoinduced living/controlled polymerization: tailoring for bioconjugation," Chemical Science, 5(9), pp. 3568-3575.
[32] Wilson, P., Nicolas, J., and Haddleton, D. M., 2015, "Polymer–Protein/Peptide Bioconjugates," Chemistry of Organo-Hybrids: Synthesis and Characterization of Functional Nano-Objects, pp. 466-502.
[33] Averick, S., Mehl, R. A., Das, S. R., and Matyjaszewski, K., 2015, "Well-defined biohybrids using reversible-deactivation radical polymerization procedures," J. Controlled Release, 205, pp. 45-57.

[34] Bhattacharjee, S., Liu, W., Wang, W. H., Weitzhandler, I., Li, X., Qi, Y., Liu, J., Pang, Y., Hunt, D. F., and Chilkoti, A., 2015, "Site-Specific Zwitterionic Polymer Conjugates of a Protein Have Long Plasma Circulation," Chembiochem : a European journal of chemical biology, 16(17), pp. 2451-2455.
[35] Averick, S. E., Bazewicz, C. G., Woodman, B. F., Simakova, A., Mehl, R. A., and Matyjaszewski, K., 2013, "Protein–polymer hybrids: Conducting ARGET ATRP from a genetically encoded cleavable ATRP initiator," Eur. Polym. J., 49(10), pp. 2919-2924.
[36] Alconcel, S. N. S., Baas, A. S., and Maynard, H. D., 2011, "FDA-approved poly(ethylene glycol)-protein conjugate drugs," Polymer Chemistry, 2(7), pp. 1442-1448.
[37] Schlesinger, N., 2004, "Management of acute and chronic gouty arthritis: present state-of-the-art," Drugs, 64(21), pp. 2399-2416.
[38] Sherman, M. R., Saifer, M. G., and Perez-Ruiz, F., 2008, "PEG-uricase in the management of treatment-resistant gout and hyperuricemia," Advanced drug delivery reviews, 60(1), pp. 59-68.
[39] Sroda, K., Rydlewski, J., Langner, M., Kozubek, A., Grzybek, M., and Sikorski, A. F., 2005, "Repeated injections of PEG-PE liposomes generate anti-PEG antibodies," Cellular & molecular biology letters, 10(1), pp. 37-47.
[40] Bailon, P., and Berthold, W., 1998, "Polyethylene glycol-conjugated pharmaceutical proteins," Pharm Sci Technol To, 1(8), pp. 352-356.
[41] Shen, M. C., Martinson, L., Wagner, M. S., Castner, D. G., Ratner, B. D., and Horbett, T. A., 2002, "PEO-like plasma polymerized tetraglyme surface interactions with leukocytes and proteins: in vitro and in vivo studies," J Biomat Sci-Polym E, 13(4), pp. 367-390.
[42] Qi, Y., and Chilkoti, A., 2015, "Protein–polymer conjugation — moving beyond PEGylation," Curr. Opin. Chem. Biol., 28, pp. 181-193.
[43] Keefe, A. J., and Jiang, S. Y., 2012, "Poly(zwitterionic)protein conjugates offer increased stability without sacrificing binding affinity or bioactivity," Nat. Chem., 4(1), pp. 60-64.
[44] Liu, M., Johansen, P., Zabel, F., Leroux, J. C., and Gauthier, M. A., 2014, "Semi-permeable coatings fabricated from comb-polymers efficiently protect proteins in vivo," Nat. Commun., 5, p. 5526.
[45] Ulbrich, K., Strohalm, J., Plocova, D., Oupicky, D., Subr, V., Soucek, J., Pouckova, P., and Matousek, J., 2000, "Poly[N-(2-hydroxypropyl)methacrylamide] conjugates of bovine seminal ribonuclease. Synthesis, physicochemical, and preliminary biological evaluation," J Bioact Compat Pol, 15(1), pp. 4-26.
[46] Caliceti, P., Schiavon, O., and Veronese, F. M., 2001, "Immunological properties of uricase conjugated to neutral soluble polymers," Bioconjugate Chem., 12(4), pp. 515-522.
[47] Gaertner, F. C., Luxenhofer, R., Blechert, B., Jordan, R., and Essler, M., 2007, "Synthesis, biodistribution and excretion of radiolabeled poly(2-alkyl-2-oxazoline)s," J. Controlled Release, 119(3), pp. 291-300.
[48] Mero, A., Pasut, G., Via, L. D., Fijten, M. W. M., Schubert, U. S., Hoogenboom, R., and Veronese, F. M., 2008, "Synthesis and characterization of poly(2-ethyl 2-oxazoline)-conjugates with proteins and drugs: Suitable alternatives to PEG-conjugates?," J. Controlled Release, 125(2), pp. 87-95.
[49] Stuart, M. A. C., Huck, W. T. S., Genzer, J., Muller, M., Ober, C., Stamm, M., Sukhorukov, G. B., Szleifer, I., Tsukruk, V. V., Urban, M., Winnik, F., Zauscher, S., Luzinov, I., and Minko, S., 2010, "Emerging applications of stimuli-responsive polymer materials," Nat. Mater., 9(2), pp. 101-113.

[50] Stayton, P. S., Shimoboji, T., Long, C., Chilkoti, A., Ghen, G., Harris, J. M., and Hoffman, A. S., 1995, "Control of protein-ligand recognition using a stimuli-responsive polymer," Nature, 378(6556), pp. 472-474.
[51] Kawano, T., Niidome, Y., Mori, T., Katayama, Y., and Niidome, T., 2009, "PNIPAM Gel-Coated Gold Nanorods for Targeted Delivery Responding to a Near-Infrared Laser," Bioconjugate Chem., 20(2), pp. 209-212.
[52] Nelson, D. M., Ma, Z., Leeson, C. E., and Wagner, W. R., 2012, "Extended and sequential delivery of protein from injectable thermoresponsive hydrogels," Journal of Biomedical Materials Research Part A, 100A(3), pp. 776-785.
[53] Shen, Y. Q., Zeng, F. Q., Zhu, S. P., and Pelton, R., 2001, "Novel cationic macromonomers by living anionic polymerization of (dimethylamino)ethyl methacrylate," Macromolecules, 34(2), pp. 144-150.
[54] Roth, P. J., Davis, T. P., and Lowe, A. B., 2012, "Comparison between the LCST and UCST Transitions of Double Thermoresponsive Diblock Copolymers: Insights into the Behavior of POEGMA in Alcohols," Macromolecules, 45(7), pp. 3221-3230.
[55] Meyer, D. E., and Chilkoti, A., 2002, "Genetically Encoded Synthesis of Protein-Based Polymers with Precisely Specified Molecular Weight and Sequence by Recursive Directional Ligation: Examples from the Elastin-like Polypeptide System," Biomacromolecules, 3(2), pp. 357-367.
[56] Azzaroni, O., Brown, A. A., and Huck, W. T. S., 2006, "UCST Wetting Transitions of Polyzwitterionic Brushes Driven by Self-Association," Angew. Chem., 118(11), pp. 1802-1806.
[57] Vamvakaki, M., Billingham, N. C., and Armes, S. P., 1999, "Synthesis of controlled structure water-soluble diblock copolymers via oxyanionic polymerization," Macromolecules, 32(6), pp. 2088-2090.
[58] Zhou, L., Yuan, W., Yuan, J., and Hong, X., 2008, "Preparation of double-responsive SiO2-g-PDMAEMA nanoparticles via ATRP," Mater. Lett., 62(8–9), pp. 1372-1375.
[59] Jochum, F. D., and Theato, P., 2013, "Temperature- and light-responsive smart polymer materials," Chem. Soc. Rev., 42(17), pp. 7468-7483.
[60] Vomasta, D., Hogner, C., Branda, N. R., and Konig, B., 2008, "Regulation of human carbonic anhydrase I (hCAI) activity by using a photochromic inhibitor," Angew Chem Int Edit, 47(40), pp. 7644-7647.
[61] Kolb, H. C., Finn, M. G., and Sharpless, K. B., 2001, "Click chemistry: Diverse chemical function from a few good reactions," Angew Chem Int Edit, 40(11), pp. 2004-+.
[62] Willner, I., and Rubin, S., 1993, "Reversible Photoregulation of the Activities of Proteins," React Polym, 21(3), pp. 177-186.
[63] Ercole, F., Davis, T. P., and Evans, R. A., 2010, "Photo-responsive systems and biomaterials: photochromic polymers, light-triggered self-assembly, surface modification, fluorescence modulation and beyond," Polymer Chemistry, 1(1), pp. 37-54.
[64] Schmaljohann, D., 2006, "Thermo- and pH-responsive polymers in drug delivery," Advanced Drug Delivery Reviews, 58(15), pp. 1655-1670.
[65] Sonaje, K., Chen, Y.-J., Chen, H.-L., Wey, S.-P., Juang, J.-H., Nguyen, H.-N., Hsu, C.-W., Lin, K.-J., and Sung, H.-W., 2010, "Enteric-coated capsules filled with freeze-dried chitosan/poly(γ-glutamic acid) nanoparticles for oral insulin delivery," Biomaterials, 31(12), pp. 3384-3394.
[66] Hoffman, A. S., 2013, "Stimuli-responsive polymers: Biomedical applications and challenges for clinical translation," Advanced Drug Delivery Reviews, 65(1), pp. 10-16.

[67] Kang, H. C., and Bae, Y. H., 2007, "pH-tunable endosomolytic oligomers for enhanced nucleic acid delivery," Adv. Funct. Mater., 17(8), pp. 1263-1272.
[68] Min, K. H., Kim, J.-H., Bae, S. M., Shin, H., Kim, M. S., Park, S., Lee, H., Park, R.-W., Kim, I.-S., Kim, K., Kwon, I. C., Jeong, S. Y., and Lee, D. S., 2010, "Tumoral acidic pH-responsive MPEG-poly(β-amino ester) polymeric micelles for cancer targeting therapy," J. Controlled Release, 144(2), pp. 259-266.
[69] Lim, W. K., Rosgen, J., and Englander, S. W., 2009, "Urea, but not guanidinium, destabilizes proteins by forming hydrogen bonds to the peptide group," Proc Natl Acad Sci U S A, 106(8), pp. 2595-2600.
[70] Yancey, P. H., and Somero, G. N., 1980, "Methylamine Osmoregulatory Solutes of Elasmobranch Fishes Counteract Urea Inhibition of Enzymes," J Exp Zool, 212(2), pp. 205-213.
[71] Yancey, P. H., Clark, M. E., Hand, S. C., Bowlus, R. D., and Somero, G. N., 1982, "Living with Water-Stress - Evolution of Osmolyte Systems," Science, 217(4566), pp. 1214-1222.
[72] Meersman, F., Bowron, D., Soper, A. K., and Koch, M. H. J., 2009, "Counteraction of Urea by Trimethylamine N-Oxide Is Due to Direct Interaction," Biophys. J., 97(9), pp. 2559-2566.
[73] Venkatesu, P., Lee, M.-J., and Lin, H.-m., 2007, "Trimethylamine N-oxide counteracts the denaturing effects of urea or GdnHCl on protein denatured state," Arch. Biochem. Biophys., 466(1), pp. 106-115.
[74] Zou, Q., Bennion, B. J., Daggett, V., and Murphy, K. P., 2002, "The Molecular Mechanism of Stabilization of Proteins by TMAO and Its Ability to Counteract the Effects of Urea," J. Am. Chem. Soc., 124(7), pp. 1192-1202.
[75] Wang, A. J., and Bolen, D. W., 1997, "A naturally occurring protective system in urea-rich cells: Mechanism of osmolyte protection of proteins against urea denaturation," Biochemistry, 36(30), pp. 9101-9108.
[76] Welch, W. J., and Brown, C. R., 1996, "Influence of molecular and chemical chaperones on protein folding," Cell Stress Chaperon, 1(2), pp. 109-115.
[77] Cho, S. S., Reddy, G., Straub, J. E., and Thirumalai, D., 2011, "Entropic Stabilization of Proteins by TMAO," J. Phys. Chem. B, 115(45), pp. 13401-13407.
[78] Arakawa, T., and Timasheff, S. N., 1985, "The Stabilization of Proteins by Osmolytes," Biophys. J., 47(3), pp. 411-414.
[79] Bennion, B. J., and Daggett, V., 2003, "The molecular basis for the chemical denaturation of proteins by urea," Proc. Natl. Acad. Sci. U. S. A., 100(9), pp. 5142-5147.
[80] Hu, C. Y., Lynch, G. C., Kokubo, H., and Pettitt, B. M., 2010, "TMAO influence on the backbone of proteins: an oligoglycine model," Proteins, 78(3), pp. 695-704.
[81] Germann, W. J., and Stanfield, C. L., 2005, "Principles of human physiology."
[82] McClintic, J. R., 1980, Basic anatomy and physiology of the human body, Wiley, New York.
[83] Shaji, J., and Patole, V., 2008, "Protein and Peptide Drug Delivery: Oral Approaches," Indian J. Pharm. Sci., 70(3), pp. 269-277.
[84] Bernkop-Schnurch, A., 2005, "Thiomers: A new generation of mucoadhesive polymers," Advanced Drug Delivery Reviews, 57(11), pp. 1569-1582.
[85] Schmitz, T., Leitner, V. M., and Bernkop-Schnurch, A., 2005, "Oral heparin delivery: Design and in vivo evaluation of a stomach-targeted mucoadhesive delivery system," J. Pharm. Sci., 94(5), pp. 966-973.

[86] Smart, J. D., 2005, "The basics and underlying mechanisms of mucoadhesion," Advanced Drug Delivery Reviews, 57(11), pp. 1556-1568.
[87] Sogias, I. A., Williams, A. C., and Khutoryanskiy, V. V., 2008, "Why is chitosan mucoadhesive?," Biomacromolecules, 9(7), pp. 1837-1842.
[88] Fuhrmann, G., Grotzky, A., Lukić, R., Matoori, S., Luciani, P., Yu, H., Zhang, B., Walde, P., Schlüter, A. D., Gauthier, M. A., and Leroux, J.-C., 2013, "Sustained gastrointestinal activity of dendronized polymer–enzyme conjugates," Nat Chem, 5(7), pp. 582-589.
[89] Gonzalez-Mariscal, L., Betanzos, A., Nava, P., and Jaramillo, B. E., 2003, "Tight junction proteins," Prog. Biophys. Mol. Biol., 81(1), pp. 1-44.
[90] Citi, S., and Cordenonsi, M., 1998, "Tight junction proteins," Biochim. Biophys. Acta, 1448(1), pp. 1-11.
[91] Noda, S., Tanabe, S., and Suzuki, T., 2013, "Naringenin enhances intestinal barrier function through the expression and cytoskeletal association of tight junction proteins in Caco-2 cells," Molecular nutrition & food research, 57(11), pp. 2019-2028.
[92] Willott, E., Balda, M. S., Fanning, A. S., Jameson, B., Van Itallie, C., and Anderson, J. M., 1993, "The tight junction protein ZO-1 is homologous to the Drosophila discs-large tumor suppressor protein of septate junctions," Proc Natl Acad Sci U S A, 90(16), pp. 7834-7838.
[93] Aungst, B. J., 2000, "Intestinal permeation enhancers," J. Pharm. Sci., 89(4), pp. 429-442.
[94] Lindmark, T., Schipper, N., Lazorova, L., de Boer, A. G., and Artursson, P., 1998, "Absorption enhancement in intestinal epithelial Caco-2 monolayers by sodium caprate: assessment of molecular weight dependence and demonstration of transport routes," Journal of drug targeting, 5(3), pp. 215-223.
[95] Kotze, A. F., Thanou, M. M., Luebetaen, H. L., de Boer, A. G., Verhoef, J. C., and Junginger, H. E., 1999, "Enhancement of paracellular drug transport with highly quaternized N-trimethyl chitosan chloride in neutral environments: in vitro evaluation in intestinal epithelial cells (Caco-2)," J. Pharm. Sci., 88(2), pp. 253-257.
[96] Kotze, A. F., Luessen, H. L., de Leeuw, B. J., de Boer, B. G., Verhoef, J. C., and Junginger, H. E., 1997, "N-trimethyl chitosan chloride as a potential absorption enhancer across mucosal surfaces: in vitro evaluation in intestinal epithelial cells (Caco-2)," Pharm. Res., 14(9), pp. 1197-1202.
[97] Veronese, F. M., 2001, "Peptide and protein PEGylation: a review of problems and solutions," Biomaterials, 22(5), pp. 405-417.
[98] Sharma, S., Kaur, P., Jain, A., Rajeswari, M. R., and Gupta, M. N., 2003, "A Smart Bioconjugate of Chymotrypsin," Biomacromolecules, 4(2), pp. 330-336.
[99] Hoffman, A. S., Stayton, P. S., Bulmus, V., Chen, G., Chen, J., Cheung, C., Chilkoti, A., Ding, Z., Dong, L., Fong, R., Lackey, C. A., Long, C. J., Miura, M., Morris, J. E., Murthy, N., Nabeshima, Y., Park, T. G., Press, O. W., Shimoboji, T., Shoemaker, S., Yang, H. J., Monji, N., Nowinski, R. C., Cole, C. A., Priest, J. H., Harris, J. M., Nakamae, K., Nishino, T., and Miyata, T., 2000, "Really smart bioconjugates of smart polymers and receptor proteins," Journal of Biomedical Materials Research, 52(4), pp. 577-586.
[100] Gil, E. S., and Hudson, S. M., 2004, "Stimuli-reponsive polymers and their bioconjugates," Prog. Polym. Sci., 29(12), pp. 1173-1222.
[101] Schild, H. G., 1992, "Poly(N-isopropylacrylamide): experiment, theory and application," Prog. Polym. Sci., 17(2), pp. 163-249.

[102] Chen, L., Honma, Y., Mizutani, T., Liaw, D. J., Gong, J. P., and Osada, Y., 2000, "Effects of polyelectrolyte complexation on the UCST of zwitterionic polymer," Polymer, 41(1), pp. 141-147.
[103] Plunkett, K. N., Zhu, X., Moore, J. S., and Leckband, D. E., 2006, "PNIPAM Chain Collapse Depends on the Molecular Weight and Grafting Density," Langmuir, 22(9), pp. 4259-4266.
[104] Yan, M., Ge, J., Dong, W., Liu, Z., and Ouyang, P., 2006, "Preparation and characterization of a temperature-sensitive sulfobetaine polymer–trypsin conjugate," Biochem. Eng. J., 30(1), pp. 48-54.
[105] Chen, G. H., and Hoffman, A. S., 1993, "Preparation and Properties of Thermoreversible, Phase-Separating Enzyme-Oligo(N-Isopropylacrylamide) Conjugates," Bioconjugate Chem., 4(6), pp. 509-514.
[106] Heredia, K. L., Bontempo, D., Ly, T., Byers, J. T., Halstenberg, S., and Maynard, H. D., 2005, "In situ preparation of protein - "Smart" polymer conjugates with retention of bioactivity," J. Am. Chem. Soc., 127(48), pp. 16955-16960.
[107] Murata, H., Cummings, C., Koepsel, R., Russell, A.J., 2013, "Polymer-based protein engineering can rationally tune enzyme solubility, kinetics, and stability," Biomacromolecules.
[108] Hedstrom, L., 2002, "Serine protease mechanism and specificity," Chem. Rev., 102(12), pp. 4501-4523.
[109] Dodson, G., and Wlodawer, A., 1998, "Catalytic triads and their relatives," Trends Biochem. Sci, 23(9), pp. 347-352.
[110] Ciampolini, M., and Nardi, N., 1966, "Five-Coordinated High-Spin Complexes of Bivalent Cobalt, Nickel, andCopper with Tris(2-dimethylaminoethyl)amine," Inorg. Chem., 5(1), pp. 41-44.
[111] Yang, Z., Domach, M., Auger, R., Yang, F. X., and Russell, A. J., 1996, "Polyethylene glycol-induced stabilization of subtilisin," Enzyme Microb. Technol., 18(2), pp. 82-89.
[112] Kumar, S., and Hein, G. E., 1970, "Concerning Mechanism of Autolysis of Alpha-Chymotrypsin," Biochemistry, 9(2), pp. 291-&.
[113] Shao, Q., He, Y., White, A. D., and Jiang, S. Y., 2012, "Different effects of zwitterion and ethylene glycol on proteins," J. Chem. Phys., 136(22).
[114] Rodríguez-Martínez, J. A., Solá, R. J., Castillo, B., Cintrón-Colón, H. R., Rivera-Rivera, I., Barletta, G., and Griebenow, K., 2008, "Stabilization of α-chymotrypsin upon PEGylation correlates with reduced structural dynamics," Biotechnol. Bioeng., 101(6), pp. 1142-1149.
[115] Hoffman, A. S., and Stayton, P. S., 2007, "Conjugates of stimuli-responsive polymers and proteins," Prog. Polym. Sci., 32(8-9), pp. 922-932.
[116] Lackey, C. A., Murthy, N., Press, O. W., Tirrell, D. A., Hoffman, A. S., and Stayton, P. S., 1999, "Hemolytic activity of pH-responsive polymer-streptavidin bioconjugates," Bioconjugate Chem., 10(3), pp. 401-405.
[117] Zhang, Q., Vanparijs, N., Louage, B., De Geest, B. G., and Hoogenboom, R., 2014, "Dual pH- and temperature-responsive RAFT-based block co-polymer micelles and polymer-protein conjugates with transient solubility," Polymer Chemistry.
[118] Strozyk, M. S., Chanana, M., Pastoriza-Santos, I., Pérez-Juste, J., and Liz-Marzán, L. M., 2012, "Protein/Polymer-Based Dual-Responsive Gold Nanoparticles with pH-Dependent Thermal Sensitivity," Adv. Funct. Mater., 22(7), pp. 1436-1444.

[119] Cummings, C., Murata, H., Koepsel, R., and Russell, A. J., 2013, "Tailoring enzyme activity and stability using polymer-based protein engineering," Biomaterials, 34(30), pp. 7437-7443.
[120] Fuhrmann, G., Grotzky, A., Lukic, R., Matoori, S., Luciani, P., Yu, H., Zhang, B., Walde, P., Schluter, A. D., Gauthier, M. A., and Leroux, J. C., 2013, "Sustained gastrointestinal activity of dendronized polymer-enzyme conjugates," Nat Chem, 5(7), pp. 582-589.
[121] Murata, H., Cummings, C. S., Koepsel, R. R., and Russell, A. J., 2013, "Polymer-Based Protein Engineering Can Rationally Tune Enzyme Activity, pH-Dependence, and Stability," Biomacromolecules, 14(6), pp. 1919-1926.
[122] Naito, H., Takewa, Y., Mizuno, T., Ohya, S., Nakayama, Y., Tatsumi, E., Kitamura, S., Takano, H., Taniguchi, S., and Taenaka, Y., 2004, "Three-dimensional cardiac tissue engineering using a thermoresponsive artificial extracellular matrix," Asaio J, 50(4), pp. 344-348.
[123] Zhou, P., Yu, S. B., Liu, Z. H., Hu, J. M., and Deng, Y. Z., 2005, "Electrophoretic separation of DNA using a new matrix in uncoated capillaries," J. Chromatogr. A, 1083(1-2), pp. 173-178.
[124] Zhang, Z., Finlay, J. A., Wang, L., Gao, Y., Callow, J. A., Callow, M. E., and Jiang, S., 2009, "Polysulfobetaine-Grafted Surfaces as Environmentally Benign Ultralow Fouling Marine Coatings," Langmuir, 25(23), pp. 13516-13521.
[125] Smith, R. S., Zhang, Z., Bouchard, M., Li, J., Lapp, H. S., Brotske, G. R., Lucchino, D. L., Weaver, D., Roth, L. A., Coury, A., Biggerstaff, J., Sukavaneshvar, S., Langer, R., and Loose, C., 2012, "Vascular Catheters with a Nonleaching Poly-Sulfobetaine Surface Modification Reduce Thrombus Formation and Microbial Attachment," Science Translational Medicine, 4(153), p. 153ra132.
[126] Arotcarena, M., Heise, B., Ishaya, S., and Laschewsky, A., 2002, "Switching the inside and the outside of aggregates of water-soluble block copolymers with double thermoresponsivity," J. Am. Chem. Soc., 124(14), pp. 3787-3793.
[127] Weaver, J. V. M., Armes, S. P., and Butun, V., 2002, "Synthesis and aqueous solution properties of a well-defined thermo-responsive schizophrenic diblock copolymer," Chem. Commun.(18), pp. 2122-2123.
[128] Kulkarni, S., Schilli, C., Muller, A. H. E., Hoffman, A. S., and Stayton, P. S., 2004, "Reversible meso-scale smart polymer-protein particles of controlled sizes," Bioconjugate Chem., 15(4), pp. 747-753.
[129] Boyer, C., Bulmus, V., Liu, J. Q., Davis, T. P., Stenzel, M. H., and Barner-Kowollik, C., 2007, "Well-defined protein-polymer conjugates via in situ RAFT polymerization," J. Am. Chem. Soc., 129(22), pp. 7145-7154.
[130] Li, H. M., Li, M., Yu, X., Bapat, A. P., and Sumerlin, B. S., 2011, "Block copolymer conjugates prepared by sequentially grafting from proteins via RAFT," Polymer Chemistry, 2(7), pp. 1531-1535.
[131] Li, M., Li, H. M., De, P., and Sumerlin, B. S., 2011, "Thermoresponsive Block Copolymer-Protein Conjugates Prepared by Grafting-from via RAFT Polymerization," Macromol. Rapid Commun., 32(4), pp. 354-359.
[132] Kulkarni, S., Schilli, C., Grin, B., Muller, A. H. E., Hoffman, A. S., and Stayton, P. S., 2006, "Controlling the aggregation of conjugates of streptavidin with smart block copolymers prepared via the RAFT copolymerization technique," Biomacromolecules, 7(10), pp. 2736-2741.
[133] Kumar, A., and Venkatesu, P., 2012, "Overview of the Stability of α-Chymotrypsin in Different Solvent Media," Chem. Rev., 112(7), pp. 4283-4307.

[134] Turner, K. M., Pasut, G., Veronese, F. M., Boyce, A., and Walsh, G., 2011, "Stabilization of a supplemental digestive enzyme by post-translational engineering using chemically-activated polyethylene glycol," Biotechnol. Lett., 33(3), pp. 617-621.
[135] Xu, J., Ye, J., and Liu, S., 2007, "Synthesis of Well-Defined Cyclic Poly(N-isopropylacrylamide) via Click Chemistry and Its Unique Thermal Phase Transition Behavior," Macromolecules, 40(25), pp. 9103-9110.
[136] Simakova, A., Averick, S. E., Konkolewicz, D., and Matyjaszewski, K., 2012, "Aqueous ARGET ATRP," Macromolecules, 45(16), pp. 6371-6379.
[137] Tsarevsky, N. V., Pintauer, T., and Matyjaszewski, K., 2004, "Deactivation efficiency and degree of control over polymerization in ATRP in protic solvents," Macromolecules, 37(26), pp. 9768-9778.
[138] Zhang, Y., Furyk, S., Sagle, L. B., Cho, Y., Bergbreiter, D. E., and Cremer, P. S., 2007, "Effects of Hofmeister Anions on the LCST of PNIPAM as a Function of Molecular Weight†," The Journal of Physical Chemistry C, 111(25), pp. 8916-8924.
[139] Reineke, J., Cho, D. Y., Dingle, Y. L., Cheifetz, P., Laulicht, B., Lavin, D., Furtado, S., and Mathiowitz, E., 2013, "Can bioadhesive nanoparticles allow for more effective particle uptake from the small intestine?," J. Controlled Release, 170(3), pp. 477-484.
[140] Xu, Q., Boylan, N. J., Cai, S., Miao, B., Patel, H., and Hanes, J., 2013, "Scalable method to produce biodegradable nanoparticles that rapidly penetrate human mucus," J. Controlled Release, 170(2), pp. 279-286.
[141] Baldwin, R. L., 1996, "How Hofmeister ion interactions affect protein stability," Biophys. J., 71(4), pp. 2056-2063.
[142] Chen, J. P., and Hoffman, A. S., 1990, "Polymer Protein Conjugates .2. Affinity Precipitation Separation of Human Immuno-Gamma-Globulin by a Poly(N-Isopropylacrylamide)-Protein-a Conjugate," Biomaterials, 11(9), pp. 631-634.
[143] Callahan, D. J., Liu, W. E., Li, X. H., Dreher, M. R., Hassouneh, W., Kim, M., Marszalek, P., and Chilkoti, A., 2012, "Triple Stimulus-Responsive Polypeptide Nanoparticles That Enhance Intratumoral Spatial Distribution," Nano Lett., 12(4), pp. 2165-2170.
[144] McDaniel, J. R., Dewhirst, M. W., and Chilkoti, A., 2013, "Actively targeting solid tumours with thermoresponsive drug delivery systems that respond to mild hyperthermia," International journal of hyperthermia : the official journal of European Society for Hyperthermic Oncology, North American Hyperthermia Group, 29(6), pp. 501-510.
[145] Hong, J., Gong, P.-J., Yu, J.-H., Xu, D.-M., Sun, H.-W., and Yao, S., 2006, "Conjugation of α-chymotrypsin on a polymeric hydrophilic nanolayer covering magnetic nanoparticles," J. Mol. Catal. B: Enzym., 42(3–4), pp. 99-105.
[146] Falatach, R., Li, S., Sloane, S., McGlone, C., Berberich, J. A., Page, R. C., Averick, S., and Konkolewicz, D., 2015, "Why synthesize protein–polymer conjugates? The stability and activity of chymotrypsin-polymer bioconjugates synthesized by RAFT," Polymer, 72, pp. 382-386.
[147] Sandanaraj, B. S., Vutukuri, D. R., Simard, J. M., Klaikherd, A., Hong, R., Rotello, V. M., and Thayumanavan, S., 2005, "Noncovalent Modification of Chymotrypsin Surface Using an Amphiphilic Polymer Scaffold: Implications in Modulating Protein Function," J. Am. Chem. Soc., 127(30), pp. 10693-10698.
[148] Blow, D. M., 1969, "The study of alpha-chymotrypsin by x-ray diffraction. The Third CIBA Medal Lecture," Biochem. J, 112(3), pp. 261-268.

[149] Scheidig, A. J., Hynes, T. R., Pelletier, L. A., Wells, J. A., and Kossiakoff, A. A., 1997, "Crystal structures of bovine chymotrypsin and trypsin complexed to the inhibitor domain of Alzheimer's amyloid beta-protein precursor (APPI) and basic pancreatic trypsin inhibitor (BPTI): engineering of inhibitors with altered specificities," Protein Science : A Publication of the Protein Society, 6(9), pp. 1806-1824.
[150] Günther, R., Thust, S., Hofmann, H.-J., and Bordusa, F., 2000, "Trypsin-specific acyl-4-guanidinophenyl esters for α-chymotrypsin-catalysed reactions," Eur. J. Biochem., 267(12), pp. 3496-3501.
[151] Wysocka, M., Lesner, A., Legowska, A., Jaskiewicz, A., Miecznikowska, H., and Rolka, K., 2008, "Designing of substrates and inhibitors of bovine alpha-chymotrypsin with synthetic phenylalanine analogues in position P(1)," Protein and peptide letters, 15(3), pp. 260-264.
[152] Asgeirsson, B., and Bjarnason, J. B., 1991, "Structural and kinetic properties of chymotrypsin from Atlantic cod (Gadus morhua). Comparison with bovine chymotrypsin," Comparative biochemistry and physiology. B, Comparative biochemistry, 99(2), pp. 327-335.
[153] Simon, L. M., Kotormán, M., Garab, G., and Laczkó, I., 2001, "Structure and Activity of α-Chymotrypsin and Trypsin in Aqueous Organic Media," Biochem. Biophys. Res. Commun., 280(5), pp. 1367-1371.
[154] Klibanov, A. M., 2001, "Improving enzymes by using them in organic solvents," Nature, 409(6817), pp. 241-246.
[155] Graham , D. Y., 1977, "Enzyme Replacement Therapy of Exocrine Pancreatic Insufficiency in Man," New Engl J Med, 296(23), pp. 1314-1317.
[156] Geokas, M. C., Conteas, C. N., and Majumdar, A. P., 1985, "The aging gastrointestinal tract, liver, and pancreas," Clinics in geriatric medicine, 1(1), pp. 177-205.
[157] Webb, S., 2010, "Drugmakers dance with autism," Nat Biotech, 28(8), pp. 772-774.
[158] Trapnell, B., Jerkins, T., Haupt, M., Chen, S., Bodhani, A., Seo, B., and Kapoor, M., 2014, "Relationship between Pancreatic Enzyme Replacement Therapy and Healthcare Use in Children with Cystic Fibrosis," Pediatr Pulm, 49, pp. 406-407.
[159] Somaraju, U. R., and Solis-Moya, A., 2014, "Pancreatic enzyme replacement therapy for people with cystic fibrosis," Cochrane database of systematic reviews(10).
[160] Lisowska, A., Kaminska, B., Grzymislawski, M., Herzig, K.-H., and Walkowiak, J., 2006, "Unresponsive or non-compliant steatorrhea in cystic fibrosis?," Journal of Cystic Fibrosis, 5(4), pp. 253-255.
[161] Fieker, A., Philpott, J., and Armand, M., 2011, "Enzyme replacement therapy for pancreatic insufficiency: present and future," Clinical and Experimental Gastroenterology, 4, pp. 55-73.
[162] DiPalma, J. A., and Collins, M. S., 1989, "Enzyme Replacement for Lactose Malabsorption Using a Beta-D-Galactosidase," Journal of Clinical Gastroenterology, 11(3), pp. 290-293.
[163] Montalto, M., Curigliano, V., Santoro, L., Vastola, M., Cammarota, G., Manna, R., Gasbarrini, A., and Gasbarrini, G., 2006, "Management and treatment of lactose malabsorption," World journal of gastroenterology, 12(2), pp. 187-191.
[164] Heyman, M. B., 2006, "Lactose Intolerance in Infants, Children, and Adolescents," Pediatrics, 118(3), pp. 1279-1286.
[165] Watson, L., 2010, "Exocrine Insufficiency and Pancreatic Enzyme Replacement Therapy in Pancreatic Cancer," Clin Oncol-Uk, 22(5), pp. 391-391.

[166] Lowe, M. E., and Whitcomb, D. C., 2015, "Next Generation of Pancreatic Enzyme Replacement Therapy: Recombinant Microbial Enzymes and Finding the Perfect Lipase," Gastroenterology, 149(7), pp. 1678-1681.
[167] Borowitz, D., Goss, C. H., Limauro, S., Konstan, M. W., Blake, K., Casey, S., Quittner, A. L., and Murray, F. T., 2006, "Study of a novel pancreatic enzyme replacement therapy in pancreatic insufficient subjects with cystic fibrosis," The Journal of Pediatrics, 149(5), pp. 658-662.e651.
[168] Davidovich-Pinhas, M., and Bianco-Peled, H., 2010, "Mucoadhesion: a review of characterization techniques," Expert Opinion on Drug Delivery, 7(2), pp. 259-271.
[169] al-Ajlan, A., and Bailey, G. S., 1997, "Purification and partial characterization of camel anionic chymotrypsin," Arch. Biochem. Biophys., 348(2), pp. 363-368.
[170] Castillo-Yanez, F. J., Pacheco-Aguilar, R., Lugo-Sanchez, M. E., Garcia-Sanchez, G., and Quintero-Reyes, I. E., 2009, "Biochemical characterization of an isoform of chymotrypsin from the viscera of Monterey sardine (Sardinops sagax caerulea), and comparison with bovine chymotrypsin," Food Chem., 112(3), pp. 634-639.
[171] Kurinomaru, T., Kameda, T., and Shiraki, K., 2015, "Effects of multivalency and hydrophobicity of polyamines on enzyme hyperactivation of α-chymotrypsin," J. Mol. Catal. B: Enzym., 115, pp. 135-139.
[172] Xenos, K., Kyroudis, S., Anagnostidis, A., and Papastathopoulos, P., 1998, "Treatment of lactose intolerance with exogenous beta-D-galactosidase in pellet form," Eur J Drug Metab Ph, 23(2), pp. 350-355.
[173] Rodriguez, E., Wood, Z. A., Karplus, P. A., and Lei, X. G., 2000, "Site-directed mutagenesis improves catalytic efficiency and thermostability of Escherichia coli pH 2.5 acid phosphatase/phytase expressed in Pichia pastoris," Arch. Biochem. Biophys., 382(1), pp. 105-112.
[174] Abian, O., Grazú, V., Hermoso, J., González, R., García, J. L., Fernández-Lafuente, R., and Guisán, J. M., 2004, "Stabilization of Penicillin G Acylase from Escherichia coli: Site-Directed Mutagenesis of the Protein Surface To Increase Multipoint Covalent Attachment," Appl Environ Microb, 70(2), pp. 1249-1251.
[175] Qi, K. K., Wu, J., Deng, B., Li, Y. M., and Xu, Z. W., 2015, "PEGylated porcine glucagon-like peptide-2 improved the intestinal digestive function and prevented inflammation of weaning piglets challenged with LPS," Animal : an international journal of animal bioscience, 9(9), pp. 1481-1489.
[176] Turner, K. M., Pasut, G., Veronese, F. M., Boyce, A., and Walsh, G., 2011, "Stabilization of a supplemental digestive enzyme by post-translational engineering using chemically-activated polyethylene glycol," Biotechnol. Lett., 33(3), pp. 617-621.
[177] Zhang, Y., and Cremer, P. S., 2006, "Interactions between macromolecules and ions: the Hofmeister series," Curr. Opin. Chem. Biol., 10(6), pp. 658-663.
[178] Yin, L., Ding, J., He, C., Cui, L., Tang, C., and Yin, C., 2009, "Drug permeability and mucoadhesion properties of thiolated trimethyl chitosan nanoparticles in oral insulin delivery," Biomaterials, 30(29), pp. 5691-5700.
[179] Park, H., and Robinson, J. R., 1987, "Mechanisms of Mucoadhesion of Poly(acrylic Acid) Hydrogels," Pharm. Res., 4(6), pp. 457-464.
[180] Rodríguez-Martínez, J. A., Rivera-Rivera, I., Solá, R. J., and Griebenow, K., 2009, "Enzymatic activity and thermal stability of PEG-α-chymotrypsin conjugates," Biotechnol. Lett., 31(6), pp. 883-887.

[181] Werle, M., and Bernkop-Schnürch, A., 2006, "Strategies to improve plasma half life time of peptide and protein drugs," Amino Acids, 30(4), pp. 351-367.
[182] Wang, W., 2000, "Lyophilization and development of solid protein pharmaceuticals," Int. J. Pharm., 203(1–2), pp. 1-60.
[183] Leach, S. A., 1963, "Release and Breakdown of Sialic Acid from Human Salivary Mucin and its Role in the Formation of Dental Plaque," Nature, 199(4892), pp. 486-487.
[184] Riccardi, C. M., Cole, K. S., Benson, K. R., Ward, J. R., Bassett, K. M., Zhang, Y., Zore, O. V., Stromer, B., Kasi, R. M., and Kumar, C. V., 2014, "Toward "Stable-on-the-Table" Enzymes: Improving Key Properties of Catalase by Covalent Conjugation with Poly(acrylic acid)," Bioconjugate Chem., 25(8), pp. 1501-1510.
[185] Cummings, C., Murata, H., Koepsel, R., and Russell, A. J., 2014, "Dramatically Increased pH and Temperature Stability of Chymotrypsin Using Dual Block Polymer-Based Protein Engineering," Biomacromolecules, 15(3), pp. 763-771.
[186] Murata, H., Cummings, C. S., Koepsel, R. R., and Russell, A. J., 2014, "Rational Tailoring of Substrate and Inhibitor Affinity via ATRP Polymer-Based Protein Engineering," Biomacromolecules, 15(7), pp. 2817-2823.
[187] Kijima, T., Yamamoto, S., and Kise, H., 1996, "Study on tryptophan fluorescence and catalytic activity of α-chymotrypsin in aqueous-organic media," Enzyme Microb. Technol., 18(1), pp. 2-6.
[188] Desie, G., Boens, N., and De Schryver, F. C., 1986, "Study of the time-resolved tryptophan fluorescence of crystalline alpha-chymotrypsin," Biochemistry, 25(25), pp. 8301-8308.
[189] Fischer, N. O., McIntosh, C. M., Simard, J. M., and Rotello, V. M., 2002, "Inhibition of chymotrypsin through surface binding using nanoparticle-based receptors," Proc. Natl. Acad. Sci. U. S. A., 99(8), pp. 5018-5023.
[190] Street, T. O., Bolen, D. W., and Rose, G. D., 2006, "A molecular mechanism for osmolyte-induced protein stability," Proceedings of the National Academy of Sciences, 103(38), pp. 13997-14002.
[191] Bennion, B. J., and Daggett, V., 2004, "Counteraction of urea-induced protein denaturation by trimethylamine N-oxide: a chemical chaperone at atomic resolution," Proc Natl Acad Sci U S A, 101(17), pp. 6433-6438.
[192] Timasheff, S. N., 2002, "Protein-solvent preferential interactions, protein hydration, and the modulation of biochemical reactions by solvent components," Proceedings of the National Academy of Sciences, 99(15), pp. 9721-9726.
[193] Swiech, K., Picanço-Castro, V., and Covas, D. T., 2012, "Human cells: New platform for recombinant therapeutic protein production," Protein Expression and Purification, 84(1), pp. 147-153.
[194] Dimitrov, D. S., 2012, "Therapeutic proteins," Methods in molecular biology, 899, pp. 1-26.
[195] Leader, B., Baca, Q. J., and Golan, D. E., 2008, "Protein therapeutics: A summary and pharmacological classification," Nat. Rev. Drug Discov., 7(1), pp. 21-39.
[196] Ecker, D. M., Jones, S. D., and Levine, H. L., 2015, "The therapeutic monoclonal antibody market," mAbs, 7(1), pp. 9-14.
[197] Hickey, A. J., 2016, "Pulmonary Drug Delivery," Drug Delivery, John Wiley & Sons, Inc, pp. 186-206.

[198] Prausnitz, M. R., and Langer, R., 2008, "Transdermal drug delivery," Nat Biotech, 26(11), pp. 1261-1268.
[199] Gaudana, R., Ananthula, H. K., Parenky, A., and Mitra, A. K., 2010, "Ocular Drug Delivery," The AAPS journal, 12(3), pp. 348-360.
[200] Batchelor, H., 2014, "Rectal Drug Delivery," Pediatric Formulations: A Roadmap, D. Bar-Shalom, and K. Rose, eds., Springer New York, New York, NY, pp. 303-310.
[201] Vyas, T. K., Shahiwala, A., Marathe, S., and Misra, A., 2005, "Intranasal Drug Delivery for Brain Targeting," Current Drug Delivery, 2(2), pp. 165-175.
[202] das Neves, J., Amaral, M. H., and Bahia, M. F., 2010, "Vaginal Drug Delivery," Pharmaceutical Sciences Encyclopedia, John Wiley & Sons, Inc.
[203] Caon, T., Jin, L., Simões, C. M. O., Norton, R. S., and Nicolazzo, J. A., 2015, "Enhancing the Buccal Mucosal Delivery of Peptide and Protein Therapeutics," Pharm. Res., 32(1), pp. 1-21.
[204] Moroz, E., Matoori, S., and Leroux, J.-C., 2016, "Oral delivery of macromolecular drugs: Where we are after almost 100 years of attempts," Advanced Drug Delivery Reviews, 101, pp. 108-121.
[205] Toorisaka, E., Hashida, M., Kamiya, N., Ono, H., Kokazu, Y., and Goto, M., 2005, "An enteric-coated dry emulsion formulation for oral insulin delivery," J. Controlled Release, 107(1), pp. 91-96.
[206] Fukui, E., Miyamura, N., Uemura, K., and Kobayashi, M., 2000, "Preparation of enteric coated timed-release press-coated tablets and evaluation of their function by in vitro and in vivo tests for colon targeting," Int. J. Pharm., 204(1–2), pp. 7-15.
[207] Carvalho, F. C., Bruschi, M. L., Evangelista, R. C., and Gremiao, M. P. D., 2010, "Mucoadhesive drug delivery systems," Braz J Pharm Sci, 46(1), pp. 1-17.
[208] Pridgen, E. M., Alexis, F., Kuo, T. T., Levy-Nissenbaum, E., Karnik, R., Blumberg, R. S., Langer, R., and Farokhzad, O. C., 2013, "Transepithelial Transport of Fc-Targeted Nanoparticles by the Neonatal Fc Receptor for Oral Delivery," Science Translational Medicine, 5(213).
[209] Naik, A., Pechtold, L. A. R. M., Potts, R. O., and Guy, R. H., 1995, "Mechanism of oleic acid-induced skin penetration enhancement in vivo in humans," J. Controlled Release, 37(3), pp. 299-306.
[210] Williams, A. C., and Barry, B. W., 2012, "Penetration enhancers," Advanced Drug Delivery Reviews, 64, pp. 128-137.
[211] Gupta, V., Hwang, B. H., Doshi, N., and Mitragotri, S., 2013, "A permeation enhancer for increasing transport of therapeutic macromolecules across the intestine," Journal of controlled release : official journal of the Controlled Release Society, 172(2), pp. 541-549.
[212] Southwell, D., and Barry, B. W., 1983, "Penetration Enhancers for Human-Skin - Mode of Action of 2-Pyrrolidone and Dimethylformamide on Partition and Diffusion of Model Compounds Water, Normal-Alcohols, and Caffeine," J Invest Dermatol, 80(6), pp. 507-514.
[213] Whitehead, K., and Mitragotri, S., 2008, "Mechanistic analysis of chemical permeation enhancers for oral drug delivery," Pharm. Res., 25(6), pp. 1412-1419.
[214] Karande, P., Jain, A., and Mitragotri, S., 2004, "Discovery of transdermal penetration enhancers by high-throughput screening," Nat. Biotechnol., 22(2), pp. 192-197.
[215] Karande, P., Jain, A., Ergun, K., Kispersky, V., and Mitragotri, S., 2005, "Design principles of chemical penetration enhancers for transdermal drug delivery," Proc Natl Acad Sci U S A, 102(13), pp. 4688-4693.

[216] Whitehead, K., Karr, N., and Mitragotri, S., 2008, "Safe and effective permeation enhancers for oral drug delivery," Pharm. Res., 25(8), pp. 1782-1788.
[217] Lamson, N. G., Cusimano, G., Suri, K., Zhang, A., and Whitehead, K. A., 2016, "The pH of Piperazine Derivative Solutions Predicts Their Utility as Transepithelial Permeation Enhancers," Mol Pharmaceut, 13(2), pp. 578-585.
[218] Muller, A. H. E., Millard, P. E., Mougin, N. C., and Boker, A., 2008, "POLY 544-Fast ATRP of N-isopropylacrylamide in water and its application to bioconjugates," Abstr Pap Am Chem S, 236.
[219] Gupta, V., Doshi, N., and Mitragotri, S., 2013, "Permeation of Insulin, Calcitonin and Exenatide across Caco-2 Monolayers: Measurement Using a Rapid, 3-Day System," PloS one, 8(2), p. e57136.
[220] Sambuy, Y., De Angelis, I., Ranaldi, G., Scarino, M. L., Stammati, A., and Zucco, F., 2005, "The Caco-2 cell line as a model of the intestinal barrier: influence of cell and culture-related factors on Caco-2 cell functional characteristics," Cell Biology and Toxicology, 21(1), pp. 1-26.
[221] Press, B., and Di Grandi, D., 2008, "Permeability for intestinal absorption: Caco-2 assay and related issues," Current drug metabolism, 9(9), pp. 893-900.